Optimized Thermoelectric Cooling Strategies for High Performance Electronic Systems

by

Ali-Reza Asarizadeh

A thesis

presented to the University of Waterloo

in fulfillment of the

thesis requirement for the degree of

Master of Applied Science

in

Chemical Engineering and Mechanical Engineering

Waterloo, Ontario, Canada, 2015

Author’s Declaration

I hereby declare that I am the sole author of this thesis. This is the true copy of the thesis, including any required final revisions, as accepted by my examiners.

I understand that my thesis may be made electronically available to the public.

Abstract

Thermoelectric components (TECs) and other electronic cooling components such as micro-heat sinks have been shown to provide effective cooling for integrated circuits (ICs). A review of available literature has shown effective temperature control using these components separately, and to a lesser extent, using configurations containing multiple approaches for cooling to sub-ambient levels. However, little data are available for sizing thermal management packages focusing on shrinking the device footprint. This suggests that more experimental data of multi-component cooling strategies are needed to leverage the advantages and demonstrate superior cooling performance on a smaller scale. In some electronics devices, such as spectrometers or photodetectors, the quality of spectral data obtained is adversely affected by increases in device temperature. Physically speaking, this is due to the fact that, at higher temperatures, the charged particles are stimulated and released from the boundary region, a process known as thermionic emission. Reducing the local temperature will help minimize the effects of heat generation and the overall noise associated with this heat buildup.

The thesis sets out to assess the feasibility and practicality of implementing a TEC-based thermal management system for use in electronic packaging and in particular, for spectrometers in the nanophotonics industry. A heat sink and fan were used as auxiliary components to aid the heat dissipation process. The key areas that needed to be addressed include surface temperature stability, sub-ambient cooling capability, and scale down potential of the overall device. Cooling of surfaces down to at least -10°C (from ambient) was conducted using several heat sink and thermoelectric device configurations. Temperature stability was demonstrated through low temperature fluctuations (0.2°C/h surface warm up rate) for a 5 hour timeframe. Preliminary results demonstrate a 78% reduction of heat sink size down to 57 cm^3 (surface area 172 cm^2) while maintaining a -10°C surface temperature. Maximum surface cooling down to -22.4°C was achieved using 254 cm^3 heat sink volume (surface area 1443 cm^2). The results also show a strong correlation between available heat sink surface area and cooling performance. Continuing improvements such as introducing a phase change liquid and further size reductions to key components (fans, TEC, heat sinks, etc.) can potentially help scale down the thermal management system even more.

Acknowledgements

I would like to acknowledge Dr. Richard Culham, Dr. Ioannis (John) Chatzis, Dr. Ali Elkamel and Dr. John Medley for reviewing my MASc. thesis. I would like to particularly thank Dr. Culham and Dr. Chatzis for their continued and unwavering support in helping me complete the degree as co-supervisors.

I also would like to acknowledge Arsen Hajian and Andrew Cenko from Tornado Spectral Systems for providing technical support and other in-kind contributions.

Finally, I would like to thank NSERC for approving and providing the necessary funding to complete this research through an Engage Grant (Project #: EGP 459062-13).

Dedication

I dedicate my MASc. thesis to my incredible family [Zahra, Kamran and Moe] as they helped me greatly during my studies. I also dedicate this work to my amazing fiancé Amel Badri who was always supportive and motivating. A special mention goes to Glenyce Hutter and Judy Caron whose contributions I will always remember.

Table of Contents

List of Figures

List of Tables

Nomenclature

E_0	=	Ground State Energy [J]
I_{max}	=	Maximum Current [A]
I_N	=	Dark Current Produced [A]
K	=	Boltzmann's Constant [1.3805 x 10^{-23} J/K]
Q_{max}	=	Maximum Power Output [W]
Q	=	Heat Flow [W]
Q_h	=	Hot Side Heat Flow [W]
Q_c	=	Cold Side Heat Flow [W]
Q_i	=	Heat Flow for Configuration i (i = 1, 2, 3, etc.) [W]
Q_{TEC}	=	Heat Dissipation in TEC Module [W]
q	=	Heat Flux [W/cm^2]
A	=	Area [cm^2]
A_i	=	Heat Sink Surface Area for Configuration i (i = 1, 2, 3, etc.) [cm^2]
h_i	=	Heat Transfer Coefficient for Configuration i (i = 1, 2, 3, etc.) [cm^2]
z	=	Thickness [cm]
R_t	=	Total Thermal Resistance [K/W]
R_i	=	Thermal Resistance at Junction Point i (i = 1, 2, 3, etc.) [K/W]
R_h	=	Heat Pipe Evaporator Convective Thermal Resistance [K/W]
$R_{p,e}$	=	Thermal Resistance of Heat Pipe Wall at Evaporator [K/W]
$R_{w,e}$	=	Thermal Resistance of Wick at Evaporator [K/W]
R_v	=	Thermal Resistance of Vapor Flow From Evaporator to Condenser [K/W]
$R_{w,c}$	=	Thermal Resistance of Wick at Condenser [K/W]

$R_{p,c}$	=	Thermal Resistance of Heat Pipe Wall at Condenser [K/W]
R_c	=	Heat Pipe Condenser Convective Thermal Resistance [K/W]
R_{conv}	=	Thermal Convection Resistance of Heat Sink [K/W]
R_b	=	Thermal Conduction Resistance of Heat Sink Base [K/W]
$R_{b,sp}$	=	Thermal Spreading Resistance at Heat Sink Base [K/W]
R_{cons}	=	Thermal Constriction Resistance [K/W]
$R_{c,sp}$	=	Thermal Spreading Resistance at TEC Cold Side [K/W]
R_{cont}	=	Thermal Contact Resistance [K/W]
$R_{c,air}$	=	Thermal Contact Resistance Using Air as Interstitial Material [K/W]
$R_{c,grease}$	=	Thermal Contact Resistance Using Grease as Interstitial Material [K/W]
$R_p(0)$	=	Dynamic Resistance at 0 Bias Voltage [Ω/cm]
R_m	=	TEC Electrical Resistance [Ω]
S_m	=	TEC Effective Seebeck Coefficient [V/K]
K_m	=	TEC Thermal Conductance [W/K]
S/V	=	Specific Surface Area [cm^{-1}]
V	=	Voltage [V]
I	=	Current [A]
T	=	Local Temperature [K]
$\overline{T}$	=	Average TEC Temperature [K]
T_{max}	=	Maximum Temperature [K]
T_{min}	=	Minimum Temperature [K]
T_a	=	Ambient Temperature [K]
T_i	=	Temperature at Junction i (i = 1, 2, 3, etc.) [K]
T_h	=	Temperature at TEC Hot Side [K]
T_c	=	Temperature at TEC Cold Side [K]

T_{bc}	=	Temperature at Heat Sink Base Center [K]
T_b	=	Temperature at Heat Sink Base Edge [K]
$\overline{T}_{\mathrm{h}}$	=	Average TEC Hot Side Temperature [K]
$\overline{T}_{\mathrm{c}}$	=	Average TEC Cold Side Temperature [K]
$\overline{T}_{\mathrm{f}}$	=	Average Heat Sink Fin Temperature [K]
$\overline{T}_{\mathrm{b}}$	=	Average Heat Sink Base Edge Temperature [K]
T_d	=	Surface Temperature of Target Cooling Zone [K]
$T_{b,max}$	=	Maximum Heat Sink Base Temperature [K]
$T_{pw,e}$	=	Heat Pipe Temperature at Evaporator – Wick Interface [K]
$T_{pw,c}$	=	Heat Pipe Temperature at Condenser – Wick Interface [K]
$T_{v,e}$	=	Vapor Temperature at Evaporator [K]
$T_{v,c}$	=	Vapor Temperature at Condenser [K]
$T_{p,e}$	=	Heat Pipe Temperature at Evaporator Wall [K]
$T_{p,c}$	=	Heat Pipe Temperature at Condenser Wall [K]
T_∞	=	Ambient Temperature [K]
r_i	=	Inside Radius of Heat Pipe [cm]
r_o	=	Outside Radius of Heat Pipe [cm]
L	=	Length [cm]
W	=	Width [cm]
k	=	Material Thermal Conductivity [W/cm K]
V_B	=	Barrier Height [m]
V_{max}	=	Maximum Voltage [V]
Z	=	Figure of Merit [1/K]
$\mathrm{Z}\overline{T}$	=	Dimensionless Figure of Merit

GREEK

α	=	Material Seebeck Coefficient [V/K]
ΔT	=	Temperature Difference Across TEC [°C]
ΔT_i	=	Temperature Difference Across TEC for Configuration i [°C]
ΔT_{max}	=	Maximum Temperature Difference Across TEC [°C]
$\Delta T_{operational}$	=	Temperature Difference Between TEC Hot and Cold Side [°C]
$\Delta T_{ambient}$	=	Temperature Difference Between Ambient and TEC Cold Side [°C]
$\Delta \upsilon$	=	Bandwidth Frequency [Hz]
σ	=	Material Electrical Conductivity [1/ Ω/cm]

"All truths are easy to understand once they are discovered; the point is to discover them."

- ***Galileo Galilei***

Chapter 1 – Introduction

Heat is an unavoidable by-product of all power operated electronics. As electric current flows through the components heat is released due to the inherent resistance to this flow within the component materials. Basically, the heat that is generated is similar to the heat generated from friction. As the electrons travel through the various conductors, they collide with other particles transferring their kinetic energy to heat. Over time, the buildup of heat can lead to reduced electronic device performance and malfunction or even outright device failure. Other sources of heat generation include core losses in inductors and transformers, increased resistance for high frequency signals due to the skin effect and switching losses in transistors. Switching losses arise from short periods of high power loads passing through transistors as they constantly switch between on and off states. The switch from on to off and vice versa in transistors is very rapid and thus heat generation from switching losses only becomes significant at high switching speeds resulting from being in a constant state of peak power transmission. In most integrated circuits (IC), 70 - 90% of the heat generated is via switching losses [Burris – 2015].

Reliability and safety are the main driving factors for thermal management in electronics. Since heat concentrates at junctions within the IC, a maximum junction temperature is usually designated by the manufacturers (typically 150°C). Exceeding the maximum junction temperature can lead to excessive heat buildup resulting in fire or combustion within the electronic component. Even if the device can be operated safely at high temperatures, the operating junction temperature is known to have a significant impact on the life and reliability of the component. The general rule of thumb is that for every 10°C drop in operating junction temperature, the life of the component doubles [Burris – 2015]. This is particularly important for continual-use devices such as cell phones and laptops. Most highly complex, highly functional modern-day electronics applications require some form of thermal management to regulate heat dissipation and maintain operating temperatures at or below safe levels for reliable performance.

As the complexity of our electronic systems grow, there will be additional heat sources and regions requiring cooling that must be managed. It is projected in Fig. 1.1, that by the year 2020,

the computing power per second of electronics will equal that of a human brain and all human brains combined by the year 2050.

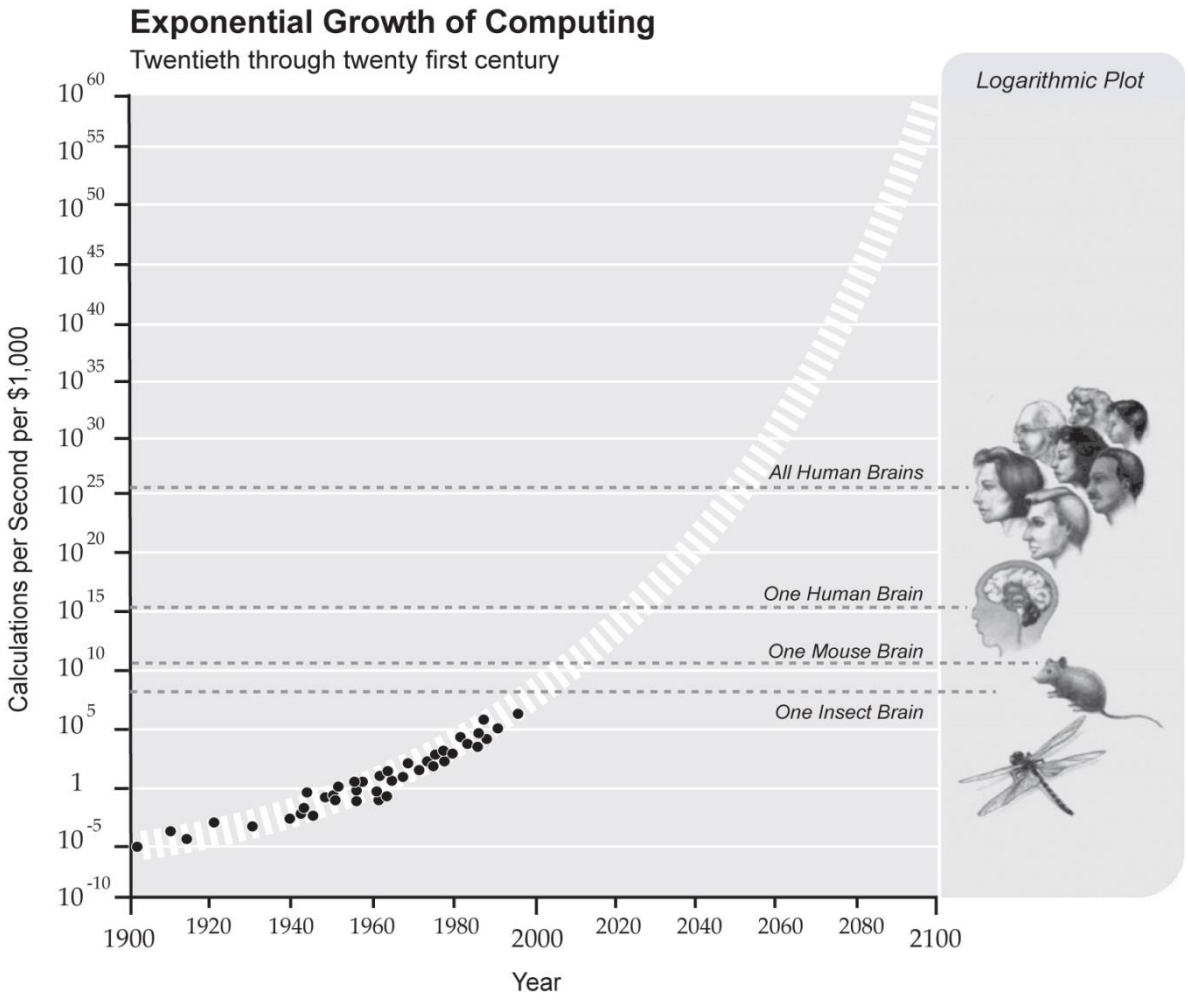

Figure 1.1: Projected Growth in Computing Power [Adapted From: Kurzweil – 2005]

As this complexity and computing power continues to grow, so will the need for cooling and thermal regulation of the component systems. Standard bulk heat transfer techniques are inefficient and provide limited localized control. By developing active cooling techniques, one will be able to target specific structures on various electronic platforms that need cooling. By focusing on only those structures requiring cooling, one will gain significant flexibility and efficiency in heat management. This will allow higher performance solutions with reduced size, weight and power requirements in the future.

Typically, these cooling strategies are utilized to cool hot surfaces often present in central processing units (CPUs) and related electronic components. Some applications, such as in optoelectronic switches and spectrometers, have the added requirement that temperatures must be regulated to operate within a very narrow range to ensure that operating specifications are achieved to precise tolerances. In special cases, as is discussed in this thesis, sub-ambient cooling is highly desirable in order to improve electronic device performance. For example, detector assemblies in spectrometers are highly sensitive to temperature fluctuations and this can cause a low signal-to-noise data response. Other devices such as light emitting diodes (LEDs) and fuses also respond to increased temperatures in a manner that reduces the component lifetime [Wilcox – 2011]. Therefore, adequate thermal design consideration is critical in the product development stage and novel methods of cooling that are scalable are most desirable.

Electronic cooling components such as micro-heat sinks have been shown to provide effective cooling for integrated circuits (ICs) [21, 24, 26, 29, 52, 58]. A review of available literature has shown effective temperature control using these components separately, and to a lesser extent, using configurations containing multiple approaches (thermoelectrics and advanced heat sinks for example). However, little data are available for sizing thermal management packages focusing on shrinking the overall device footprint without sacrificing performance. Of particular interest is sub-ambient cooling directly at the surface of electronic devices. Few experiments have focused on sub-ambient surface-level cooling which is critical for equipment such as spectrometers and photodetectors. This suggests that more experimental data of multi-component cooling strategies are needed to leverage the advantages and demonstrate reliable localized cooling on a smaller scale.

This work will examine the feasibility of using thermoelectric devices and auxiliary components, such as heat sinks, in an active cooling configuration designed to achieve temperature stability at the surface-level. Experiments will focus on key parameters such as stable device surface temperature, heat sink surface area, rate of heat dissipation (heat flux) and power input requirements. The methodology involves the examination of the thermal resistance network established between the heat source within the electronic component and the cooling medium. All relevant thermal resistances will be quantified for the purpose of determining which resistive

paths control heat flow and which are secondary. It is only through an assessment of this nature that an effective thermal optimization can occur, allowing operating temperatures to be controlled in a safe and effective manner.

By combining the advantages of the various available cooling strategies, effective thermal management can be achieved. The applications for such a technology can range from telecommunications and automotive to medical as well as many other industry sectors. A brief examination of the cooling requirements for integrated circuits will help in the assessment and production of an effective thermal management strategy.

1.1 Thermal Management of Integrated Circuits (ICs)

Integrated circuits are found in many products around the world and in many different sectors of the economy. As the years progress, more and more complex circuits necessitate the need for enhanced thermal management techniques.

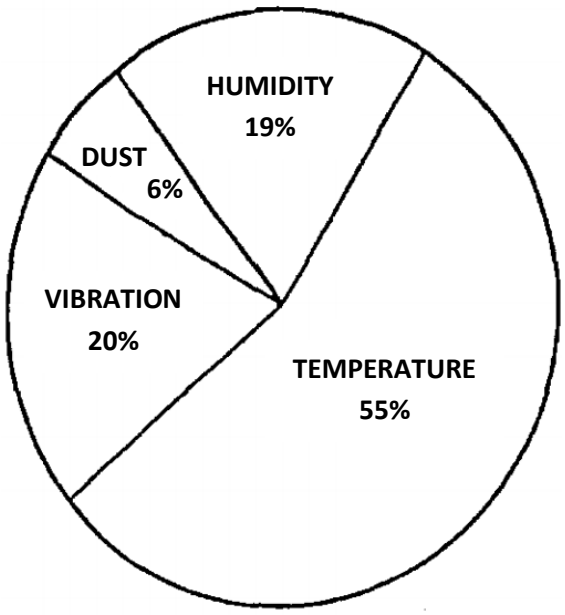

Figure 1.2: Primary Causes of Circuit Failure
[Adapted From: Yeh – 1995]

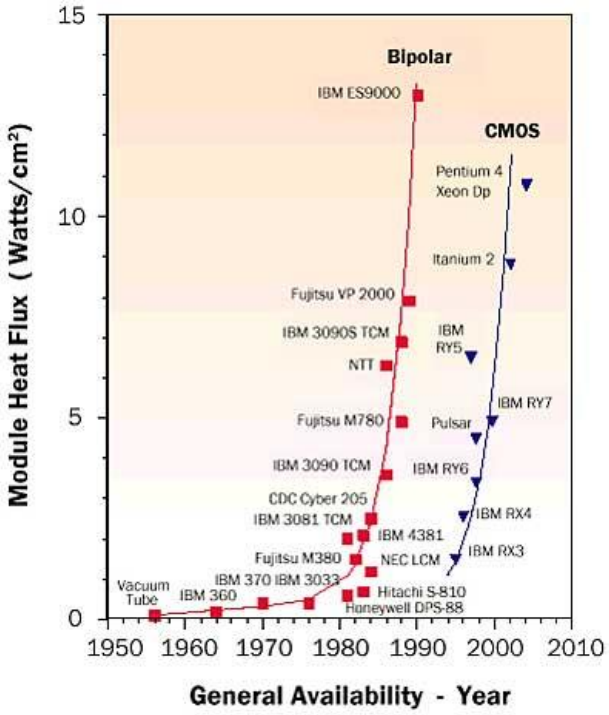

Figure 1.3: CPU Heat Flux Progression
[Adapted From: Ellsworth – 2005]

As evidenced by Fig. 1.2, it is reported that more than 50% of all electronics failures are directly or indirectly related to temperature [Yeh – 1995]. Also, with increasing power densities of CPUs, as seen in Fig. 1.3, one would expect the heat dissipation requirements to increase accordingly. This trend is not new as can be seen with the surge of heat flux in bipolar circuit technology in the early 80's and then again in the mid 90's [Ellsworth – 2005]. In fact, Moore's law predicts that the number of transistors in CPUs will double every 2 years. As shown in Fig. 1.4, this is a trend that has continued in a predictive manner for the past 40 years.

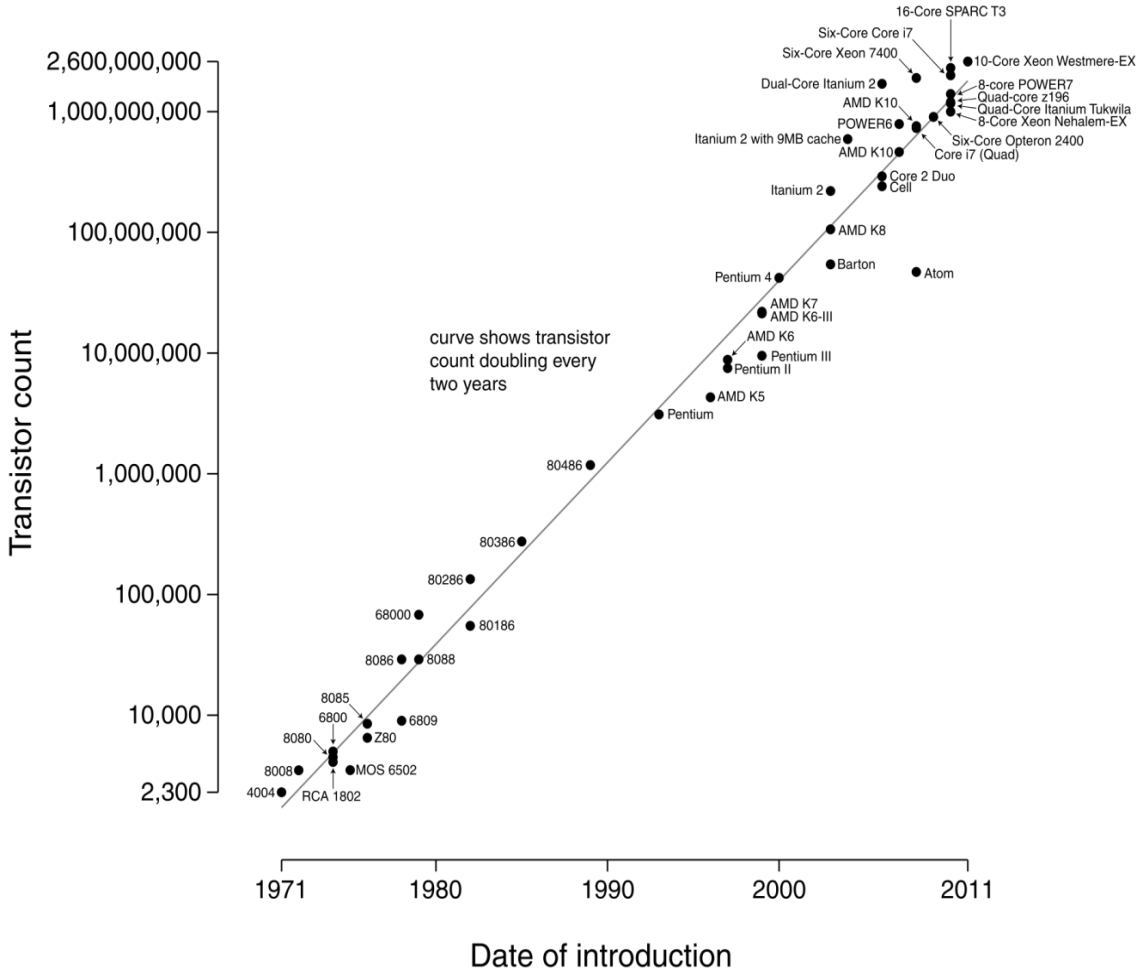

Figure 1.4: CPU Transistor Count Timeline [Adapted From: Wgsimon – 2011]

This has prompted the discussion about the limits of conventional cooling methods and the viability of new innovative thermal management strategies for high heat flux applications.

To better understand heat flow through electronic components one must refer to Fourier's Law. Considering a plate as seen in Fig. 1.5 with adiabatic conditions at the edges (one-dimensional heat flow), Fourier's Law states that the time rate of heat transfer (Q) through a material of thickness (z) is proportional to the negative gradient in the temperature (ΔT) and to the cross-sectional area (A), at right angles to that gradient through which the heat flows.

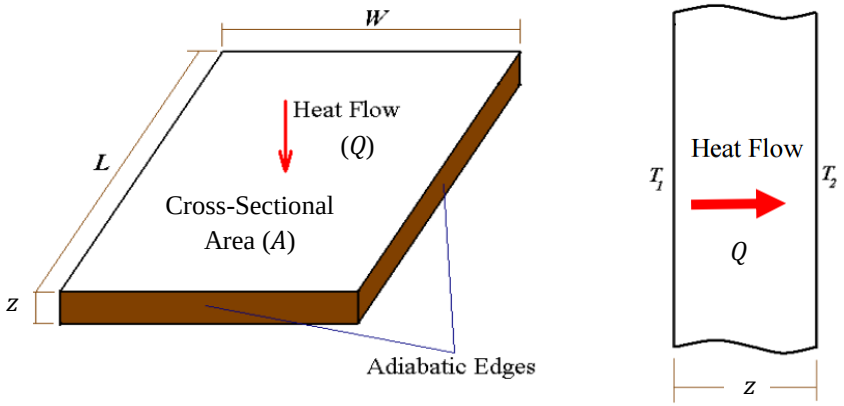

Figure 1.5: One-Dimensional Heat Flow through a Plate [Adapted From: Sparrow – 2010]

The relationship between the heat flux (q) and device temperature is stated in Eq. (1.2).

$$Q = -kA\frac{\Delta T}{z} \tag{1.1}$$

$$q = \frac{Q}{A} = -k\frac{\Delta T}{z} \tag{1.2}$$

Thus the heat flux in W/cm^2 is determined by the material thermal conductivity k in W/(cm K), the temperature gradient across the device ΔT in K, and the thickness of the device z in cm. With respect to thermal management in integrated circuits, the heat flux or the heat dissipation rate is a critical performance metric. A CPU requires a heat dissipation rate of 120 – 150 W on a 1 cm square wafer [Upadhya et al. – 2004]. In the past, a heat dissipation rate of 100 W/cm^2 provided sufficient cooling in most cases but future heat dissipation requirements are expected to range up to 300 W/cm^2 [Thome – 2006].

There are two primary reasons for the increase in heat flux in CPU's: the speed of information relay and the number of gates on the chip. A little more than a decade ago, a 0.18 μm component size appeared to be a limiting factor in CPU design [Azar – 2000]. Today, geometries down to 20 nm are becoming the standard or even outdated as seen in Fig 1.6.

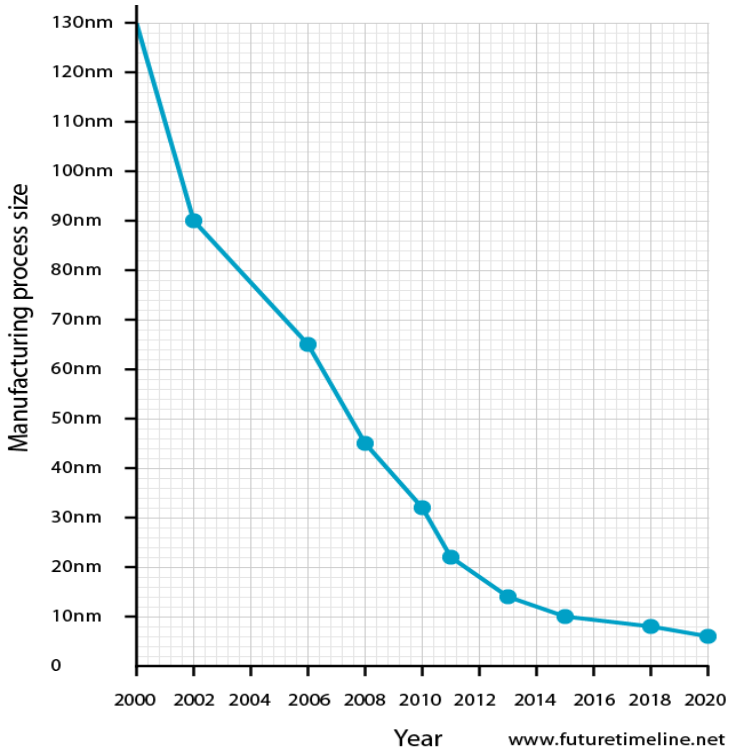

Figure 1.6: Microchip Transistor Size Timeline [Adapted From: Futuretimeline.net – 2012]

Figure 1.6 illustrates the decline in microchip component sizes for various products with no significant sign of a plateau. If the assumption is made that the lower limit of part size is on the atomic scale, then it appears that the above trend will continue until at some point the limit will switch to the manufacturing and fabrication of such devices. Therefore, if part sizes continue to trend downward and the power levels of electronics increase or even remain the same, the localized heat flux increases and heat dissipation becomes a more important issue.

CPUs and similar electronic components tend to heat up rapidly when in continuous use and require cooling to prevent overheating. Although, it is generally not the transient response that is the problem but the elevated temperatures over a long period of time that can lead to issues of reliability. In other instances where device overheating may not be a concern, it is still desirable to cool some electronic components below ambient temperatures due to resulting effects on overall device performance and in particular, the speed of information relay [Wolpert and Ampadu – 2012]. There are many situations where this is the case such as in spectrometer equipment where a reduction of detector temperature yields a higher quality of spectral data or in

refrigeration applications where sensitive materials like food and medical samples need to be kept in a sub-ambient environment for a prolonged period of time. Thus, it is important for a robust thermal management configuration to be able to achieve sub-ambient cooling for a prolonged period to demonstrate reliability and versatility if necessary.

Finally, not only are electronic devices shrinking in size as noted previously, they are also becoming more and more portable over time. The era of ultrathin laptops, tablets, and smartphones may indicate a shift in consumer preference from strict performance to include convenience through portability. Hence, a slim stand-alone thermal management configuration is surely preferential and provides many advantages over conventional bulky heat sink schemes. This portability factor provides yet another challenge when attempting to design a thermal management configuration that can suit many electronic applications.

Keeping in mind these factors, an assessment of the various existing thermal management technologies is carefully reviewed in order to determine the most appropriate solution.

1.2 Thermal Management Technology

Many cooling techniques are available for use but their utility depends largely on the application in question and the limitations specific to each case (i.e. geometry, power requirements, temperature constraints, noise constraints, etc.). A multi-component configuration approach is more likely to be selected rather than any individual technique due to advantages and disadvantages of each proposed technology.

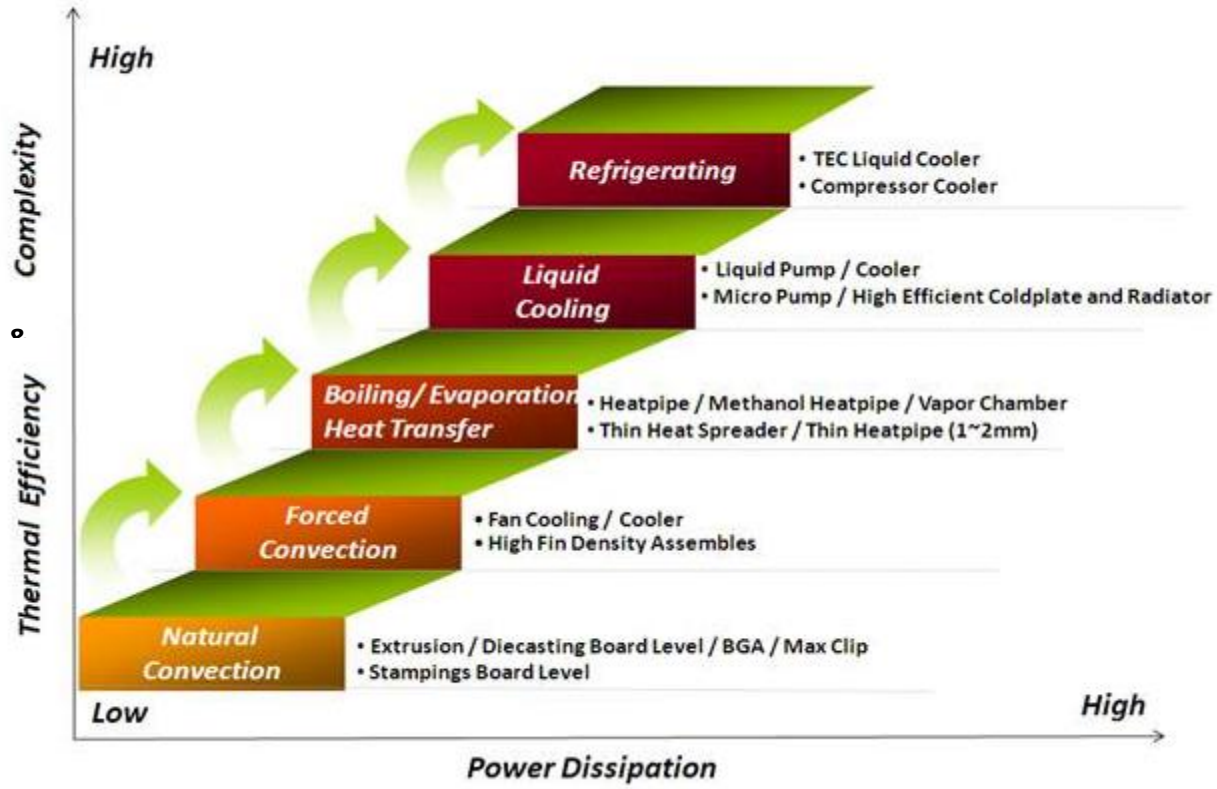

Figure 1.7: Relative Power Dissipation of Various Cooling Technologies
[Adapted From: Asia Vital Components – 2010]

Figure 1.7 displays the common approaches to thermal management in terms of their relative dissipative capacities and increasing efficiency and complexity. A closer look at each technology, highlighting the advantages and disadvantages, can be used to determine an optimal configuration based on key criteria (operating conditions, size, etc.).

1.2.1 Natural and Forced Air Convection Cooling

Natural convection is on the lower end of the heat dissipation spectrum and is typically used in applications where simplicity is required and/or a secondary power source is not available. Although natural convection applications may involve the use of advanced finned heat sinks, they essentially rely heavily on environmental conditions such as temperature gradients, which lead to buoyancy effects, as well as surface orientation to aid in cooling. In natural convection, fluid motion across the desired area occurs through natural means and density changes in the transfer medium resulting from thermal gradients leading to fluid buoyancy. Since the fluid velocity associated with this cooling approach is rather low (less than 1 m/s in electronic applications), the heat transfer rate encountered is also quite low, typically an order of magnitude lower than observed in most forced convection applications [Tada – 2002]. However, in forced convection cooling, a steady supply of convective air flow (produced externally) can provide up to 50 W/cm^2 of heat dissipation depending on the available surface area exposed for convection [Lasance – 2005].

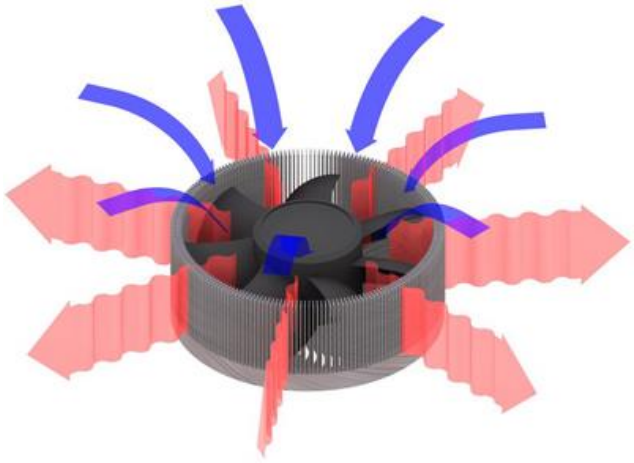

Figure 1.8: Fan & Fin Heat Sink [Adapted From: Domingo – 2011]

Figure 1.8 illustrates a fan and heat sink configuration designed to dissipate heat radially through carefully spaced metallic fins. The amount of heat dissipated is a function of the air temperature, fin material properties (thermal conductivity), exposed surface area of the fins and the speed of air flow around the fins. An advantage of forced convection over natural convection is the ability

to position the fan and cooling solution in any orientation independent of the gravity vector (which is a prerequisite for buoyancy driven flow). A drawback of this active cooling approach is that it will require input power as well as the inclusion of moving mechanical parts, potentially introducing vibration as well as gradual wear and tear over time.

1.2.2 Heat Pipes

Heat pipes are classified as passive cooling components that utilize a working fluid to carry away heat from the source and transfer it over the length of a pipe to a secondary cooling component required to actually dissipate the heat (i.e. heat sink). The fluid is returned via a wick structure within the pipe that drives the fluid back to the source to complete the loop using capillary forces. Many different geometries and lengths of pipe can be used but for the sake of simplicity, Fig. 1.9 illustrates a single straight heat pipe along with the mechanism of heat transfer.

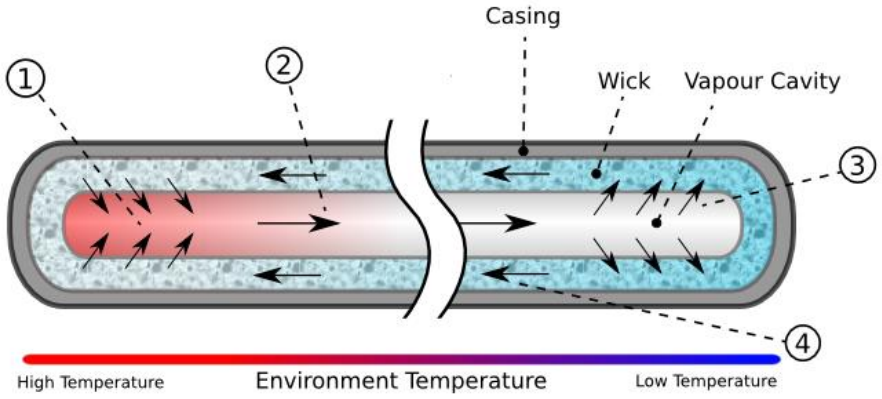

Figure 1.9: Heat Pipe Cross-Section [Adapted From: van Es and van Gerner – 2013]

The working fluid in liquid phase is heated up in section 1 via sensible heating until the fluid approaches the boiling temperature at the local vapor pressure. At a fixed temperature, the fluid begins to evaporate leading to a mixed phase in section 2 (evaporator end). The vapor phase flows toward section 3 at a constant temperature carrying the latent heat of vaporization that was absorbed in sections 1 and 2. The heated vapor then begins to condense in section 3 (condenser end) thereby transferring the heat to the surroundings. Heat pipe configurations, on average, dissipate 100 W/cm^2 with heat flux rates up to 300 W/cm^2 made possible with assembly upgrades [Lasance – 2005]. Although there is potential for a high heat transfer rate, it is

important to note that the effectiveness of a heat pipe is a function of pipe length, quality of wick structure (liquid return rate), condenser temperature (liquid condensation rate) and the contact resistance at both the evaporator and condenser sections. If the pipe is too short, it may require fans and other heat sinks to aid in heat dissipation to ensure that the working fluid does not completely vaporize inside the pipe causing a "dry out" condition and pressure build up.

1.2.3 Liquid Cooling

There are several different liquid cooling techniques that have been investigated in the past. The most popular methods being immersion cooling, spray cooling, and microchannel cold plate cooling. In immersion cooling (or pool cooling), the target device is actually submerged in a dielectric liquid causing vapor bubbles to form in the liquid pool upon sufficient heating. These bubbles rise to the liquid surface where they are cooled and condensed back into liquid form similar to condensation in a heat pipe. Heat dissipation rates of up to 100 W/cm^2 are possible using this method with the obvious drawback being the necessity of a dielectric liquid that is compatible with the target device. In most cases water cannot be used due to its chemical and electrical properties [Lasance – 2005]. Figure 1.11 illustrates an immersion cooling setup.

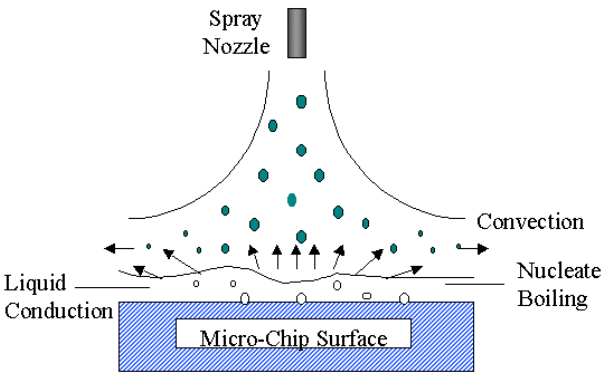

Figure 1.10: Spray Cooling Diagram
[Adapted From: Silk – 2004]

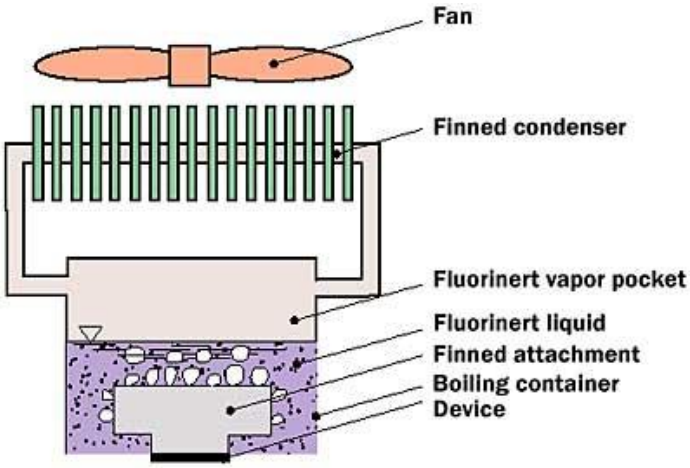

Figure 1.11: Immersion Cooling Setup
[Adapted From: Lasance – 2005]

Spray cooling methods also involve direct liquid contact with the target device, all be it in the form of a mist that vaporizes immediately after contact. Nucleate boiling occurs rapidly and heat is carried away as a result of convection. Heat dissipation rates greater than 270 W/cm^2 have been reported using this approach. Disadvantages here include the need for a high pressure spray nozzle as well as a constant supply of liquid coolant [Lasance – 2005]. Figure 1.10 demonstrates spray cooling of a micro-chip surface.

Cold plate cooling is a form of active cooling that involves pumping a liquid coolant through a metal plate that carries heat away from the target device in a loop-like fashion. The inlet contains virgin coolant that is at a desired preset temperature and the outlet is liquid that is at a higher temperature due to heat transfer from the heat source. Figure 1.12 illustrates several schemes.

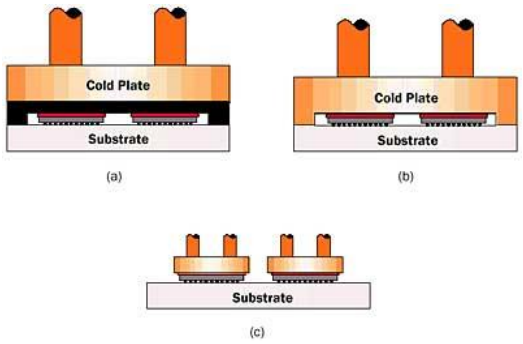

Figure 1.12: (a) Separable Cold Plate Cooling (b) Integrated Cold Plate Cooling
(c) Individual Cold Plate Cooling [Adapted From: Ellsworth – 2005]

In scheme (a) the cold plate is detachable from the target devices with an inlet and outlet stream. In scheme (b) the cold plate is merged with the devices as a bulk module and in (c) each target device is equipped with its own cold plate component. Standard cold plate cooling methods report a heat dissipation rate of approximately 400 W/cm^2 [Ellsworth – 2005]. However, experiments involving the use of microchannels in the cold plates demonstrate heat flux capabilities of 790 W/cm^2 [Tuckerman and Pease – 1981]. With recent advancements in fabrication techniques and enhanced technology, heat dissipation rates as high as 1300 W/cm^2 have been reported [Lasance – 2005]. The advantages here include leveraging both a higher surface area and two-phase flow to obtain these higher heat fluxes. On the downside, there may

be a high pressure drop associated with the fluid flow and a certain amount of input energy required for fluid pumping.

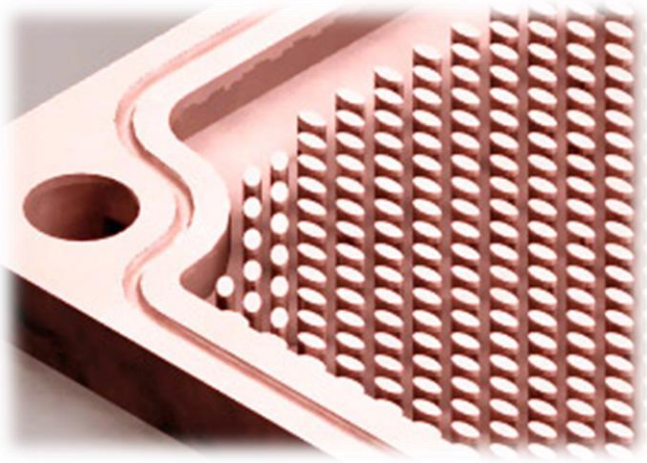

Figure 1.13: Microchannel Cold Plate
[Adapted From: Frostytech.com – 2010]

Various geometries have been investigated and each presents its own challenge regarding heat transfer and fluid flow. Georgia Tech previously developed a novel method of fabricating microchannels directly onto the backs of integrated circuitry designed to cool at the source, although this method has not been fully embraced by the electronics industry [Toon – 2005].

1.2.4 Solid-State Thermoelectric Cooling

A thermoelectric Peltier cooler (TEC) is another active cooling strategy that has been recently adopted for use in thermal management of electronics. The concept was first invented in 1834 by French physicist Jean Charles Athanase Peltier who discovered that running an electric current through two dissimilar metals can pump heat from one area to another. This was the reverse of the Seebeck effect which describes the generation of an electric current through two dissimilar metals in the presence of a thermal gradient [MacDonald – 1962]. The Peltier effect is demonstrated graphically below in Figures 1.14 and 1.15.

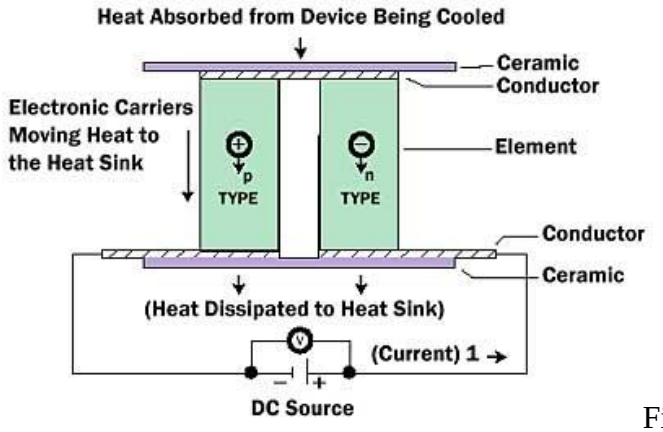

Figure 1.15: Schematic of Peltier Cooler (1 p-n Junction) [Adapted From: Lasance – 2005]

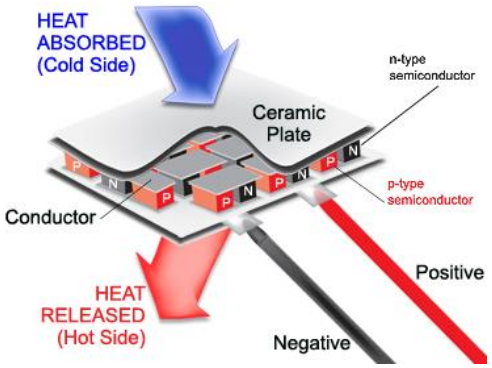

Figure 1.14: Thermoelectric Device Breakdown [Adapted From: Buyincoins.com – 2014]

The dissimilar metals are referred to as "p" and "n" types depending on which charge carriers are transferring the heat and are setup in a junction. When current is applied through the junction it causes a flow of electrons (negatively charged) in one direction and "holes" (positively charged) in the other. This flow also results in the absorption of heat at the cold side which is then ejected at the hot side. The thermoelectric device is comprised of several of these p-n junctions connected together in series and/or parallel as seen in Figure 1.14. The junctions are sandwiched between electrically conducting surfaces to complete the circuit and attached to the external non-conductive ceramic contact surfaces. This results in a device with a thin profile (mm in thickness) that can be used in various applications where small form factors are ideal [MacDonald – 1962]. Thermoelectric device performance is quantified by its figure of merit ($Z\bar{T}$) as defined in Eq. (1.3)

$$Z\bar{T} = \frac{\alpha^2 \sigma}{k}\bar{T} \tag{1.3}$$

where α is the material Seebeck coefficient, σ is the material electrical conductivity and k is the material thermal conductivity. For over 40 years the value of the figure of merit has been 1 or lower though advancements of thin film nano-materials has allowed values greater than 2 to be achieved [Mayer and Ram – 2006]. However, the figure of merit alone is not indicative of the performance capability of the thermoelectric device. Heat dissipation at the hot junction is

critical in determining the feasibility and efficiency of the device in any application. Simple TECs can dissipate 160 W/cm^2 and possibly up to 800 W/cm^2 by upgrading to a superlattice structure and reducing the device size [Lasance – 2005]. Figure 1.16 demonstrates this potential as a function of the input current required.

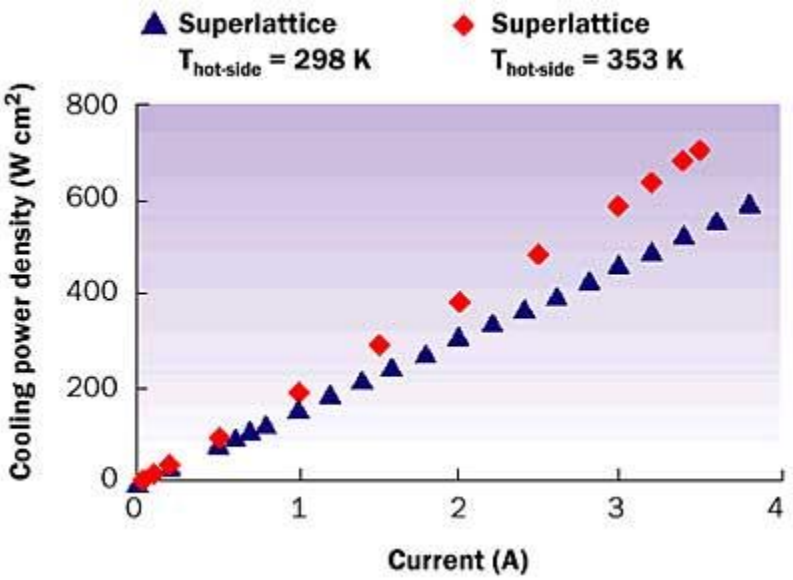

Figure 1.16: Estimated TEC Heat Flux as a Function of Current
[Adapted From: Lasance – 2005]

Table 1.1 shows a comparison of the TEC-based cooling approach against the other methods mentioned previously in the key areas of interest.

Table 1.1: Technology Comparison

Cooling Method	Size	Performance	Stability	Portability	Total Favourable Score
Natural Convection	Acceptable	Insufficient	Environmentally Driven	Acceptable	2/4
Forced Convection	Acceptable	Insufficient	Acceptable	Acceptable	3/4
Heat Pipes	Requires a Minimum Length	Insufficient	Acceptable	Acceptable	2/4
Liquid Cooling	Bulky	Acceptable	Acceptable	Not Practical	2/4
TEC	Acceptable	Acceptable	Acceptable	Acceptable	4/4

Performance was deemed acceptable if the technology could provide sub-ambient cooling to some degree since it is a requirement for the intended application. Liquid cooling (cryogenic) and TEC cooling solutions currently provide the best forms of sub-ambient cooling as stand-alone systems. Heat pipes as well as natural and forced convection systems alone cannot provide significant sub-ambient cooling. Other factors include whether or not the eventual proposed cooling system will be portable and relatively easy to move from location to location as well as be small enough to fit reasonably into electronic device packaging. In this case, liquid cooling is not practical because it requires attachments to pumps and available liquid sources or holding tanks. TECs on the other hand, can easily be hooked up to a battery and occupy relatively little space. Heat pipes cannot be too small as mentioned previously due to the possibility of a pressure build up. Although a TEC requires some input power, the advantages can outweigh the disadvantages in an appropriate multi-component configuration as demonstrated in the previous instances. As a result, the effectiveness of a multi-component TEC-based cooling system will be the primary focus of this MASc. thesis while leveraging the advantages of some auxiliary components mentioned previously.

1.3 Motivation

There are two main motivations for conducting the proposed research. The first is to understand the fundamental road blocks to heat transfer in advanced cooling configurations through thermal resistance analysis and the second is the immediate demand or utility of these kinds of devices in industrial applications.

1.3.1 Thermal Resistance Analysis

In order to better understand the impediments to the overall heat transfer mechanism, it is necessary to analyze the thermal resistance at each stage of the process. This is typically done using a thermal resistance network analysis which is designed to mimic an electrical circuit with heat flow (Q) instead of current flow. The idea is to map the thermal gradient as the heat travels from point to point and quantify the thermal resistance along the path at each juncture. This way, it is possible to identify the key areas to focus on and those that are less significant.
Figure 1.17 below demonstrates a generic thermal resistance network for a common CPU cooling scenario.

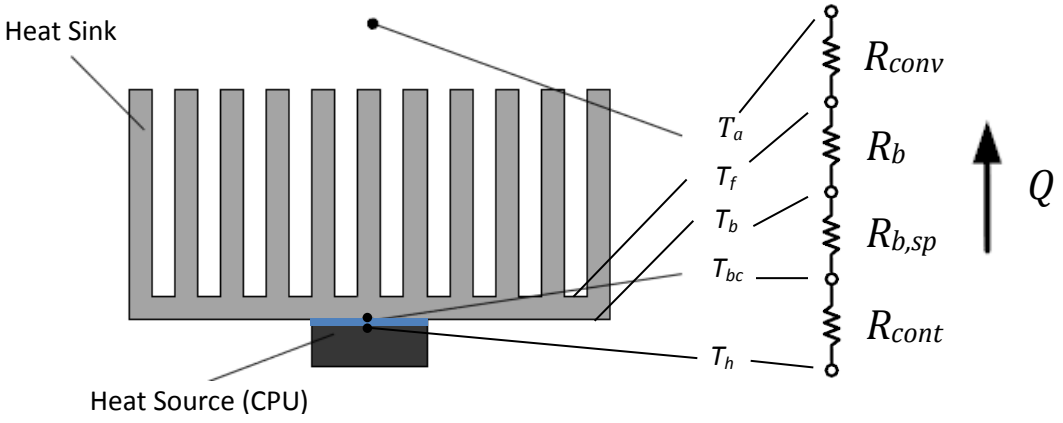

Figure 1.17: Thermal Resistance Network for CPU Cooling
[Adapted From: Chang et al. – 2007]

The resistance network is broken down into four main categories: contact resistance between heat source and heat sink base center (R_{cont}), spreading resistance from heat sink base center to

heat sink base edge ($R_{b,sp}$), conduction resistance from heat sink base to heat sink fins (R_b), and convection resistance from heat sink fins to the ambient (R_{conv}). Each of these contributes to the overall resistance and ultimately the heat flow observed. It is important to note that it is true that there are multiple resistance paths for each individual fin in the heat sink array but for the sake of simplicity the resistances have been lumped together for a total convection resistance.

Thermal resistance can be a function of many controllable parameters such as geometry, material properties, boundary conditions, etc. It is through the selection and control of these parameters that the designer can manage and control thermal issues, leading to improved reliability and better functionality. Knowing that $R_i = \Delta T / Q$, for a fixed value of Q, as the resistance goes down so too does ΔT. If the ambient temperature is roughly fixed, then the operating temperature of the source will go down in a linear manner. This thesis will investigate these resistances and quantify their effect on the overall heat flow of a TEC-based heat sink. Also, by examining these thermal resistances, the dynamic between heat sink surface area and heat flow can be analyzed in a similar fashion.

1.3.2 Applications of Interest

Passive cooling strategies have been used for some time now and have been sufficient for addressing heat transfer issues in electronic systems as noted earlier. However, the growth of computing power over time has highlighted the need for advanced cooling methods. In some cases, sub-ambient cooling is highly desirable and sought after. These applications include spectroscopy, detailed imaging, and refrigeration just to name a few. In spectroscopy for example, a detector is used to convert wave signals to data (known as spectra) that is processed further. The quality of spectra has been shown to be related to the detector temperature and the amount of noise generated in the data [21, 24, 40]. Figures 1.18 and 1.19 depict two different photodetectors and their relative sizes.

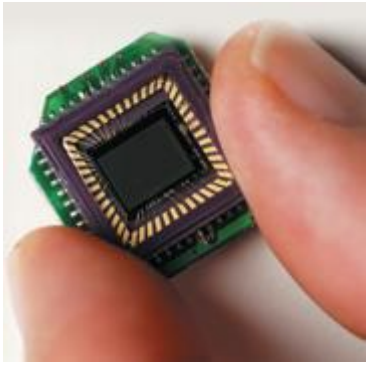

Figure 1.19: Photodetector Chip
[Adapted From: intechopen.com – 2012]

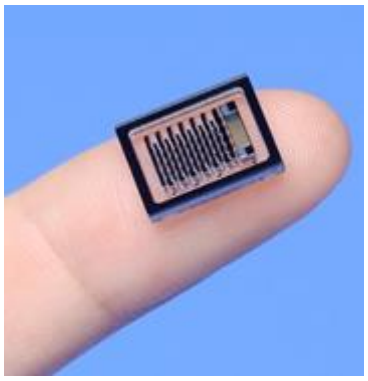

Figure 1.18: Micro-Photomultiplier Tubes (μPMT)
[Adapted From: hamamatsu.com – 2013]

These detectors are often sub-components in a larger instrument such as a spectrometer or camera. Cooling the detector components results in better system performance and a higher resolution in the acquired data. Also, as can be seen from Fig. 1.18 and Fig. 1.19, a bulky cooling configuration is not desirable or practical in this situation. Figures 1.20 and 1.21 are images taken by a cooled and uncooled thermal imaging camera of hand prints left on a wall after two minutes that demonstrates the quality difference in spectral data visually.

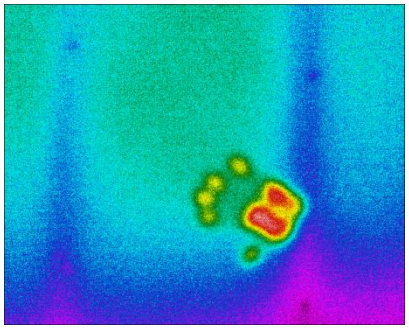

Figure 1.20: Thermal Image from Cooled Camera [Adapted From: flir.com – 2015]

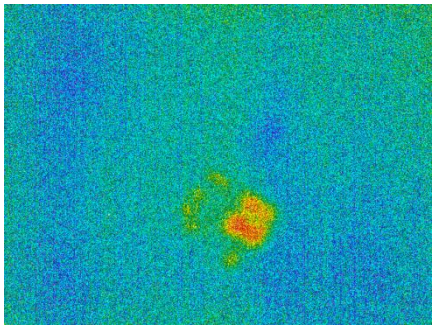

Figure 1.21: Thermal Image from Uncooled Camera [Adapted From: flir.com – 2015]

Clearly, the uncooled image displays significant distortion and noise when compared to the cooled image taken with the same camera. This sensitivity difference indicates that the cooled camera is able to perceive spectral data more precisely than its uncooled counterpart. Therefore it is of paramount importance that the detector temperature of such systems be cooled at a reliable and adequate level in order to provide a higher signal-to-noise ratio in photodetector systems.

However, sustained cooling for how long is considered reliable? What degree of cooling is adequate? What kind of limitations, such as device size and portability, are present? These questions are addressed to a greater extent in Chapter 2 in order to provide a framework that can be used as a basis for the research.

1.4 Summary

As the trend in electronic systems moves in the direction of higher power densities the need for a stand-alone cooling method with minimal liabilities increases. In the past a heat dissipation rate of 100 W/cm^2 was sufficient but modern heat dissipation demands involve heat fluxes up to 300 W/cm^2 and higher. Although strict heat dissipation of hot objects is important, in some industrial applications, localized sub-ambient cooling is highly preferential, such as in spectrometer equipment. As a result, localized sub-ambient cooling will be the main focus of this thesis.

Thermoelectric devices (TECs) and other electronic cooling components such as micro-heat sinks have been shown to provide effective cooling for integrated circuits (ICs). A brief overview of previously researched cooling methods has been presented along with the associated advantages and disadvantages. The ability to provide localized sub-ambient cooling was the main performance characteristic used to determine the most suitable technology to be optimized. For this reason, a TEC-based multi-component thermal management configuration is of particular interest for further investigation. Other forms of cooling were considered too bulky or non-portable and did not provide sufficient cooling to be considered viable. The TEC-based design was selected after careful review and evaluation of available cooling technologies via a comparison chart.

Several key factors are considered in this multi-component approach and will be emphasized in this document. Sub-ambient cooling performance, temperature reliability / stability and form factor (size) reduction are among the top parameters that will be addressed. Optimization of the vital parameters will be conducted at each stage of the development in order to demonstrate a proof of concept. A look into input power requirements and other similar factors will be noted. Resistance mapping of the thermal gradient across a TEC-based heat sink will guide the evaluation and determine areas of primary focus and those that are less significant. Experiments will be geared in this direction in order to demonstrate the feasibility of TEC-based thermal management schemes for future portable electronic devices.

Thermoelectric coolers have been successfully used in various applications and are of particular use in the spectrometer industry and specifically in detector assemblies. This demonstrates a potential opening in the market for broader use of TEC-based thermal management schemes.

A review of the thermal management demands of this industry sector is presented in the literature review section in order to provide a benchmark for the performance criteria. This is followed by the design of experiments used to assess the feasibility of the TEC-based cooling systems in the main criteria as previously discussed. The results are also analyzed and compared to those found in the literature. Final conclusions and recommendations are given at the end that suggests ways to improve upon the designs proposed in this thesis.

Chapter 2 – Literature Review

The following literature review is intended to outline previous research conducted in regards to TEC-based thermal management and give a brief overview of the various applications in which the technology is used. An order of magnitude assessment of the thermal resistances involved is conducted in order to simplify and target a specific area for improvement. However, there will be added emphasis on sub-ambient cooling in the nanophotonics and spectroscopy industries which are the applications of particular interest. Some background in this field of research is provided in order to better understand the market for sub-ambient thermal management.

2.1 Nanophotonics and Spectroscopy

Nanophotonics, in general, refers to the study of the behaviour of light (photons) in the nano-scale. This branch of science has progressed due to the ability to fabricate equipment on the nanometer scale and involves two main categories of interest; studying the properties of light in the nanometer scale and enabling efficient devices for use in engineering and related applications [Prasad – 2004].

On the other hand, spectroscopy is the study of the interaction between matter and radiated energy. Traditionally, spectroscopy involves experimentation using visible light, although it has since expanded vastly to include any interaction with radiated energy of any form (i.e. sub-atomic particles, sound waves, etc.). Devices used to conduct such experiments are commonly referred to as spectrometers and they produce spectral data (interaction response as a function of wavelength or frequency) for analysis [Yadav – 2005]. Spectrometers can be used for all sorts of applications but a common use is in the area of high resolution imaging. For example, hyperspectral imaging can be used to map geological features of a rock formation or identify toxic chemicals in exhaust gas releases [Chamberland et al. – 2005].

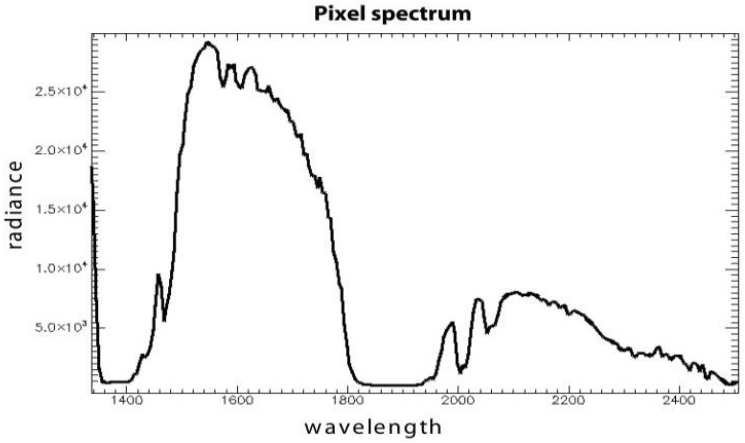

Figure 2.1: Spectral Data from Hyperspectral Imaging of Geological Features (Rock Face) [Adapted From: Virtual Outcrop Geology Group – 2014]

Figure 2.1 demonstrates results produced using the hyperspectral imaging technique whereby a pixel spectrum is also analyzed by the spectrometer. More information regarding spectral imaging will be provided in the next section as it pertains to the target application of the proposed research.

Combining the two subject areas into one we get Nanophotonic Spectroscopy, which by extension means the study of the interaction between photons and matter at the nano-scale. This field of research is specifically used in the development of advanced imaging devices with very high resolutions. The literature review will focus on thermal management issues facing the nanophotonics imaging industry as well as a review of the solutions available to date.

2.1.1 Optical Coherence Tomography (OCT) Imaging

Optical Coherence Tomography (OCT) is a signal acquisition method which uses near-infrared light to produce 2-D (cross-sectional) and even 3-D images inside a desired scattering medium or sample. In OCT, light is scattered through a sample and the reflected light is captured and processed further to produce the final image, very similar to ultrasound techniques which use sound waves instead of light. Below is a typical OCT configuration diagram that displays the process and its various components [Tornado Spectral Systems – 2013].

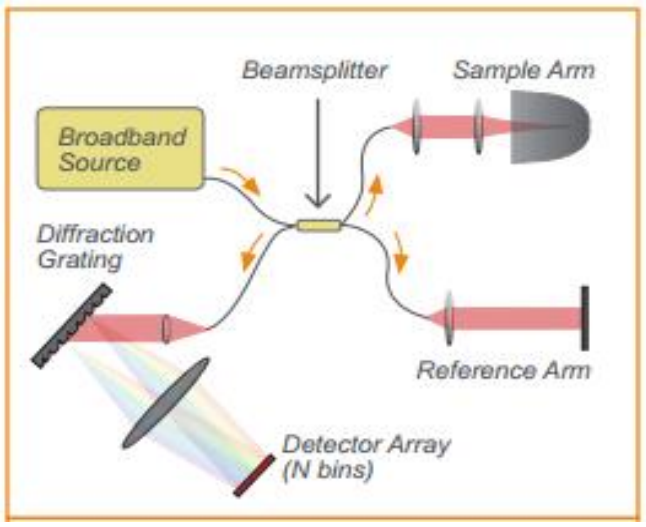

Figure 2.2: SD-OCT System Schematic [Adapted From: Tornado Spectral Systems – 2013]

As depicted in Fig. 2.2, the scattered rays are re-collected at the detector array which is actually where the spectrometer is positioned. From there the data are processed further and the image is sent to the display screen. Figures 2.3 and 2.4 are examples of the final images produced using the OCT technique in both 2-D and 3-D respectively.

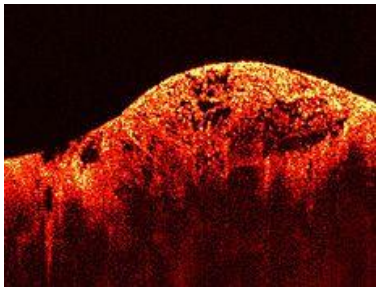

Figure 2.3: 2-D OCT Image of Sarcoma Cancer [Adapted From: Boppart – 2007]

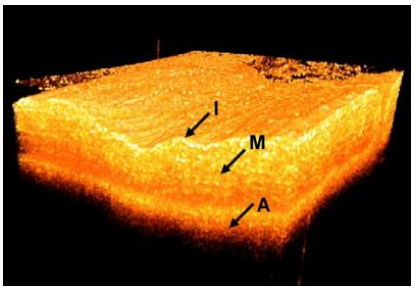

Figure 2.4: 3-D OCT Image of in Vitro Porcine Artery Wall [Adapted From: Thorlabs – 2014]

The quality of the images generated is determined to a great extent by the level of interference or noise associated with the incoming signal. At the detector, it is critical that interference and noise is reduced to a minimum to obtain the highest quality spectra for analysis and ultimately sharp and precise images. Thus detector noise, otherwise known as dark noise or dark current will be the subject of the next section.

2.1.2 Dark Current and Noise in Photodetectors

As mentioned in the previous section, photodetectors and spectrometers process signal data from incoming light and relay that information downstream to be displayed or analyzed. However, not all of the data results from the detection of scattered light (through the sample) and some interference from other sources should be expected in any photonic experiment. One such form of interference is referred to as dark noise or dark current.

Dark current refers to a relatively small electric current that is generated within photosensitive devices even when there is no light entering the detector. It is the result of random electrons and holes generated within the depletion layer of a device that are then swept by the high electric field. The rate of charged particle production leading to dark current flow is related to the defects present in the material composition of the detector or device layer and the device temperature [Janesick – 2001]. For example, a typical photodiode produces dark current according to Eq. (2.1).

$$I_N = \sqrt{\frac{4KT\Delta v}{R_P(0)}} \tag{2.1}$$

where I_N is the dark current produced, K is Boltzmann's constant, T is the temperature of the device, Δv is the bandwidth frequency and $R_p(0)$ is the dynamic resistance of the diode at 0 bias voltage. It is clear that the dark current will be reduced in proportion to the square root of the temperature as the device temperature is reduced [Kleinfeld – 1979].

Physically speaking, this is due to the fact that, at higher temperatures, the charged particles are stimulated and released from the boundary region, a process known as thermionic emission. It is also important to note that as temperature rises, it may become easier for particles to "tunnel" through the device layer and generate dark current as well. This action is referred to as thermally assisted tunneling and is more prevalent in quantum well infrared photodetectors (QWIP). Both types of dark current behaviours are depicted below in Fig. 2.5 [Hickey – 2002].

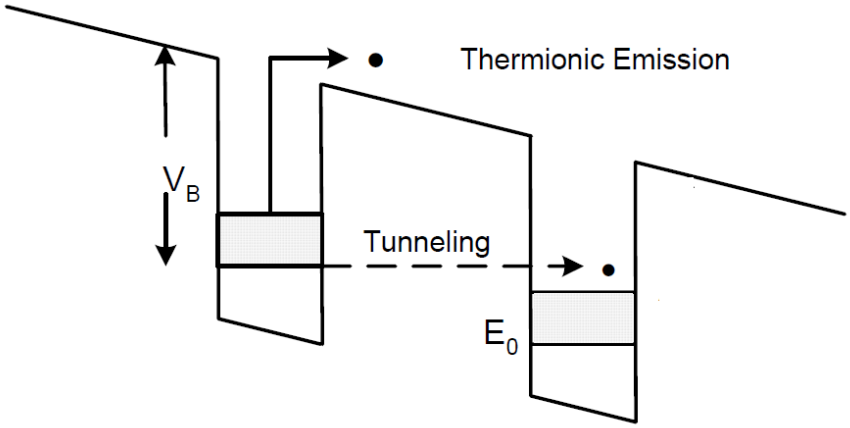

Figure 2.5: Dark Current Behaviour in QWIP
[Adapted From: Hickey – 2002]

In some cases, a device is doped with silicon or other elements to increase electron concentration and to produce a sufficient amount of photocurrent. These charge carriers can easily "boil off" at room temperature due to thermal excitation and generate dark current in the absence of light. In the case of the QWIP, a plot of dark current production versus bias voltage at various temperatures clearly illustrates this dynamic [Hickey – 2002].

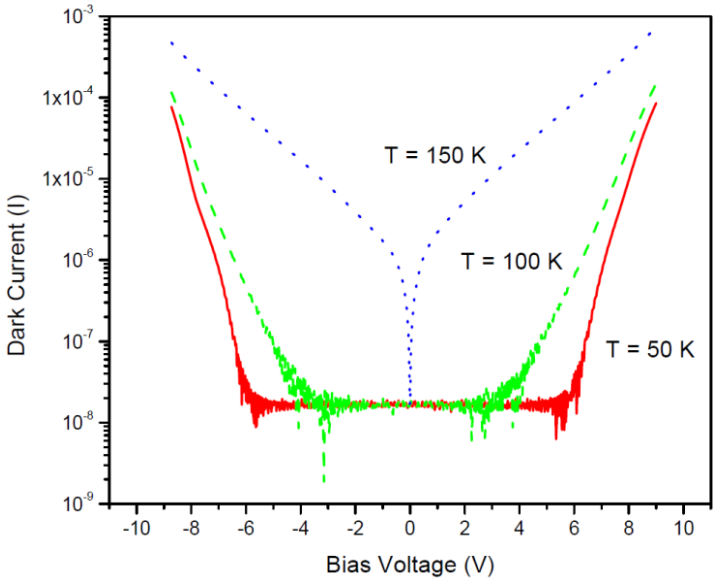

Figure 2.6: Current vs Bias Voltage at Various Temperatures
[Adapted From: Hickey – 2002]

It becomes evident that dark current is highly temperature sensitive above 150 K for QWIP and similar devices. Reducing the local temperature will help minimize the effects of dark current generation and the overall noise associated with this current. In the next section a review of the potential solutions will be provided and investigated.

2.2 Sub-Ambient Thermal Management in Spectrometers

There are various methods that can be employed to deal with the thermal management issues present in electronics as mentioned in the introduction. These include active cooling strategies as well as passive cooling techniques. However, in the literature there are two main strategies that are employed regarding the cooling of spectrometers; cryogenic liquid cooling and thermoelectric cooling. These methods will be discussed in detail in this section in an effort to determine which is better suited for the desired application along with the advantages and disadvantages of each technology.

2.2.1 Cryogenic Liquid-Cooled Detectors

Cryogenics is a branch of science dealing with material behaviour at very low temperatures (usually < 80 K). To obtain temperatures this low one must use certain cryogens such as liquid nitrogen or solid neon (heat absorbed through boiling and sublimation respectively). These substances were first used in the field of astronomy and later in particle physics for sensing neutrinos and other subatomic particles [Timmerhaus and Reed – 2007].

The advantage of this method is the ability to achieve incredibly low temperatures which is the ultimate goal. However, this method is used mainly for bulky station-like systems that are not portable. Another downside is the hazardous nature of the cryogens themselves which requires extra care when handling them. Figure 2.7 is an example of such a system used in the detector assembly of an advanced cooled grating spectrometer (CGS-4).

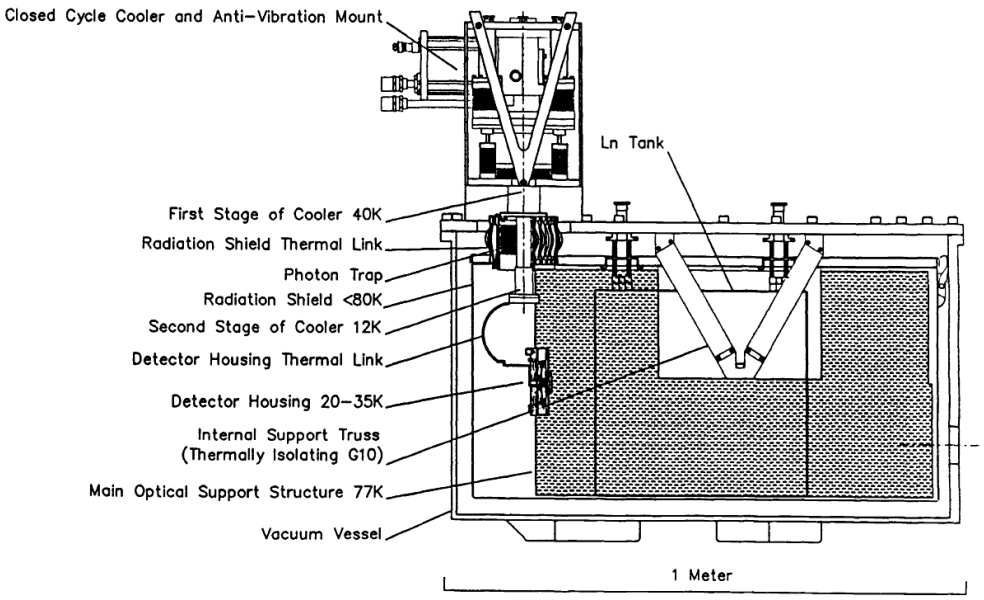

Figure 2.7: Advanced Cooled Grating Spectrometer (CGS-4) Diagram
[Adapted From: Mountain et al. – 1990]

At an approximate weight of 85 kg that includes a 10 L can of liquid nitrogen that is attached, the CGS-4 spectrometer facility is clearly not characterized as portable. Although not all cryogenic cooling methods are necessarily this large, they do contain the hazardous component which may be required to be monitored for safety reasons [Mountain et al. – 1990].

2.2.2 Thermoelectric Peltier-Cooled Detectors

The development of thermoelectric devices for use in spectrometers has gained pace over the years. Several examples of thermoelectrically cooled detectors can be found in the literature. A CdZnTe detector used for X-ray astronomy was successfully cooled to between -30°C and -40°C by a 3-stage Peltier device, significantly improving the energy resolution [Bale et al. – 1999]. In another instance, thermoelectric cooling of CCD detectors in a two-channel Fabry-Perot interferometer was preferable over cryogenic cooling (liquid nitrogen) due to read out errors caused by the latter system [Shiokawa et al. – 2003]. Yet another example is provided in the field of quantum key distribution (QKD) where information bits are encoded on single photons and exchanged between two entities. In order for QKD to work well, the single photon detector should have a reasonably high efficiency and low dark count rate (ratio of incorrect counts due to

noise to total counts). It was observed that at 10% detection efficiency, a thermoelectrically cooled detector based on an avalanche photodiode (APD) results in a dark count probability of 6 x 10^{-5} and 2.8 x 10^{-5} at -40°C and -60°C respectively [Stucki et al. – 2001].

So it is clear that there are advantages/disadvantages to thermoelectric cooling over cryogenic cooling but what is the difference in performance? A recent study comparing the two techniques aims to answer this question. The study involved comparing a thermoelectrically cooled Si-PIN diode (XR-100CR) to a cryogenically cooled Si(Li) detector. The results of the study are presented in Fig. 2.8.

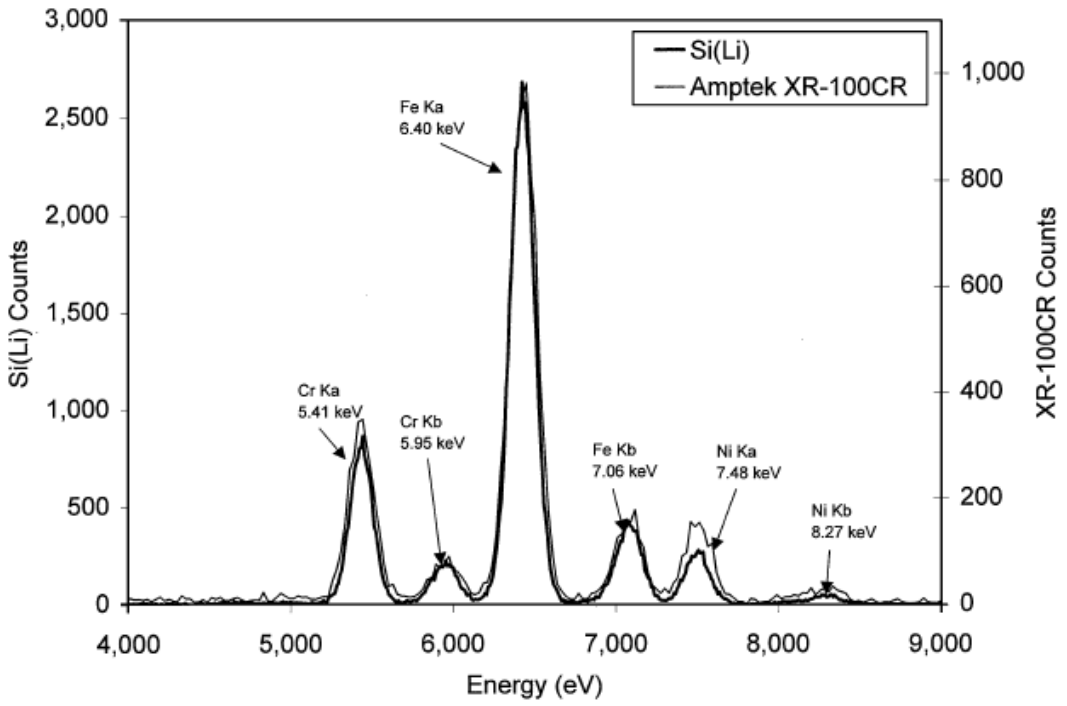

Figure 2.8: Spectra of X-Rays Emitted by Stainless Steel Alloy, Energy Resolution Comparison XR-100 (Dark Line) & Si(Li) Detector (Thin Line) [Adapted From: Redus et al. – 2001]

As shown above, the energy resolution of the Si(Li) detector is slightly better but the peaks in each case are equally well distinguished. The thermoelectrically cooled diode performs nearly as well as the cryogenically cooled detector. This new generation of thermoelectrically cooled detectors and diodes has enabled the successful completion of various projects. Most notably, the XR-100 silicon detector was used on the Mars Pathfinder mission to help measure the composition of soil and rocks on Mars [Rieder et al. – 1997]. In laboratory electronics, a two

stage thermoelectric cooler was used to cool the field-effective transistors (FETs) to 220 K that otherwise would contribute significant noise in the data absent any cooling [Redus et al. – 2001]. After looking at the various advantages and disadvantages of each technology it was decided that the thermoelectric option would be explored further.

2.3 Thermal Resistance Network Analysis

In order to fully understand the bottlenecks to heat transfer an assessment of the thermal resistance network is required. If the thermal resistance at a particular junction on the device can be lowered, an improvement of the heat dissipation quantity can be expected according to Eq. (2.2) and (2.3)

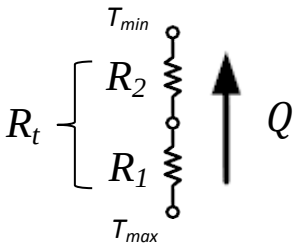

Figure 2.9: Simple Thermal Resistance Network

$$Q = \frac{T_{max} - T_{min}}{R_t} \quad (2.2)$$

$$R_t = \sum_{i=1}^{n} R_i \quad (2.3)$$

where R_t is the total absolute thermal resistance of the network in °C/W or K/W and Q is the heat flow in W. The total resistance is calculated by summing up the individual resistances along the network path. An order of magnitude assessment quantifying these individual thermal resistances will help determine the location of dominant resistance. The types of thermal resistance encountered depend on the type of technology used, and generally speaking, the more complex the configuration the greater the number of resistive layers as each additional contact point introduces a new resistance to heat flow. This will be demonstrated in the next section as various thermal networks are compared.

2.3.1 Order of Magnitude Assessment

In the introduction, a thermal resistance network was shown for a common microchip cooling scenario with a single heat sink. In this section, a look at other thermal resistance networks including TEC-based configurations will be reviewed. Past research to this end has revealed the need for a more detailed understanding of the relationship between the overall thermal resistance of a heat sink configuration and its individual component resistances. For example, studies detailing the individual thermal resistances in heat pipes have shown that although the total thermal resistance of a typical copper heat pipe may be quite low, the overall thermal resistance

of a heat pipe configuration including a dissipative heat sink at the condenser is significantly higher [Riffat – 2004].

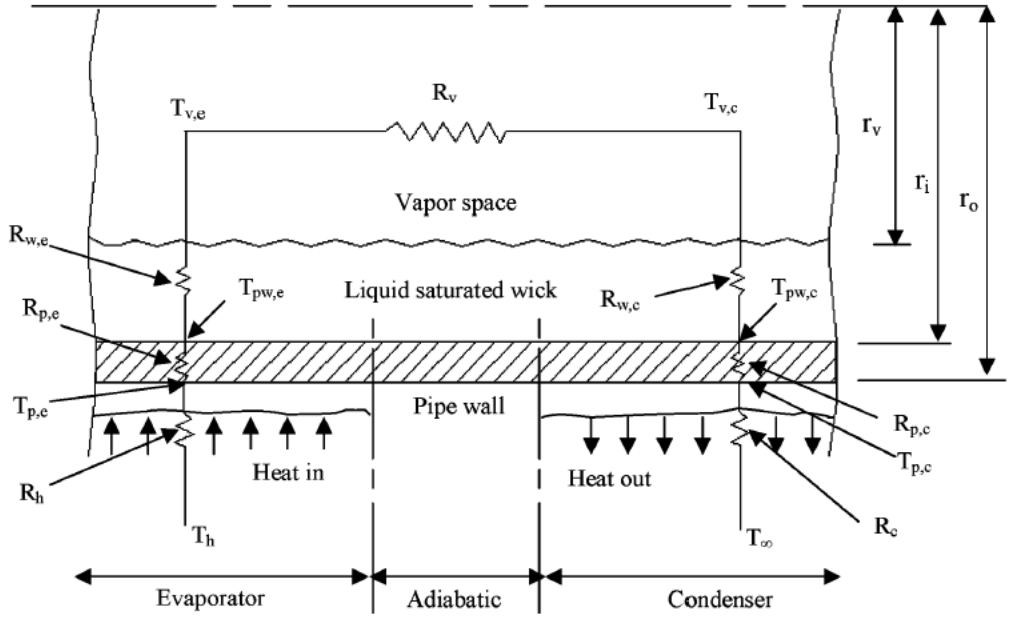

Figure 2.10: Thermal Resistance Network of a Heat Pipe [Adapted From: Kumar – 2007]

Figure 2.10 illustrates the thermal resistance network of a copper heat pipe as well as the various thermal resistance junctures within the pipe structure. In this scenario, the thermal resistances are observed at the ambient-pipe wall boundary (R_h and R_c), through the pipe wall itself ($R_{p,e}$ and $R_{p,c}$), through the saturated wick ($R_{w,e}$ and $R_{w,c}$) and finally through the vapor space (R_v) inside the heat pipe. The thermal resistance of the heat pipe internals is often grouped together to simplify the network ($R_{HP} = R_{p,e} + R_{p,c} + R_{w,e} + R_{w,c} + R_v$). In one study, researchers reported an overall thermal resistance of 1.30 K/W and component resistances of 0.123 K/W, 0.09 K/W and 1.087 K/W for R_h, R_{HP} and R_c respectively for cooling a 60°C target heat source using an air-cooled heat sink at the condenser [Kumar – 2007]. It becomes apparent that over 90% of the thermal resistance observed along the thermal pathway described in Figure 7 resides at the pipe wall-ambient convective boundary, R_c. The ratio of R_{HP} to R_c is roughly 1 to 8.3. In another study where a liquid heat exchanger was used at the condenser, a heat pipe resistance (R_{HP}) as low as 0.02 K/W and a ratio of 1 to 15.1 (R_{HP} to R_c) was reported [Riffat – 2004]. In both situations, the dominant resistance is the convection resistance at the condenser.

Thermoelectric-based cooling configurations involve a very different and much more linear thermal resistance network. Figure 2.11 illustrates a simple cooling configuration and the notable individual resistances.

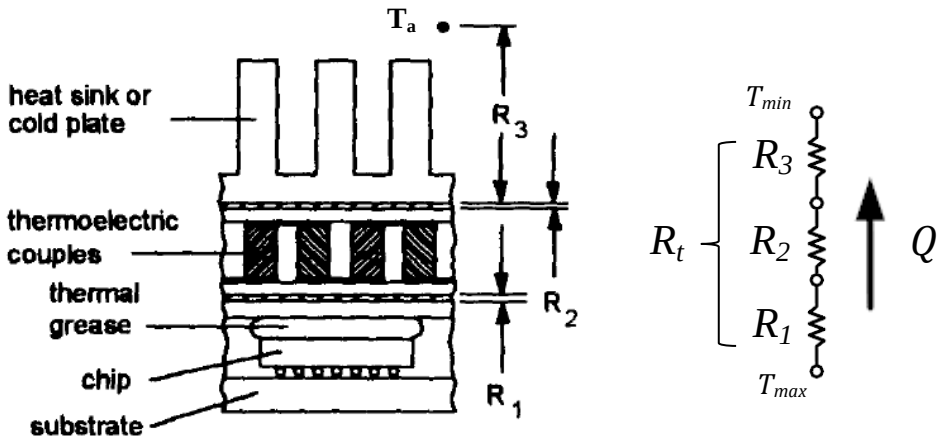

Figure 2.11: A Simple TEC-Based Cooling Configuration [Adapted From: Simons – 2000]

Although it is true that each individual fin of the heat sink contributes its own thermal resistance, the bulk thermal resistance of the heat sink is sufficient for understanding the general behaviour of the heat transfer process. A study conducted on the above cooling arrangement reported thermal resistance values of 0.0054 K/W, 0.0054 K/W and 0.116 K/W for R_1, R_2 and R_3 respectively for air cooling of a 40°C heat source [Simons – 2000]. Similar to heat pipe configurations, the dominant thermal resistance was observed at the convection cooling layer representing 91% of the total thermal resistance. The thermal resistance of the TEC itself is generally not considered since it is a heat pump with a negative resistance value. For a water cooling arrangement, a thermal resistance of 0.0168 K/W was reported. A more detailed thermal network analysis for a TEC-based cooling configuration is shown in Fig. 2.12.

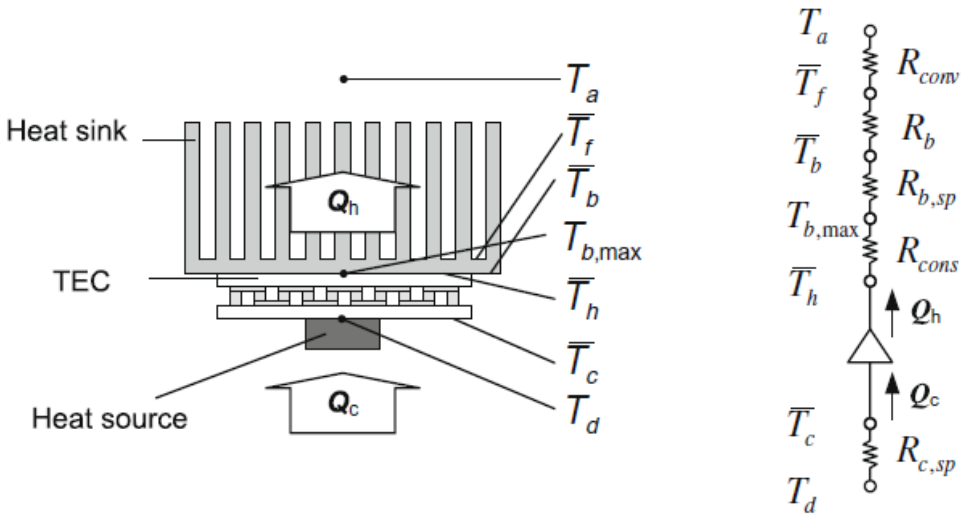

Figure 2.12: Detailed TEC-Based Configuration and Thermal Network
[Adapted From: Chang et al. – 2009]

In this setup, the individual resistances include: heat source spreading resistance ($R_{c,sp}$), constriction resistance (R_{cons}), heat sink base spreading resistance ($R_{b,sp}$), heat sink base resistance (R_b) and convection resistance (R_{conv}). Studies conducted using this setup have reported thermal resistance values of -0.0194 K/W, 0.0477 K/W, 0.0114 K/W and 0.1905 K/W for R_{cons}, $R_{b,sp}$, R_b and R_{conv} respectively. The spreading resistance at the heat source was 0.001 K/W and thus was considered negligible. The constriction resistance is generally negative and not a significant barrier to the overall heat transfer and is also negligible. Again, the convective thermal resistance is the dominant resistance, and in this case, represents 76% of the total positive thermal resistance [Chang et al. – 2009].

2.3.2 Focus Areas and Limitations

After a careful review of the literature, three main convective heat transfer solutions are often considered: natural convection, forced air convection, and forced water heat exchangers. Results of another comparative study indicate thermal resistance values of 6.46 K/W, 2.84 K/W and 0.36 K/W for natural, forced-air, and water-based heat exchangers respectively [Riffat – 2004]. As stated previously, water-cooled forced convection heat exchangers provide a high level of performance, but the main drawback is that they need a convenient source of cooling water. Without a source of cooling water, a forced convection water heat exchanger would require a

pump and radiator along with the associated fittings and tubing. The added resistance of the radiator would increase the overall thermal resistance. Natural convection just does not provide sufficient cooling for modern day high power electronics. Forced air-cooled systems are therefore often a more attractive solution.

A challenging aspect of sub-ambient cooling strategies involves mitigation of condensation within electronic packaging. Condensation occurs when device operating temperatures drop below the dew-point temperature resulting in localized water droplet formation. This can be problematic in electronic equipment causing short circuits, corroding of sensitive device internals as well as introducing a safety risk. Efforts to control condensation in electronic systems include placing enclosure heaters to keep temperatures above the dew-point [Coulton – 2015]. However, if the goal is to maximize photodetector performance through sub-ambient and even sub-zero cooling, other methods of condensation control will likely be required. A few suggestions are given in the following chapters regarding condensation control although more research into this specific topic is required to obtain a more permanent solution.

It is evident after reviewing the literature that the thermal resistance at the convective boundary needs to be improved in order to enhance the dissipative performance of a TEC-based cooling system. A forced air cooling configuration remains ideal for carrying out experiments to this end. Areas that require more investigation include the effect of increased surface area of the heat sink on the convective thermal resistance and the heat flux observed. In the subsequent sections, a three step experimental process will be outlined with a review of the results from each experiment. The goal of the research will be to make improvements to the viability of thermoelectrics for use in spectrometers and other electronic devices by taking into consideration both performance and form factor. The specific effect of heat sink surface area on the convective thermal resistance and the overall heat flux will be analyzed. The focus will be to cool a surface that mimics the detector surface in spectrometers or photodetectors below ambient temperature.

Chapter 3 – Experiment Design and Procedure

The main challenge in spectrometer applications is to maintain a cool stable temperature at the detector. Keeping a stable temperature is important to ensure consistent high quality spectra in the final data produced by a spectrometer as mentioned in the introduction. In addition, the region of desired cooling is rather small (on the order of microns) which adds another level of complexity in terms of testing. This is why miniature thermoelectric devices and micro heat sinks are essential. Figures 3.1(a) and 3.1(b) display the physical features of a traditional spectrometer assembly.

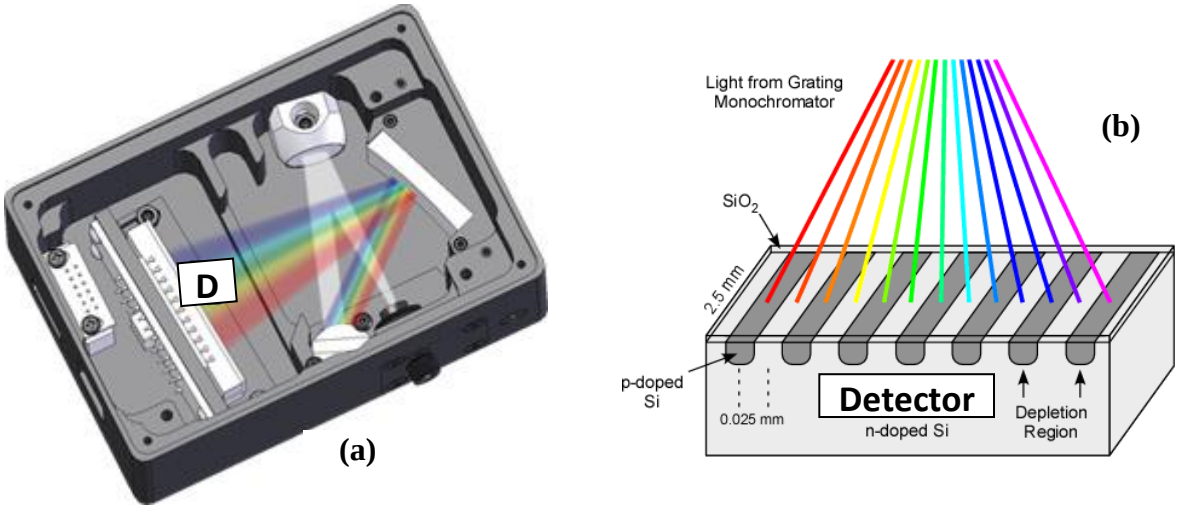

Figure 3.1: (a) Traditional Detector Assembly in Spectrometers (b) Detector Close Up [Adapted From: (a) BWTEK.com – 2015 (b) Dunnivant – 2008]

As depicted in Fig. 3.1(a), the detector array is labeled "D" in the spectrometer assembly. Figure 3.1(b) shows a potential detector width of only 2.5 mm which re-emphasizes the need for localized cooling. However, before declaring micro heat sinks as viable solutions, a slightly larger scale demonstration prototype is necessary to provide proof of concept of the device performance.

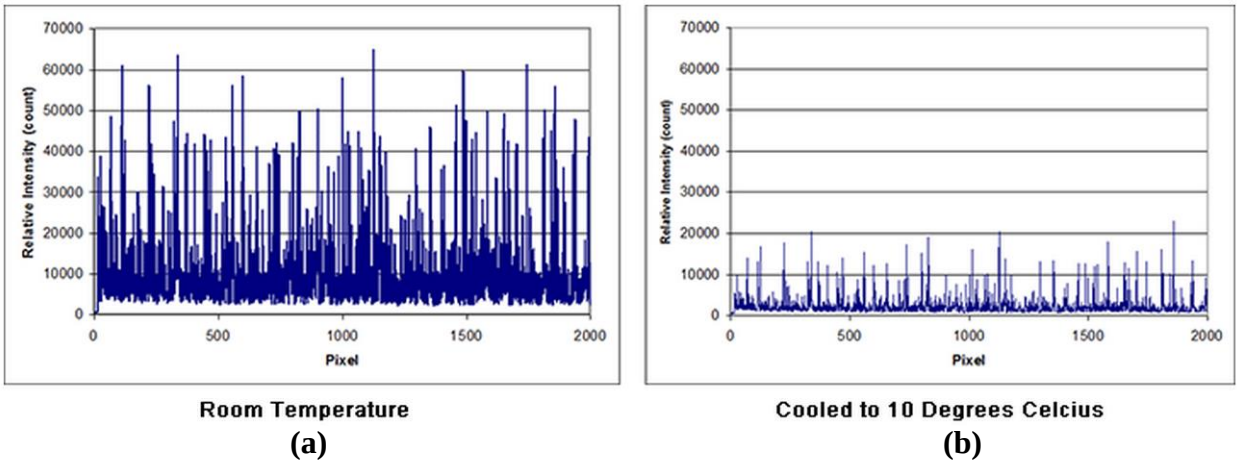

Figure 3.2: Dark Current Generation of (a) Un-cooled and (b) TEC-Cooled CCD Detector [Adapted From: BWTEK.com – 2015]

Although previous experiments have shown the benefits of sub-ambient cooling as seen in Fig. 3.2(a) and 3.2(b), optimization of these TEC-based cooling configurations have been lacking. An understanding of the relationship between heat sink surface area and cooling performance will provide a benchmark for future research and scale down attempts. The idea is to use strategically placed thermoelectric devices on the detector that will provide localized cooling and couple them with advanced heat sinks to dissipate the heat emitted on the backside. The result is an enhanced product that can be used to expand the viable market for nanophotonic spectrometers and similar microelectronics. The experimentation involves a gradual progression of the thermal management design from beginning to end in the order listed below. These test criteria were selected based on the rationale explained in Chapter 1 and Chapter 2 and follows from the need expressed by spectrometer manufacturers.

i) Maintain a stable temperature for a minimum duration of 5 hours
ii) Reduce target surface temperature to -10°C or cooler
iii) Demonstrate size reduction in the design to scale with the desired application

Each of these objectives will be discussed along with the associated testing protocols used in the experiments. The results are presented later on in Chapter 4.

3.1 Apparatus and Experiment Setup

In this section, the key components of the experimental setup will be discussed. The function as well as the selection criteria will be explained for each component. These components will form the core of the test setup with minor changes made from experiment to experiment. A description of the part details will be given to specify operating conditions and limits.

3.1.1 Test Station Setup

All the experiments were setup similar to Fig. 3.3 below. The components are interchangeable depending on the type of experiment conducted. However, in the first experiment, a simpler version of this test station (less secure) was used without the test rig frame and load cell to demonstrate the results in cases where there is poor surface-to-surface contact.

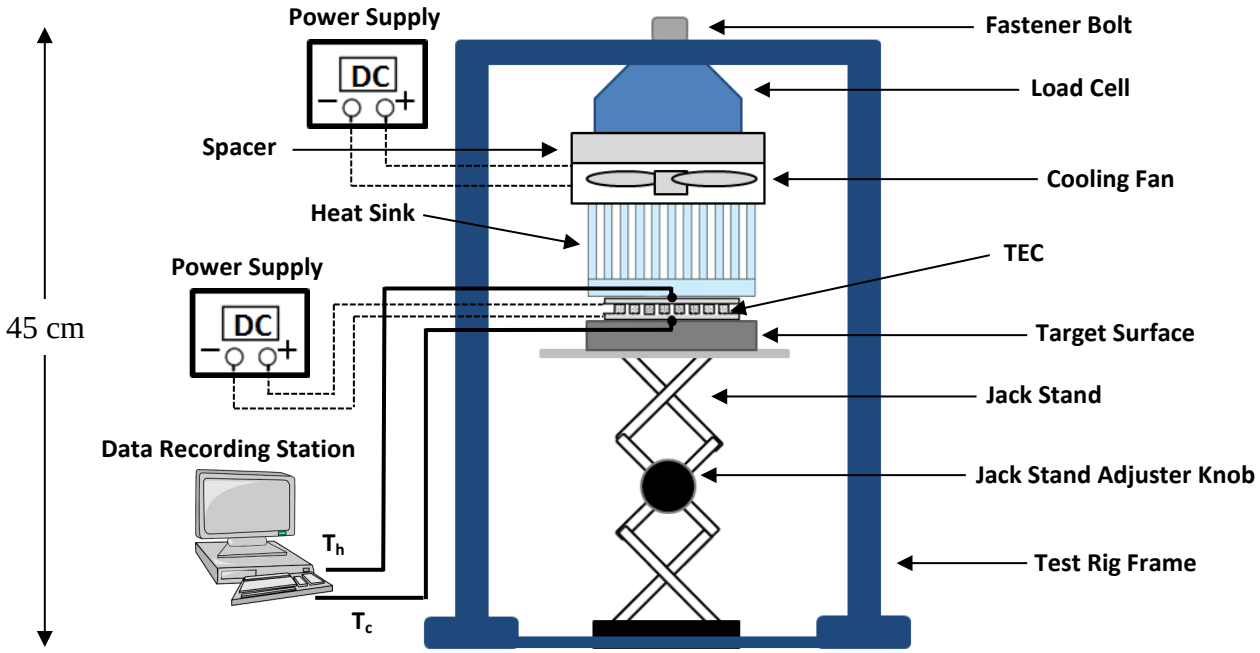

Figure 3.3: Thermoelectric Test Station Schematic Diagram

The main active cooling components include a CPU fan and also the TEC. Power is supplied to these components via DC power supplies. A passive cooling heat sink is sandwiched between the active cooling components. Temperature measurements are recorded at a computer station via

thermocouples placed at the cold and hot junctions of the TEC. A load cell is used at the top of the setup to measure contact pressure between surfaces. A jack stand platform is used to increase or decrease this pressure manually by adjusting the height of the platform. The target surface is placed between the platform and TEC. The sturdy metal test rig frame is used to securely anchor the entire setup. A spacer is used between the cooling fan and load cell in order to prevent blocking air flow to the heat sink.

Prior to turning on the cooling components, a period of 5 – 7 min was dedicated to recording the ambient temperature which is visible in the results. This period of time was monitored to ensure that the starting temperatures (ambient conditions) did not fluctuate beyond ±0.5°C for 10 consecutive readings before commencing cooling. The data were logged in a LabView recording station and converted into an excel file for later analysis. At the 7 min mark, if no significant changes have occurred in ambient conditions, the power supplies are turned on at which point active cooling begins. This is evidenced in the data as a sudden drop and sudden rise in the cold and hot side temperatures respectively. The surface pressure is monitored at the start, steady-state (middle), and final moments of each experiment to ensure proper contact is maintained between surfaces.

3.1.2 Power Supply

Two GW Model GPS-30300 DC power supplies were used to provide power to the TEC and fan components of the thermal management system. For all experiments, a fixed voltage of 27.5 V was applied to the same fan mounted on each heat sink for constant air flow comparison.

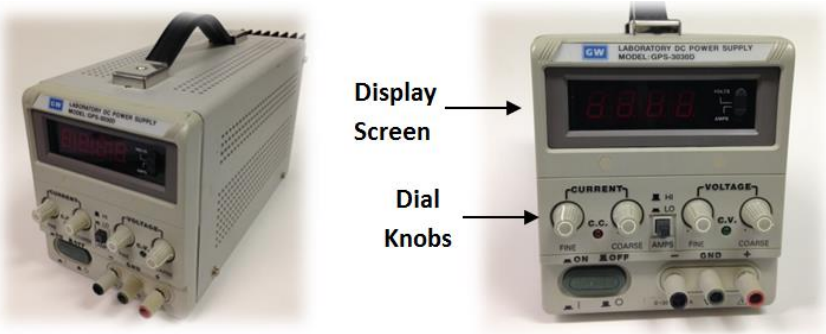

Figure 3.4: GW Model GPS-30300 DC Power Supply

The input power was calculated by multiplying the voltage and current provided by the power supplies. The voltage and current levels were manually adjusted using the rotatable dials on the power supplies and monitored throughout the experiment.

3.1.3 Test Rig Frame Structure

The test rig consists of a metallic frame measuring 45 cm in height with a closed top where contact pressure can be increased through tightening of the bottom jack stand. The jack stand will also provide the platform for the target surface, TEC, heat sink and fan. The pressure was also noted for later analysis via a load cell (calibration found in Appendix A) mounted at the top of the metallic frame as seen below. Finally, a spacer was used to maintain space between the fan and the load cell to avoid blocking air flow to the heat sink.

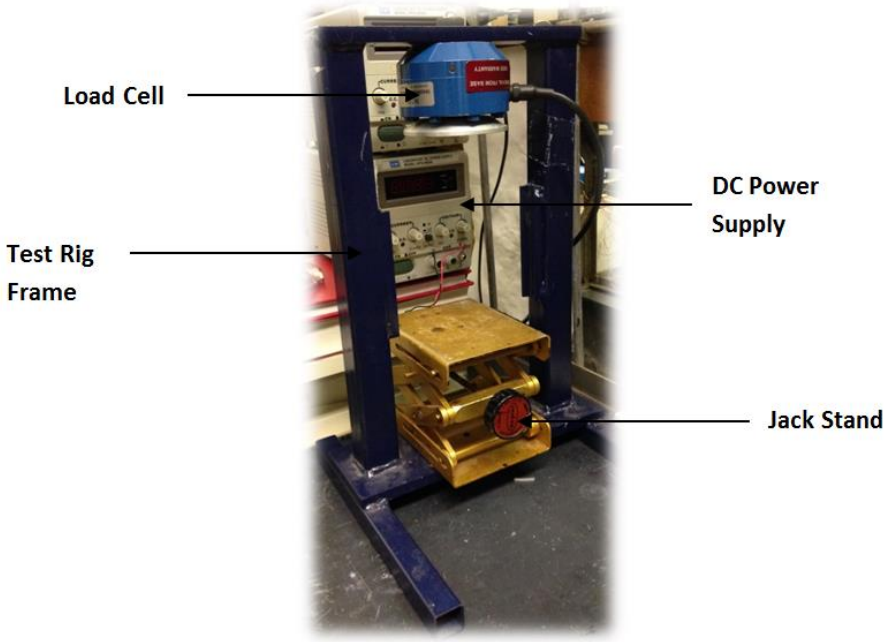

Figure 3.5: Test Rig Frame Structure with Fixed Load Cell and Secondary Jack Stand

In the initial trial experiments, the metallic frame was not used in order to compare the results from an unsecured rig to a secured one. The results of the two configurations are displayed in the next chapter and will be discussed later on. It is critical that solid contact is made between the surfaces in order to reduce the thermal resistance at each junction point. The effect of surface

pressure on heat transfer is also considered in this study in order to determine its level of significance.

3.1.4 Thermoelectric Device Selection

The central component, which is responsible for the active cooling of the desired region, is known as a thermoelectric component or TEC. Several of these devices were considered for experimentation and the following TECs (TEC 1, TEC 2) were chosen for further testing based on economics, easy-of-use, accessibility, and performance. The TECs were chosen to demonstrate proof of concept in this phase of the research. Enhanced TEC designs should be considered for future experiments. TEC 2 specifications can be found in Appendix B.

Figure 3.6: TEC 1 [Adapted From: Custom Thermoelectric – 2007]

Table 3.1: TEC 1 Specifications

Specifications	
Manufacturer	Custom Thermoelectric
Part #	12711-5L31-04CL
Internals	Bismuth Telluride
I_{max}	4.0 A
V_{max}	15.4 V
Q_{max}	33.4 W
ΔT_{max}	67 °C
T_{max}	125 °C

As mentioned in the introduction, a TEC requires some input power to pump heat from one side to the other. Initially, as power is supplied to the TEC a thermal gradient is introduced producing a cold and hot side. However, if there is no heat dissipation on the hot side of the TEC, the thermal gradient across the device will collapse resulting in a sharp temperature rise within the device in a matter of seconds depending on the rate of power supplied. A simple experiment demonstrates this dynamic by monitoring both the cold and hot sides of the TEC for a short period after supplying a constant input power when no heat dissipation is involved. The resulting device behaviour is displayed using a cooling performance curve as seen in Fig. 3.7.

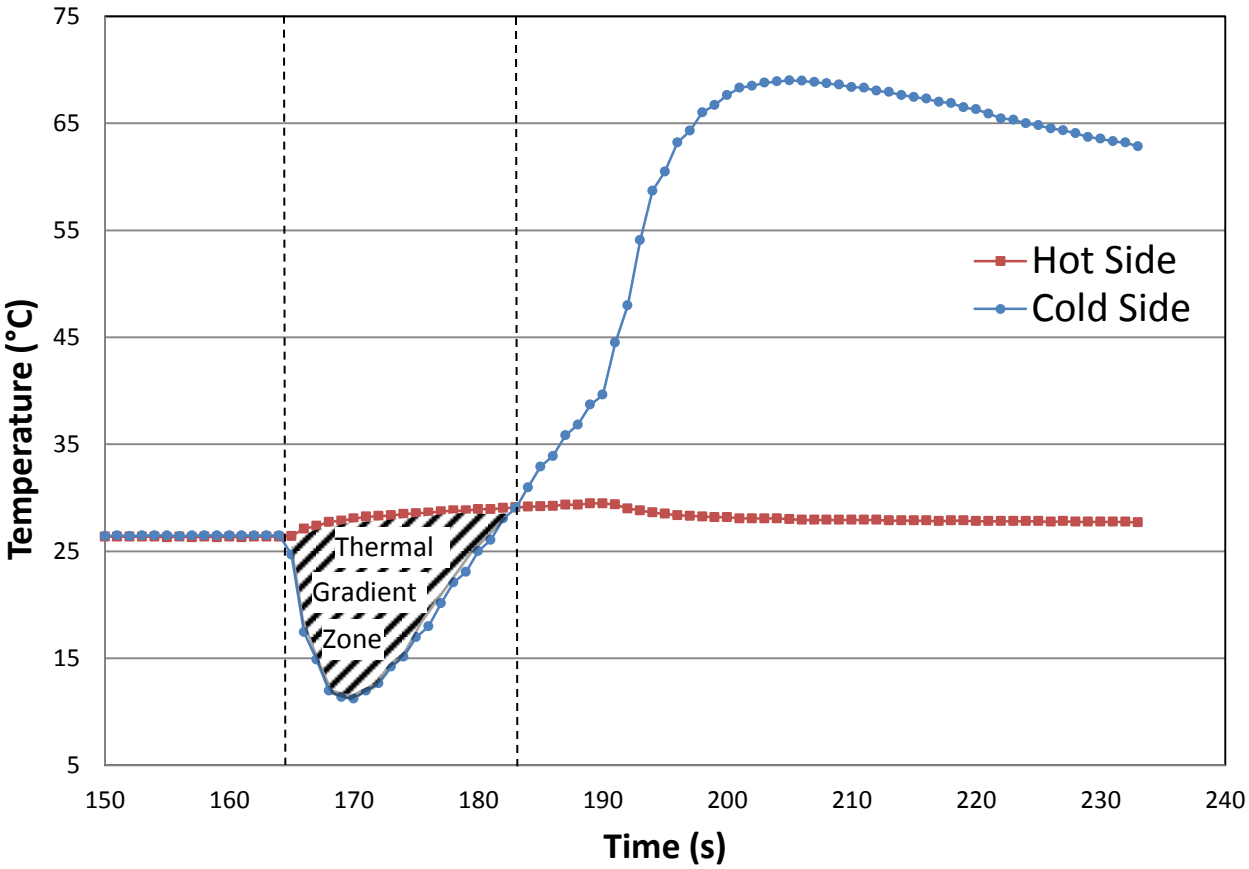

Figure 3.7: TEC 1 Performance without Heat Sink

It is clearly shown that shortly after activating cooling (9 V, 1.8 W input power at approx. 165 s) the thermal gradient begins to collapse rather quickly and fully collapses at approx. 182 s. Cooling was observed for only 17 seconds and with the cold side surface temperature only down to 12°C (ΔT_{max} = 15°C). After the thermal gradient has collapsed, the TEC starts to heat up internally from the cold side up to a threshold temperature where the device fails due to thermal shorting. The experiment was aborted at approx. 195 s before this threshold to avoid damaging the TEC. This highlights the importance of having a sufficient heat sink on the hot side capable of continually dissipating heat that is pumped through the TEC. Detailed specification sheets are provided in Appendix B regarding the specific TEC used in the described experiments. Upon careful consultation and correspondence with Tornado Spectral Systems, an innovative spectroscopy solutions provider, it was determined that a minimum of -10°C surface temperature was required to provide sufficient cooling value regarding spectrometer performance [Personal Correspondence 1 – 2014]. This metric is used as the benchmark for all experiments conducted.

3.1.5 Heat Sink Selection

The heat sink which will be used to dissipate the heat transmitted through the backside of the TEC is of critical importance as demonstrated previously. For the purposes of studying temperature stability, a basic heat sink (HS – 3) and fan was selected as seen in Figures 3.8 and 3.9. The heat sinks performance will provide a baseline from which further improvements to the design can be compared. In all, 5 aluminum-based heat sinks (HS – 1 to HS – 5) of varying specifications and dimensions were tested with the same fan mounted on top in each case.

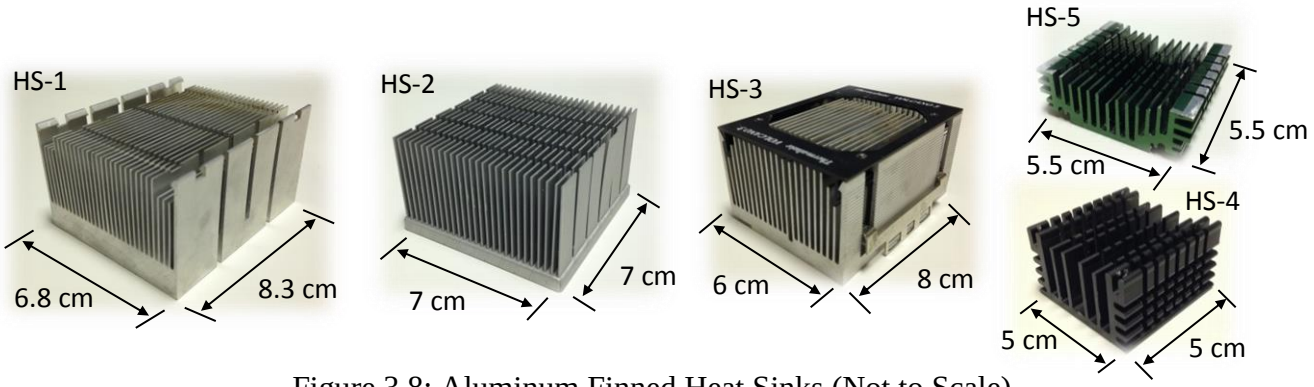

Figure 3.8: Aluminum Finned Heat Sinks (Not to Scale)

Selection of these heat sinks were conducted based on their sizes, varying surface areas, fin spacing and other factors listed in Table 3.2. The practicality of each heat sink also was considered during the selection process (i.e. not larger than a fist in effective volume).

Table 3.2: Heat Sink Specifications

	HS - 1	**HS – 2**	**HS – 3**	**HS – 4**	**HS - 5**
Material	Aluminum	Aluminum	Aluminum	Aluminum	Aluminum
Surface Treatment	Bare	Anodized	Bare	Anodized	Anodized
Effective Volume	254 cm^3	196 cm^3	192 cm^3	75 cm^3	57 cm^3
Surface Area	1444 cm^2	1177 cm^2	1025 cm^2	174 cm^2	172 cm^2
S/V Ratio	5.68 cm^{-1}	6 cm^{-1}	5.33 cm^{-1}	2.32 cm^{-1}	3.02 cm^{-1}
Fin Spacing	1.5 mm	2 mm	2 mm	1.5 mm	2 mm
Fin Thickness	1 mm	0.75 mm	1 mm	2 mm	1.5 mm
Fin Height	31 mm	35 mm	32 mm	25 mm	15 mm
Weight	426 g	166.93 g	241.47 g	65.45 g	54.39 g
Base Thickness	12 mm	5 mm	7 mm	3 mm	2.5 mm
Mounted Fan	Standard CPU cooling fan (6 cm x 6 cm x 2.5 cm)				

3.1.6 Fan Selection

Since interest is primarily focused on the effect of heat sink surface area on cooling performance, a constant rate of forced air convective cooling provided via a PAPST TYP 614NM standard CPU fan was chosen (Appendix C for specs). This cooling fan was mounted on each heat sink along with an identical spacer fan as seen in Fig. 3.9 (spacer fan not powered and only used for spacing). The input voltage applied to the cooling fan was kept at 27.5 V throughout the experiments to maintain a constant rate of air flow. Also, the fan was chosen based on dimensions that would be convenient for mounting on top of the various heat sinks.

Figure 3.9: Standard CPU Cooling Fan (PAPST TYP 614NM)

3.1.7 Surfaces to Be Cooled

As mentioned in the introduction, this study focuses on cooling electronic surfaces below ambient conditions in order to improve device performance. Since the focus application is cooling in spectroscopy and photodetectors, the interest was not in cooling a continually hot surface, but rather cooling a target surface as far below ambient as possible and to at least -10°C. The performance of the TEC in this situation can be made relevant to cases in electronic packaging where a heat source is continually present. Therefore, instead of a heater, various surfaces are used as the target for cooling. The surfaces used in the experiments include 4.5 cm x 4.5 cm x 0.3 cm pieces of rubber and copper which were selected based on their ease-of-use and physical properties. Each surface is tested on a jack stand (used as the test rig platform) as displayed in Fig. 3.10. Although, there will be added focus on experiments involving copper metal as the target surface in order to mimic the intended application in microelectronic packaging or common detector surfaces in spectrometers.

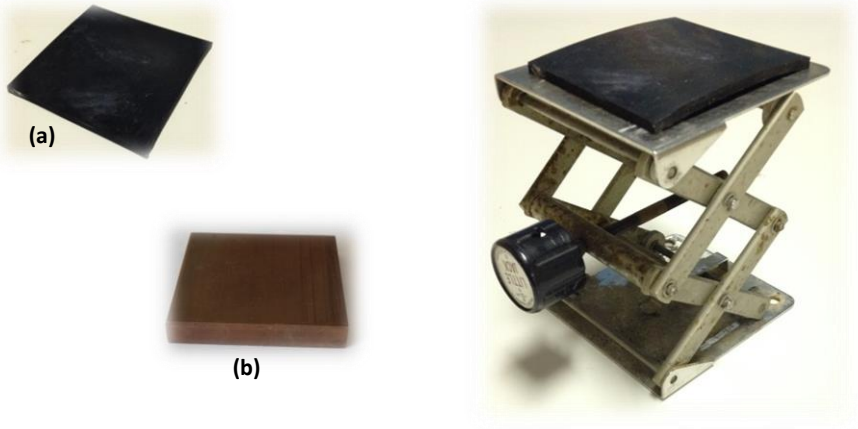

Figure 3.10: Target Surfaces (a) Rubber (b) Copper and Jack Stand Platform

Since the thermal conductivity of the surfaces vary, the subsequent results can be compared in each case to determine the effect of surface thermal conductivity on heat transfer for each type of surface.

3.1.8 Temperature Measurements and Data Acquisition

The temperature of the cold and hot side of the TEC was recorded using 2 Watlow SERV-RITE Model T-type thermocouples connected to a Keithly 2700 data acquisition system (using LabView Version 6i software). The thermocouples were placed in the center position of the cold and hot sides and held in place by TechSpray 1978-DP thermal interface compound. A small 0.018 inch channel was milled into each heat sink to accommodate the thermocouple and prevent damage at higher contact pressures.

Figure 3.11: T-Type Thermocouple for Insertion into Single Channel on Heat Sink Bottom

Figure 3.12: Data Acquisition System (Computer Station & Data Logger Module)

The thermocouples were connected to input channels on the logger board and are automatically detected by the LabView software as displayed in Fig 3.12. The channels are numbered from 0 – 15 and can be selected on the software interface. The board number by default is 0 and is also noted on the screen. The output array includes time in s, hot side temperature (T1) in °C and cold side temperature (T2) in °C. The temperatures are indexed to correspond to automatic real time plots of the output data. The output data itself are converted to an excel file saved to a specified file path. The data are collected as soon as the Boolean functions are activated and the "Run" button is selected near the top of the screen. The experiment can be halted at any time by selecting the "Abort" button. A close up view of the interface is presented in Fig. 3.13 and 3.14. Plot 1 corresponds to T1 data values and plot 2 corresponds to T2 data values. More channels may be used if necessary for measuring temperature at other points of interest.

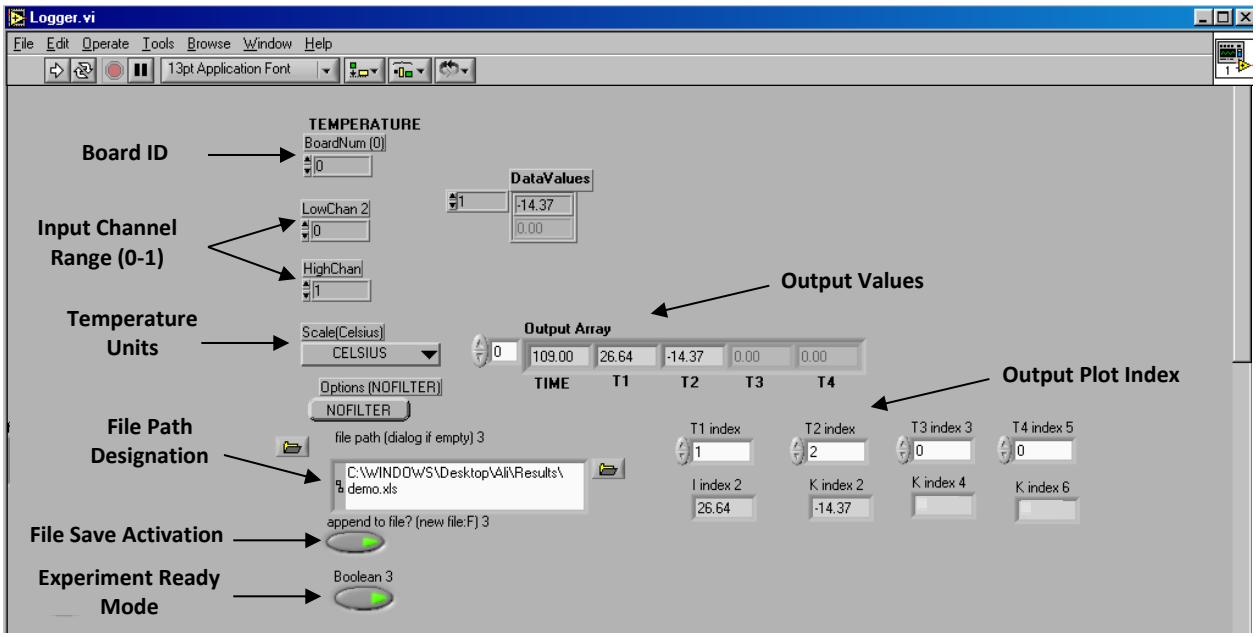

Figure 3.13: LabView Data Logger Screenshot 1

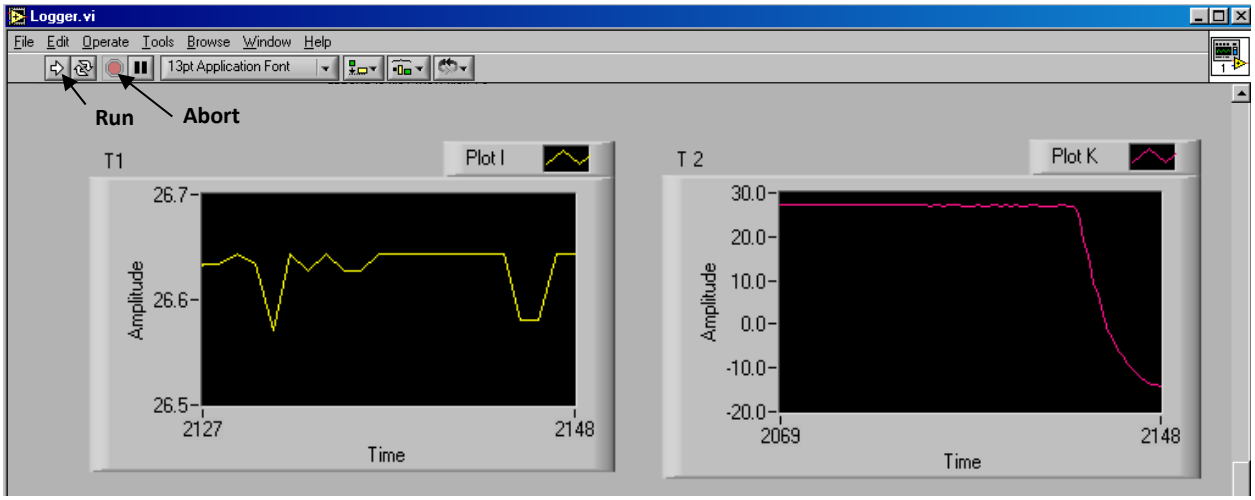

Figure 3.14: LabView Data Logger Screenshot 2

The amplitude corresponds to temperature values in degrees C which can be changed by changing the units as shown in Fig. 3.14. The time axis is set in seconds in order to capture sudden changes in temperature at a higher resolution and was converted to minutes or hours later in the excel data.

3.2 Experimental Procedure

Three experiments were designed to test the performance of the TEC-based thermal management configuration described in section 3.1. The first test focused on the stability and reliability of surface cooling for an extended duration. The second series of tests were designed to attain the maximum cooling performance using a standard heat sink (HS – 3). Finally, in the third round of experiments, the overall size of the configuration was reduced and compared in terms heat sink surface area and volume while maintaining at least -10°C at the cold side surface juncture. Multiple replicate runs were conducted to ensure consistent cooling behaviour and to detect any potential anomalies.

3.2.1 Experiment 1 – Cooling Stability and Reliability

The performance measure investigated in this experiment was the stability of the cold and hot side temperatures during active cooling. In the field of spectroscopy, the reliability of the thermal management system at the detector end is of critical importance and the consistency of the data produced at the detector is dictated, in large part, by the stability of the temperature locally. The goal was to monitor the cold and hot side temperatures over a minimum duration of 5 hours to understand the behaviour and performance characteristics of the TEC over time while taking note of cool down and warm up rates.

The first set of tests focused on the cold side of the TEC. It is important that the cold side temperature can be relied upon due to its impact on the overall performance of the electronic system it is designed to cool. Any disruption to temperature stability may yield higher than desired noise levels, overheating of key parts, and introduce various safety concerns. The active cooling experiment was carried out using a TEC (Fig. 3.6), HS – 3 (heat sink 3) and a standard pc board fan (Fig. 3.9). It is important to note that this first experiment focused purely on temperature stability while demonstrating the importance of proper surface contact and thus was conducted on a simpler test rig (requiring alignment adjustments) and without any thermal compound (needed for optimal heat transfer). The test was repeated 5 times for various durations.

The setup in this first experiment is similar to Fig. 3.3 only it is unsecured, without the metallic frame and load cell. Instead, a retort stand and clamp was used to hold the configuration in place as depicted in Fig 3.15. This was done in order to compare both setups with respect to effects of secured contact between surfaces and unsecured contact between surfaces on cooling performance.

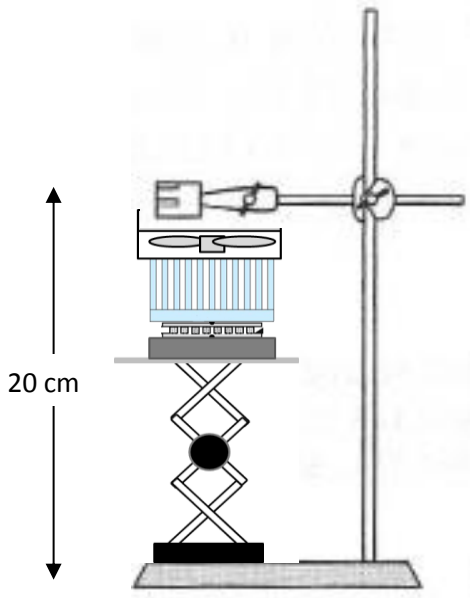

Figure 3.15: Experiment 1 Test Setup (Retort Stand and Clamp)

The components are arranged in a column stack as seen in Fig 3.15 and the fan and TEC are connected to the power supplies. After checking all components for proper fit, the data acquisition system is activated and ambient temperature is recorded for 7 min as mentioned earlier. At the 7 min mark, if ambient conditions are stable, active cooling begins as power is supplied to both the fan (27.5 V, 0.33 A) and TEC (11.7 V, 2.55 A). The experiment is allowed to run for 5 h or more and then stopped. This time duration was considered after consulting with industry partners and required for various applications. The data are gathered for analysis and the test is repeated on different days for verification purposes. The goal was to determine the behaviour the TEC-based cooling configuration over an extended period of time and the time required to reach steady-state cooling.

3.2.2 Experiment 2 – TEC Cooling Performance

The next step in the thermal management development process was to improve the actual cooling performance of the TEC-based system. A target cold side surface temperature of at least -10°C was required to demonstrate significant results. In experiment 2, the highest cooling capability was investigated using HS – 1, HS – 2, and HS – 3 heat sinks. Also, the secured version of the experimental setup was used as depicted in Fig. 3.3. The load cell was calibrated against standardized weights prior to use as seen in Appendix A. The fan input power was constant throughout the experiment at 27.5 V and 0.33 A. The TEC power was adjusted manually for each heat sink in order to obtain the maximum cooling potential. In addition to securing the test rig, thermal compound was added in between the cold and hot junctures to improve heat transfer through the region. After all components are ready and secured in position, the data acquisition system was activated. At the 7 min mark, if ambient conditions have not deviated significantly, power was supplied to the TEC and fan at which point cooling begins. Each heat sink was tested several times for at least 5 h to ensure accuracy of the data and in each case the same fan was used.

3.2.3 Experiment 3 – Configuration Scale Down

The third set of experiments is focused on reducing the structural footprint (occupying volume) of the TEC / heat sink thermal management system. The goal was to show that further reductions to the form factor of the components can be realized as improvements are made to the heat sinks by maximizing the exposed surface area. To accomplish this, a range of heat sinks were evaluated for comparison purposes. In total five heat sinks were chosen to demonstrate the relationship between the available surface area of a heat sink and the impact on overall cooling performance. The procedure is identical to section 3.2.2 with the addition of HS – 4 and HS – 5 as extra heat sinks to be tested. The cooling response was compared and presented in the results section. The sizes of the heat sinks were reduced such that a cold side junction temperature of at least -10°C was achieved. Other heat sinks that did not meet this requirement were not considered for long term study.

3.2.4 Experiment 4 – Target Surface Analysis

Finally, an analysis of the effect of different target surfaces on cooling was carried out. Specifically, neoprene rubber (thermal insulator) and copper (thermal conductor) was examined due to their vastly different thermal conductivities and physical properties. The objective here was to measure the impact of the target surfaces on the thermal resistance network pathway as well as noting the differences in the resulting condensation effects. This experiment provided more information regarding surface response effects in electronic packaging by increased understanding of the target surface behaviour under sub-ambient cooling conditions. Neoprene rubber and copper were chosen as they represent opposite ends of the spectrum with respect to thermal conductivity. Ceramic surfaces were also considered at one point but neglected in the final experiments due to difficulties experienced in machining channels into the hard ceramic surface (required for thermocouple insertion).

3.3 Experiment Design Summary

An overview of all the experiments is presented in Table 3.3. The test matrix is designed to provide an outline of all the experiments and their aims. Each experiment was devised based on the findings of the previous in a progressive manner such that the information gathered from one experiment is used to enhance or provide the foundation for the next.

Table 3.3: Experiment Test Matrix

Experiment #	Component of Interest	Focus Areas	Goal / Aim
1	TEC	Stable junction temperatures	No temperature fluctuations beyond 1°C for 5 h
2	TEC	Cold side temperature	Achieve -10°C or lower at the cold junction
3	Heat Sink Configuration (Including Fan)	Surface area and volume	Reduce overall size by 50% from starting size
4	Target Surface	Cooling and condensation	Determine optimal surface for cooling

By expanding on each experiment and addressing the various aspects of TEC-based cooling, the proof of concept will be demonstrated. The goals of the experiments where determined through correspondence with specialist in the field of spectroscopy. The ultimate goal however is to provide recommendations on how to improve current efforts to cool spectrometers and related electronics using TEC-based platforms via a better understanding of the different sub-components in the cooling configuration.

3.4 Uncertainty Analysis

In this section, the various uncertainties involved in the experimental measurements are presented. The accuracy of the equipment used in the experiments is used to determine the uncertainty (error range) of both measured and calculated properties.

3.4.1 Error Analysis Method

The uncertainty of theoretical and experimental results will be determined using the method described by Moffat [Moffat – 1999]. In this approach, any particular result R is expressed as a function of a set of individual measurements X_i as seen in Eq. (3.1).

$$R = R(X_1, X_2, X_3, \dots, X_N) \tag{3.1}$$

Each measurement can be expressed as $X_i \pm \delta X_i$ where δX_i is the error or uncertainty value. If R is of the form $R = X_1^a X_2^b X_3^c \cdots X_N^N$ then the overall uncertainty of a result (δR), as a fractional percentage, is given by Eq. (3.2) and Eq. (3.3) below.

$$\delta R = \left[\left(\frac{\partial R}{\partial X_1}\delta X_1\right)^2 + \left(\frac{\partial R}{\partial X_2}\delta X_2\right)^2 + \left(\frac{\partial R}{\partial X_3}\delta X_3\right)^2 + \cdots + \left(\frac{\partial R}{\partial X_N}\delta X_N\right)^2\right]^{1/2} \tag{3.2}$$

$$\frac{\delta R}{R} = \left[\left(\frac{\delta X_1}{X_1}a\right)^2 + \left(\frac{\delta X_2}{X_2}b\right)^2 + \left(\frac{\delta X_3}{X_3}c\right)^2 + \cdots + \left(\frac{\delta X_N}{X_N}N\right)^2\right]^{1/2} \tag{3.3}$$

Detailed calculations of the various uncertainties are presented in Appendix E. A summary of the uncertainties is presented in Table 3.4.

3.4.2 Summary of Uncertainties

The tabulated uncertainties of the key variables are listed in Table 3.4. Detailed calculations of the individual uncertainties are shown in Appendix E. The specifications provided by the manufacturer's data sheets were used to determine the accuracy level of the measured properties.

Table 3.4: Summary of Uncertainties

Variable	**Data Range**	**Uncertainty (± %)**
Temperature [°C]	-22.4°C – -10.1°C	0.089 – 0.198
Surface Pressure [psi]	7.07 psi – 28.4 psi	0.020 – 0.056
Heat Sink Surface Area [cm^2]	172 cm^2 – 1444 cm^2	11.8 – 2.3
Voltage [V]	11.7 V – 27.5 V	0.50
Current [A]	0.33 A – 2.55 A	0.50
Thermal Resistance [K/W]	0.007114 K/W – 0.54 K/W	6.0 – 26.6
Heat Flow [W]	20.09 W	18.8
Time [h]	0 h – 10 h	0 – 2.8 x 10^{-6}
Configuration Volume [cm^3]	57 cm^3 – 254 cm^3	0.028 – 0.016
Power [W]	1.8 W – 9.08 W	0.71

Chapter 4 – Results and Discussion

The following are the results gathered with respect to the experiments described previously. A discussion about each experiment and its results is also presented in order to address the key findings. The focus is on the developmental progression of a TEC-based heat sink from one stage to the next highlighting key aspects at each stage. The idea is to demonstrate viability of the proposed cooling system based on design constraints and various performance metrics. Test redundancy is used to demonstrate repeatability. Replicates of the results are conducted to ensure consistent behaviour with any anomalies explained.

4.1 Experiment 1 – Temperature Stability

In Chapter 3, it was shown that a TEC by itself could not sustain a temperature gradient for more than a few seconds without a heat sink (and fan) present to dissipate heat on the hot side. The question now is how long a TEC-based cooling configuration can sustain a temperature gradient with a heat sink? Does the heat sink stabilize the cold side temperature in a predictable manner or is the behaviour erratic? Is there a steady-state threshold and if so how long does it take to reach this threshold? To answer these questions an experiment was devised (Experiment 1) to assess the stability of the cold side temperature, and by extension the stability of the hot side temperature, using a variable surface pressure test rig. The input conditions are presented in Table 4.1 and the results of Experiment 1 are shown in Fig. 4.1.

Table 4.1: Experiment 1 Test Conditions

TEC Input Power	Fan Input Power	Surface Pressure	Ambient Conditions	Target Surface	Heat Sink Used	Test Duration
11.7 V 2.55 A	27.5 V 0.33 A	Variable Unknown	23°C Humidity 67%	Rubber (Neoprene)	HS – 3	5 – 10 h 5 replicates

4.1.1 Temperature Stability Results

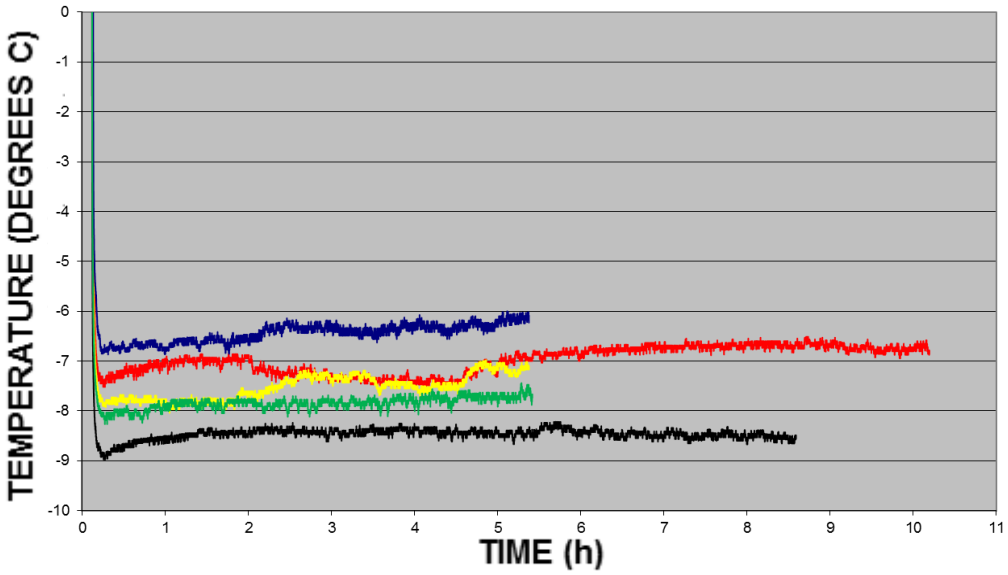

Figure 4.1: Cold Side Temperature Stability Graph of TEC 1 for Various Durations

As shown above, the test was repeated 5 times for various durations. An average warming rate 0.10°C/h was observed which was determined to be sufficient for the intended application [Personal Correspondence 2 – 2014]. The minimum cooling potential (guaranteed cooling temperature) was reached in 2 min on average. In other words, the highest temperature which was observed for the entire cooling duration occurred around the 2 min mark after cooling was initiated. However, it is noticeable that the maximum cooling potential fluctuates from -6.7°C (blue line) to -9°C (black line). This can be attributed to the variable surface pressure resulting in poor surface to surface contact. The hot side temperatures were observed to be quite stable showing nearly no change after reaching the maximum temperature in 2 min on average (more discussion about this in later sections). Also, due to improper alignment, a TEC failure was observed in one instance as a result of overheating during active cooling. Ideally, one would like to have perfect solid contact at the heat transfer boundary as thermal conductance through solid materials (tight particle packing) is generally higher than through fluids (loose particle packing). Imperfections or roughness at the surface boundary can contribute significant thermal resistance in some cases. Contact resistance can also increase if there are interstitial materials such as air pockets in between the surface interface.

4.1.2 Surface Contact Pressure

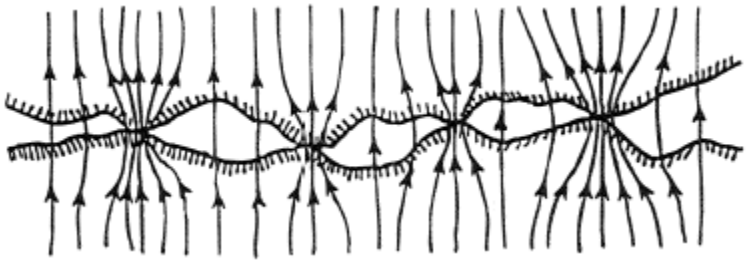

Figure 4.2: Magnified View of Heat Flow through Two Materials in Contact
[Adapted From: Thermopedia.com – 2011]

Figure 4.2 displays the contact interface formed by the pressing of two surfaces together at some arbitrary pressure. It is shown that only a fraction (3 – 5% of the apparent cross sectional area) of the total available area is actually in contact with the other surface due to roughness and imperfections in the surfaces. The varying results in Experiment 1 (Fig. 4.1) can be explained by different surface roughness profiles associated with the variable test rig. Also, since the first test rig does not include a surface pressure monitor, each run may involve a different surface pressure contributing to inconsistent junction profiles and interstitial gaps.

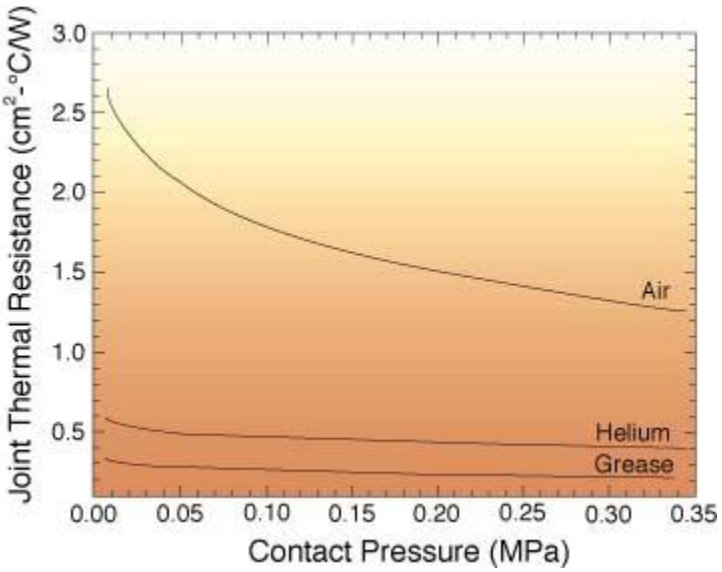

Figure 4.3: Joint thermal resistance of an aluminum heat sink-ceramic package assembly
[Adapted From: Teertstra et al. – 1997]

Detailed studies of the effects of contact pressure on thermal contact resistance at the surface boundary have been conducted in past for different interstitial materials as seen in Fig. 4.3. Generally speaking, as solid contact between surfaces increases the thermal resistance at the junction decreases. In Experiment 1, the dissipation of heat is performed through a ceramic (TEC) / aluminum (heat sink) contact boundary as previously seen in the design setup. Figure 4.3 displays contact resistances for an aluminum-ceramic surface interface at various contact pressures using various interstitial materials. As seen in Fig. 4.3, as contact pressure rises it is expected that the thermal resistance decreases regardless of the interstitial material used. However, using air as the interstitial material results in thermal resistances ranging from 2.75 cm^2 °C/W – 1.25 cm^2 °C/W for contact pressures between 0.01 MPa – 0.35 MPa. These resistance values are higher than other interstitial materials that can be used such as thermal grease. To verify this, random pressure adjustments were made to a replicate experiment at arbitrary times to observe the cooling response as a result of increased surface pressure. This was done by simply turning the jack stand knob slightly to apply more pressure. Again, since there was no pressure monitor initially, the value of the adjustment was unknown at first but was not necessary for qualitative analysis purposes. The results of the test are displayed in Fig. 4.4.

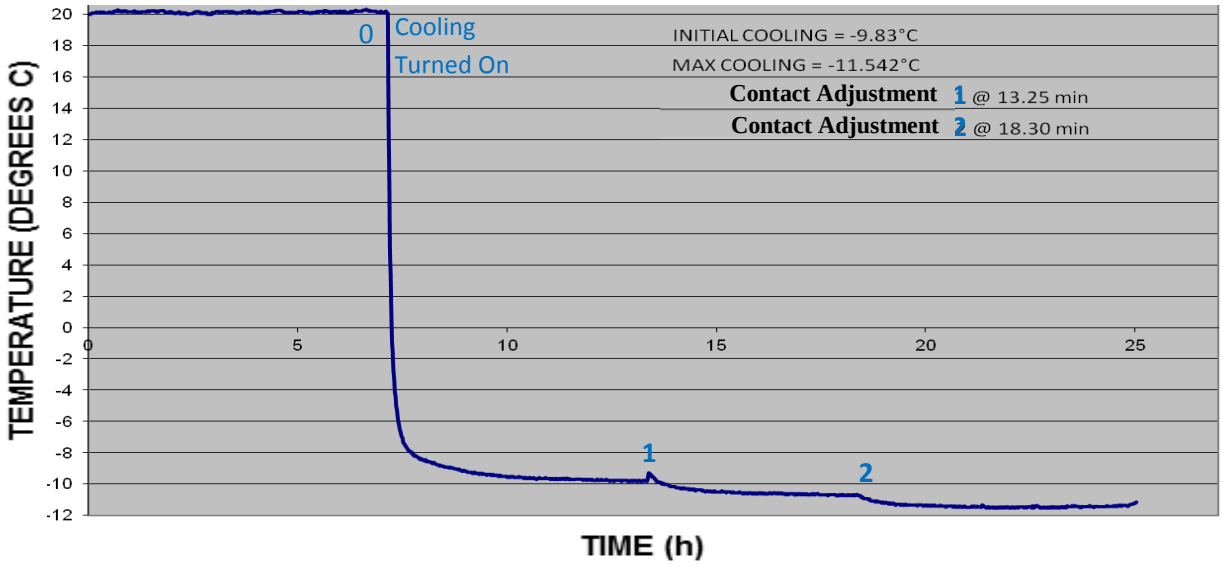

Figure 4.4: Effect of Arbitrary Contact Pressure Adjustments on Cooling Performance

Two pressure adjustments were made at 13.25 min and 18.30 min into the run and as can clearly be seen, there is a notable steady-state cooling response of roughly -1°C in both cases. This confirms that pressure at the surface boundary needs to be monitored and explored further. No change other than the increased applied surface pressure was made in the experiments in order to isolate the effect of pressure increase on cooling. Although the cold side temperatures remain fairly stable, there are great fluctuations in cooling from run to run. This is no doubt due to poor alignment attributed to the variable surface pressure test station that creates an inconsistent surface contact profile. Consistent data are necessary in order to characterize this cooling technique as reliable.

At this point the variable pressure rig has served its purpose for initial experimentation and an upgrade is needed to a pressure-monitored test rig mentioned previously. After making the necessary modifications, the secure test rig (including pressure monitoring load cell) was used for two more runs of the exact same test using the TEC and HS – 3. This time the pressure was set at 0.049 MPa (7.07 psi) for the first run and 0.20 MPa (28.3 psi) for the second run. The load cell was calibrated against standardized lab weights prior to use and the calibration curve is presented in the Appendix section. The results of these runs are displayed in Fig. 4.5.

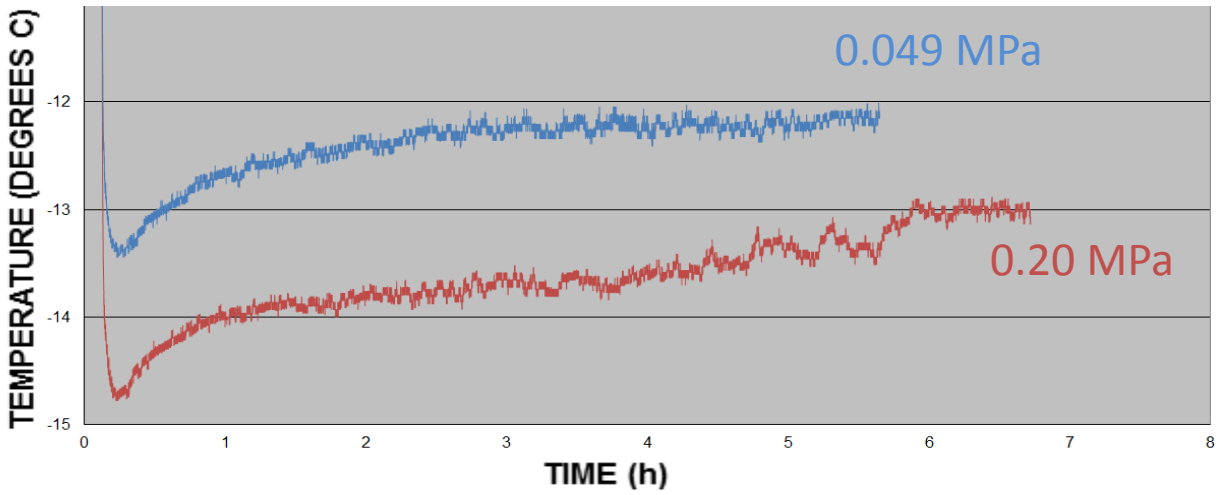

Figure 4.5: Effect of Increased Surface Pressure on Cooling Performance

It is clear that surface pressure has an effect on the cooling potential of the system. However, the change in cooling is relatively insignificant yielding only an average of 1.5°C of additional cooling in response to a fourfold increase in surface pressure after which no further cooling was observed. This is most likely due to the increased contact pressure with a higher number of solid-to-solid contact points as well as greater contact area as the asperities become deformed at the micro-level as shown in Fig. 4.2. Around an applied pressure of 0.24 MPa (35 psi), a plateau is reached where there are no further benefits to cooling as surface pressure is increased. At the plateau, a threshold pressure is reached where the surface profile no longer changes significantly to provide more contact area. Figure 4.3 validates this finding since a noticeable plateau is observed at around 0.28 MPa (40 psi) contact pressure for air as the interstitial material in between aluminum and ceramic surfaces. Thus, the contact resistance on average for the set of tests in Experiment 1 can be approximated using Fig. 4.3. For a contact pressure of 0.21 MPa (30 psi), a contact resistance of 1.5 cm^2·°C/W can be read from the graph for air as the interstitial material. If the contact area is divided out the absolute contact resistance can be determined as follows.

$$TEC_{Area} = TEC_{Length} \times TEC_{Width} = 3\ cm \times 3\ cm = 9\ cm^2 \tag{4.1}$$

$$R_{c,air} = \frac{R_{cont}}{TEC_{Area}} = \frac{1.5\ cm^2 \cdot ℃/W}{9\ cm^2} = 0.1667\ ℃/W = 0.1667\ K/W \tag{4.2}$$

A similar calculation can be done for the case of thermal grease as the interstitial material. Again, using Fig. 4-3 at a contact pressure of 0.21 MPa, a contact resistance of 0.125 cm^2·°C/W is recorded.

$$R_{c,grease} = \frac{R_{cont}}{TEC_{Area}} = \frac{0.125\ cm^2 \cdot ℃/W}{9\ cm^2} = 0.01389\ ℃/W = 0.01389\ K/W \tag{4.3}$$

Reviewing the calculations, the addition of thermal grease improves the heat transfer dynamics at the contact interface resulting in an order of magnitude drop in thermal contact resistance with the contact resistance involving air 1200 % greater than the case involving thermal grease. The

next experiment (Experiment 2) can verify this and provide additional insight into the other component thermal resistances.

4.1.3 Experiment 1 Summary

Experiment 1 highlights the importance of solid contact between surfaces and using proper interstitial materials to increase reduce thermal resistance along the interface profile while maintaining adequate surface pressure to increase contact points and heat transfer. It is clear that even slight changes made to contact profiles (between TEC and heat sink) have an effect on the cooling performance of the TEC. Although, raising the surface interface pressure fourfold did not seem to have a significant impact on relative cooling (only a 1.5°C decrease). Instead a threshold surface pressure of approximately 0.21 MPa (30 psi) was noted above which no significant additional cooling was observed.

The key findings in this experiment are that the cold side temperatures are stable (0.1°C/h warming rate) for at least a 5 h period and that sufficient contact pressure is needed to ensure maximum cooling. The focus now shifts to maximizing cooling performance (lower cold side temperatures) by incorporating the knowledge gained through Experiment 1.

4.2 Experiment 2 – Enhanced Cooling

The next step in the thermal management development process was to improve the actual cooling performance of the TEC. A target cold side temperature of at least -10°C was requested to demonstrate this as a proof of concept and although Fig. 4.5 shows cooling down to -13°C, this was not yet observed consistently. To make this enhancement in performance it was necessary to further upgrade the test configuration by adding thermal compound to the TEC / heat sink interface. This should reduce the thermal contact resistance as suggested in the previous section. The following results were obtained for the same test parameters conducted in the previous section using the TEC and HS – 3.

4.2.1 Cooling Performance Results

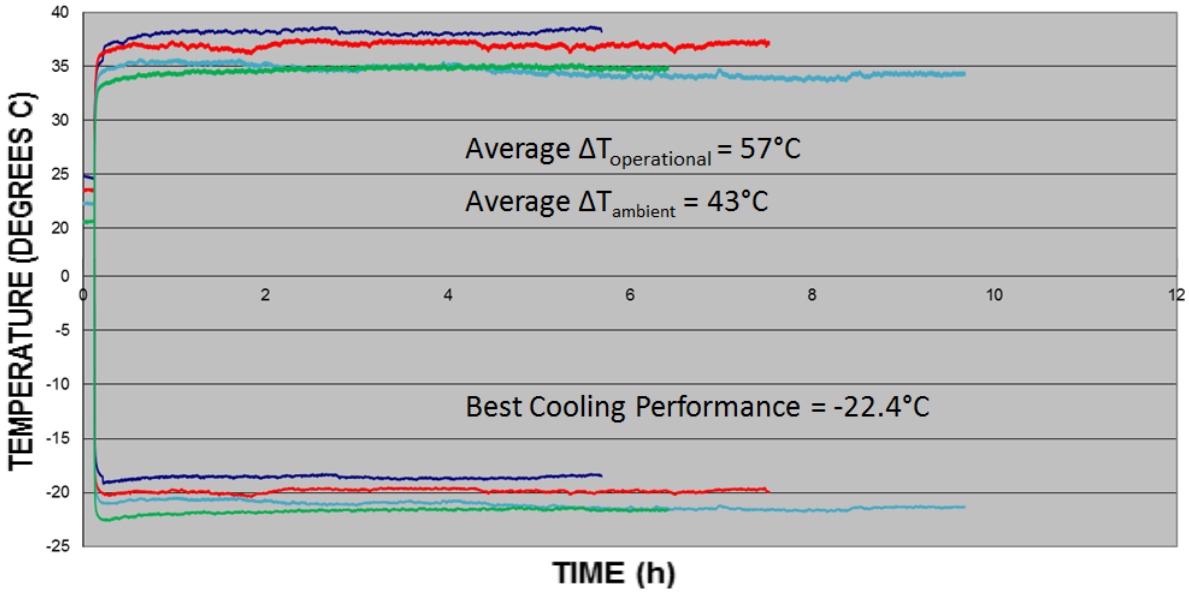

Figure 4.6: Cold and Hot Side Temperatures for TEC 1 / HS - 3 Using Enhanced Configuration

Figure 4.6 shows four test replicates on different days for the same TEC / heat sink combination (TEC, HS – 3). In this case the hot side temperatures were also displayed. It is important to note that the lowest cold side temperature achieved does depend on the ambient temperature. Also notable is the fact that the performance correlates linearly with the ambient temperature.

Corrected to operation in an ambient temperature of approx. 23°C (start of test), the average cold side temperature observed was -21°C with a ΔT = 57°C. This performance improvement confirms the importance of reducing thermal contact resistance mentioned previously. Both cold and hot junction temperatures show exceptional stability over long durations with an average warming rate of 0.11°C/h and 0.071°C/h for the cold and hot side respectively. The lowest temperature achieved at the cold side for any one run was observed to be -22.4°C which occurred on the coldest day (ambient temperature = 21°C). The results are very consistent regardless of day-to-day variations in ambient temperature (winter ≈ 20°C, summer ≈ 25°C). By removing the excess temperature (correcting to 23°C) it can be shown that there is little difference in TEC performance. This indicates that the TEC is performing reliably with minimal variations in heat pumping from run to run. Figure 4.7 illustrates a closer examination of the thermal resistance network and breaks down the results in a meaningful way for further analysis.

Table 4.2: Empirical Results

Symbol	Temp. Value
T_d	20°C
$\bar{T}_c$	-21.1°C
$\bar{T}_h$	36.2°C
$T_{b,max}$	Calculated 35.91°C
$\bar{T}_b$	34°C
$\bar{T}_f$	33.85°C
T_a	23°C

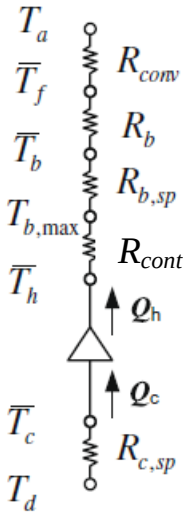

The individual thermal resistance values are displayed graphically via a thermal resistance network that represents the experimental layout. This is similar to Fig. 2.12 except for the constriction resistance which was considered negligible. The individual temperatures at each junction were measured directly from the experiment at steady-state (point at which no significant fluctuation in the cold and hot side temperatures were observed). $T_{b,max}$ was not measured due to the incredibly small distance between the TEC hot side and the heat sink base,

and instead, was back calculated using the contact thermal resistance determined from Eq. 4.3 ($R_{c,absolute\ grease} = R_{cont} = 0.01389\ K/W$).

$$R_{cont} = \frac{\Delta T}{Q_h} = \frac{\bar{T}_h - T_{b,max}}{Q_h} \tag{4.4}$$

$$T_{b,max} = \bar{T}_h - Q_h R_{cont} \tag{4.5}$$

The heat flow was determined by first calculating $R_b$which is the conduction resistance through the heat sink base with cross-sectional area A, thermal conductivity k of aluminum, and thickness L (Table 3.2). Then using Eq. 2.2, the heat flow Q_h can be calculated.

$$R_b = \frac{L}{kA} = \frac{0.0070\ m}{205\ \frac{W}{m\ K} \cdot 0.0048\ m^2} = 0.007114\ K/W \tag{4.6}$$

$$Q_h = \frac{\Delta T}{R_b} = \frac{\bar{T}_b - \bar{T}_f}{R_b} = \frac{307.15\ K - 307\ K}{0.007114\ K/W} = 20.09\ W \tag{4.7}$$

Since Q_h is constant at steady-state, $T_{b,max}$ can now be calculated using Eq. 4.5.

$$T_{b,max} = \bar{T}_h - Q_h R_{cont} = 309.35\ K - \left(20.09\ W \cdot 0.01389 \frac{K}{W}\right) = 309.06\ K\ or\ 35.91℃$$

All other component resistances can also be calculated in a similar manner. The thermal resistances $R_{b,sp}$ and R_{conv} are determined as follows.

$$R_{b.sp} = \frac{\Delta T}{Q_h} = \frac{T_{b,max} - \bar{T}_b}{Q_h} = \frac{309.06\ K - 307.15\ K}{20.09\ W} = 0.0951\ K/W \tag{4.8}$$

$$R_{conv} = \frac{\Delta T}{Q_h} = \frac{\bar{T}_f - T_a}{Q_h} = \frac{307\ K - 296.15\ K}{20.09\ W} = 0.54\ K/W \tag{4.9}$$

$R_{c,sp}$ is the spreading resistance between the target surface and the cold side of the TEC. This resistance determines how much heat can enter the cooled region. It is also calculated by dividing the temperature difference across the area of heat spreading by the cold side heat flow Q_c.

$$R_{c,sp} = \frac{\Delta T}{Q_c} = \frac{T_d - \bar{T}_c}{Q_c} = \frac{293.15\ K - 252.05\ K}{Q_c} = \frac{41.1}{Q_c} \tag{4.10}$$

A higher value of $R_{c,sp}$ should result in a lower Q_c, and ultimately, a lower level of cooling. This resistance value will be discussed more in section 4.4 as it pertains to the type of target surface used for cooling.

4.2.2 Model Comparison

Checking the resistance values against available models will help put the results in perspective. A model provided by Simons – 2010 allows one to estimate the cooling performance of thermoelectric devices using readily available vendor data. The resistance values obtained will be checked using this model and compared. In an earlier article provided by Luo – 2008, the following equations were presented for heat pumping with a thermoelectric cooling device.

$$Q_c = S_m T_c I - \frac{I^2 R_m}{2} - K_m(T_h - T_c) \tag{4.11}$$

$$Q_{TEC} = I S_m (T_h - T_c) - I^2 R_m \tag{4.12}$$

$$Q_h = Q_{TEC} + Q_c \tag{4.13}$$

However, in order to obtain estimates for heat pumping using these equations, the physical properties of the TEC need to be determined from available performance data. These properties

include the TEC Seebeck coefficient (S_m), TEC electrical resistance (R_m), and the TEC thermal conductance (K_m) [Luo – 2008].

$$S_m = 2\frac{Q_{max}}{I_{max}} \cdot \frac{1}{T_h + \Delta T_{max}} \tag{4.14}$$

$$K_m = \frac{T_h - \Delta T_{max}}{T_h + \Delta T_{max}} \cdot \frac{Q_{max}}{\Delta T_{max}} \tag{4.15}$$

$$Z = \frac{2\Delta T_{max}}{(T_h - \Delta T_{max})^2} \tag{4.16}$$

$$R_m = \frac{{S_m}^2}{K_m Z} \tag{4.17}$$

The values Q_{max}, I_{max}, and ΔT_{max} are typically given on a thermoelectric specification sheet at a set value for T_h as can be seen in Appendix B. It is also important to note that all temperature values must be in Kelvin when using these equations. Evaluating Eq. 4.11 - 4.17, the following values are obtained.

Table 4.3: TEC Specifications

Input Data 1: TEC Performance Characteristics			
Q_{max} (W)	I_{max} (A)	ΔT_{max} (K)	T_h (K)
33.4	4	67	398.2

Table 4.4: Model Estimates of TEC Properties

Output Data 1: TEC Physical Properties			
S_m (V/K)	K_m (W/K)	Z (1/K)	R_m (Ω)
0.0359	0.355	0.00122	2.972

Table 4.5: TEC Experiment Operating Conditions

Input Data 2: Operating Conditions				
T_h (K)	T_c (K)	I (A)	V (V)	T_a (K)
309.15	252.15	2.55	11.6	296.2

Table 4.6: Model Predicted Heat Pumping & Total Thermal Resistance

Output Data 2: Heat Pumping & Total Resistance			
Q_c (W)	Q_{TEC} (W)	Q_h (W)	R_t (K/W)
6.81	14.11	20.92	0.622

The total resistance was calculated using Eq. 2.2 which represents the total thermal resistance between the TEC hot side (T_h) and the ambient (T_a).

After reviewing the results it is clear that, yet again, the convective thermal resistance (R_{conv}) represents the greatest barrier to the cooling capability of the TEC. In the case of Experiment 2, R_{conv} represents 82.3% of total thermal resistance between the hot side of the TEC and the ambient. This confirms that the focus should be placed squarely on convective heat transfer in order to improve the overall device performance. The model predicted values of Q_h and R_t show agreement with the experimental results with minor deviations as seen in Table 4.7.

Table 4.7: Observed Values vs. Model Predictions

	Experimental Value	Model Value	Difference (%)
Q_h (W)	20.09	20.92	3.97
R_t (K/W)	0.6561	0.6215	5.57

Although the heat dissipation rate is relatively low (only 20 W approx.), it is important to note that the TEC used in the experiments is not advanced (1st generation device) and is only meant to show the importance of surface area of the combined heat sink assembly. Other experiments with larger budget limits can be conducted with 2nd and 3rd generation devices that can show substantially higher rates of cooling.

4.2.3 Experiment 2 Summary

The TEC used in Experiment 2 (TEC - 1) provided sufficient cooling (-21.1°C target surface temperature) when combined with heat sink HS – 3. The addition of thermal compound at the surface interface proved vital in providing consistent and enhanced cooling. After calculating the individual thermal resistances, once again it can be noted that the convective thermal resistance, R_{conv}, represents the most significant barrier to cooling (67 % of the total thermal resistance). This highlights the importance of convective heat transfer at the TEC hot side and the need for advanced heat sink designs. The experimental results show good agreement with predicted model values and are within a 5 % margin of error. Although the overall power dissipation was relatively low (20 W), the TEC used in experiment 2 is a 1^{st} generation device and was used only as a proof of concept. 2^{nd} and 3^{rd} generation devices would be able to pump significantly more heat as demonstrated in the introduction and literature review.

So it is evident that a TEC and heat sink combination can address thermal issues present in nanophotonics and related industries. The question now is if the design is feasible from a practical perspective and if its structural footprint can be reduced?

4.3 Experiment 3 - Thermal Management Scale Down

The next set of experiments is focused on reducing the structural footprint (occupying volume) of the TEC / heat sink thermal management system. The goal was to show that further reductions to the form factor of the components can be realized as improvements are made to the heat sinks by maximizing the exposed surface area. To accomplish this, a collection of heat sinks was evaluated for comparison purposes. In total five aluminum heat sinks were chosen to demonstrate that increasing the available surface area has a profound impact on the overall cooling performance.

4.3.1 Scale Down Results

	HS - 1	HS – 2	HS – 3	HS – 4	HS - 5
Surface Treatment	Bare	Anodized	Bare	Anodized	Anodized
Effective Volume	254 cm^3	196 cm^3	192 cm^3	75 cm^3	57 cm^3
Surface Area	1444 cm^2	1177 cm^2	1025 cm^2	174 cm^2	172 cm^2
S/V Ratio	5.68 cm^{-1}	6 cm^{-1}	5.33 cm^{-1}	2.32 cm^{-1}	3.02 cm^{-1}
Fin Spacing	1.5 mm	2 mm	2 mm	1.5 mm	2 mm
Fin Thickness	1 mm	0.75 mm	1 mm	2 mm	1.5 mm
Fin Height	31 mm	35 mm	32 mm	25 mm	15 mm
Weight	426 g	166.93 g	241.47 g	65.45 g	54.39 g
Base Thickness	12 mm	5 mm	7 mm	3 mm	2.5 mm

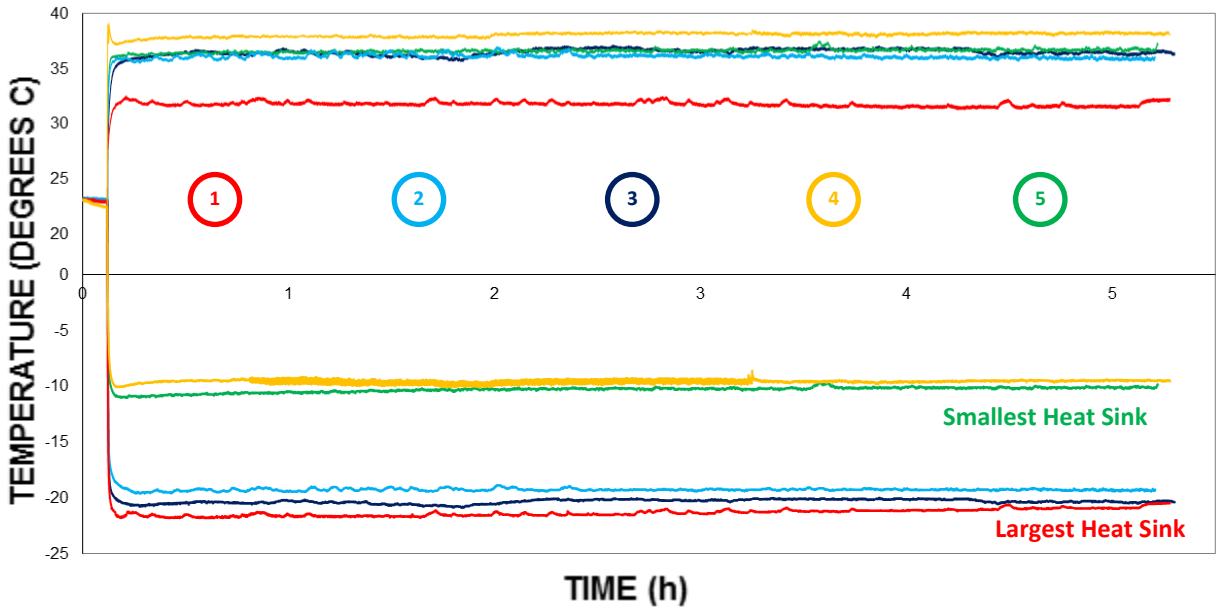

Figure 4.7: Cooling Performance of Heat Sinks (HS - 1 to HS - 5)

Figure 4.7 displays the results of repeated experiments carried out using the various heat sinks. In each case the same TEC and fan were used in order to standardize the comparison. Figure 4.7 shows a strong correlation between heat sink size and cooling capability. The largest heat sink HS – 1 was able to cool the rubber surface down to approximately -22°C while the smallest heat sink HS – 5 was able to cool the same surface to approximately -11°C. It is important to note here that the TEC input power was changed for the smaller heat sinks (HS – 4 and HS – 5) since they were not able to dissipate the same heat load as the larger heat sinks. However, one can compare HS – 1 and HS – 3 heat sinks since the TEC input power and fan speed was constant in each case (TEC 2.55 A 11.6 V, Fan 0.33 A, 27.5 V). The effect of reduced surface area can be predicted using the convective heat transfer equation (Eq. 4.18). From Fig. 4.7 the values of T_h can be read as an average over the experiment duration and compared with the predicted values.

$$Q_i = h_i A_i \Delta T_i \tag{4.18}$$

$$Q_1 = h_1 A_1 \Delta T_1$$

$$Q_3 = h_3 A_3 \Delta T_3$$

$Q_1 = Q_3$ and $h_1 = h_3$ since constant for both cases

$$\frac{Q_1}{Q_3} = \frac{h_1 A_1 \Delta T_1}{h_3 A_3 \Delta T_3} = \frac{A_1 \Delta T_1}{A_3 \Delta T_3} = 1$$

Substitute $A_3 = 0.71\ A_1$ as determined from Table 3.2

$$\frac{A_1 \Delta T_1}{0.71\ A_1 \Delta T_3} = 1$$

$$\frac{\Delta T_1}{\Delta T_3} = 0.71$$

The actual ratio observed from the experimental results in Fig. 4.7 can be calculated as follows.

$$\bar{T}_{f1} = 32℃$$
$$\bar{T}_{f3} = 35.5℃$$
$$T_a = 23℃$$

$$\Delta T_1 = \bar{T}_{f1} - T_a = 32℃ - 23℃ = 9℃$$
$$\Delta T_3 = \bar{T}_{f3} - T_a = 35.5℃ - 23℃ = 12.5℃$$

$$\frac{\Delta T_1}{\Delta T_3} = \frac{9℃}{12.5℃} = 0.72$$

Again the predicted effect of decreased surface area on heat sink temperature gradient shows good agreement with the actual observed ratio of the temperature difference. The results of Experiment 3 for all five heat sinks are presented in Table 4.8.

Table 4.8: Heat Sink Performance Breakdown

Heat Sink (#)	Volume (cm^3)	Surface Area (cm^2)	Lowest Temp. Achieved (°C)	TEC Power Input (W)	Fan Power Input (W)	S/V Ratio (cm^{-1})
1	254	1443.56	-21.8	31.4	9.21	5.68
2	196	1177.25	-19.5	30.8	9.18	6
3	192	1025.14	-20.7	31.2	9.02	5.33
4	75	173.72	-9.8	17.19	9.06	2.32
5	57	172.32	-11	16.6	9.05	3.02

The cooling performance improves with increases in both heat sink volume and surface area. A common method of capturing surface area "density" is known as the specific surface area measured in cm^{-1}. It is calculated by dividing the surface area available by the occupying volume of the object or heat sink in this case. As seen in the results, cooling capability correlates

positively with specific surface area also. This highlights the importance of high surface area heat sinks and their role in reducing the device structural footprint in future cooling applications. Metal foam heat sinks with specific surface areas of 150 cm^{-1} or higher can greatly improve the results observed above. In some cases, only minimal forced air may be required with sufficient pore densities available to dissipate the heat [Ozmat – 2007]. The porous nature of these heat sinks allows for passage of fluids with the pressure drop related to the pore density. For a given size, metallic foams can provide 5 – 10 times larger surface areas when compared to a similar sized flat plate. Some studies have shown that foam can be three times more efficient in cooling compared to pin fin heat sinks [Overclockers.com – 2005].

A further breakdown of the results, from a statistical point of view (Fig. 4.8), shows the strong correlation between the available surface area (area exposed to convection) and the overall cooling performance.

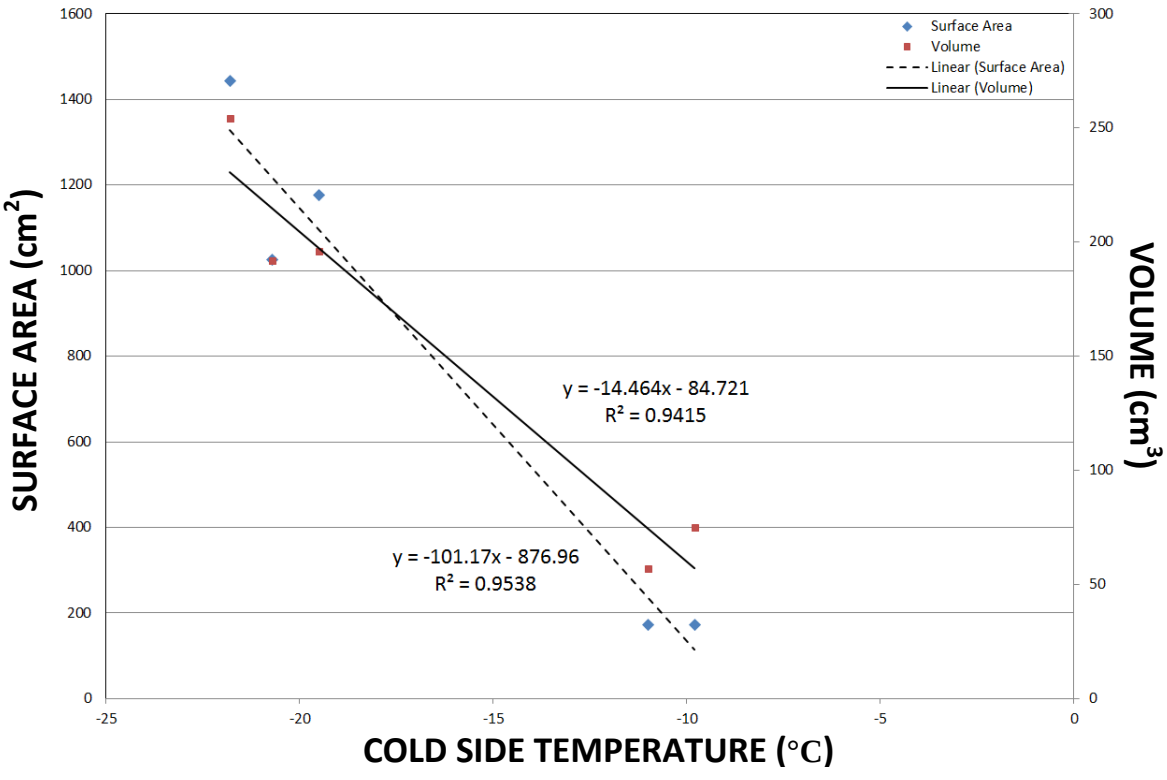

Figure 4.8: Correlation between Cooling Capability and Volume (Dark Line), Surface Area (Dashed Line)

The surface area was calculated manually by measuring the various surfaces contained in the internals of the heat sink. There is obviously some human error involved in this method but it establishes a frame of reference that can be used to assess other heat sinks. The available surface area is clearly important when it comes to cooling potential and will be the focus of future heat sink development among other items.

As for the TEC itself, one can reduce the area of cooling to a highly localized region by shrinking the TEC. A second TEC (TEC 2) was tested to demonstrate the local cooling capability of such devices. A comparative visual of this size reduction can be seen in Fig. 4.9 (a) and Fig. 4.9 (b).

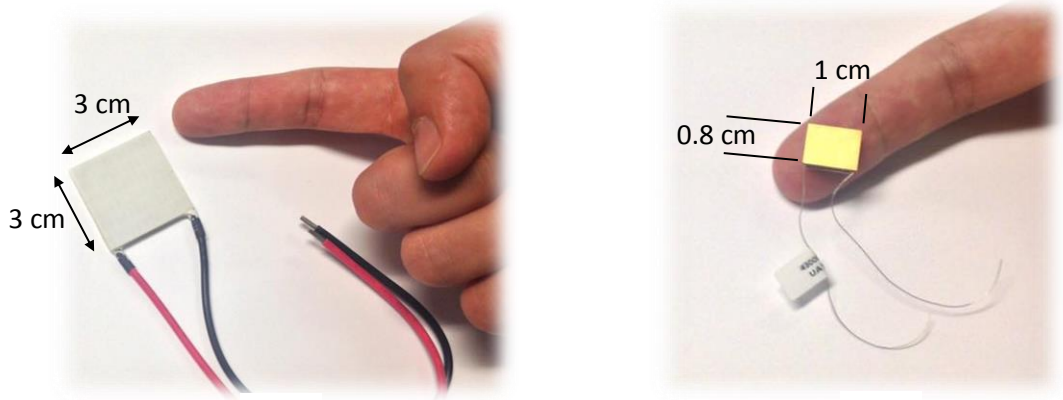

(a) (b)

Figure 4.9: (a) TEC 1 and (b) TEC 2 Size Comparison

Preliminary results for TEC 2, displayed in Fig. 4.10, show cooling down to -8°C on average which just falls short of the required surface temperature of -10°C. However TEC 1 and TEC 2 represent 1st and 2nd generation devices and with advances being made in the field of thermoelectrics, smaller and more powerful devices can be expected to be developed in the near future. Couple this with advances in high surface area heat sinks and the prospect of addressing an even more localized cooling region becomes more realistic and practical.

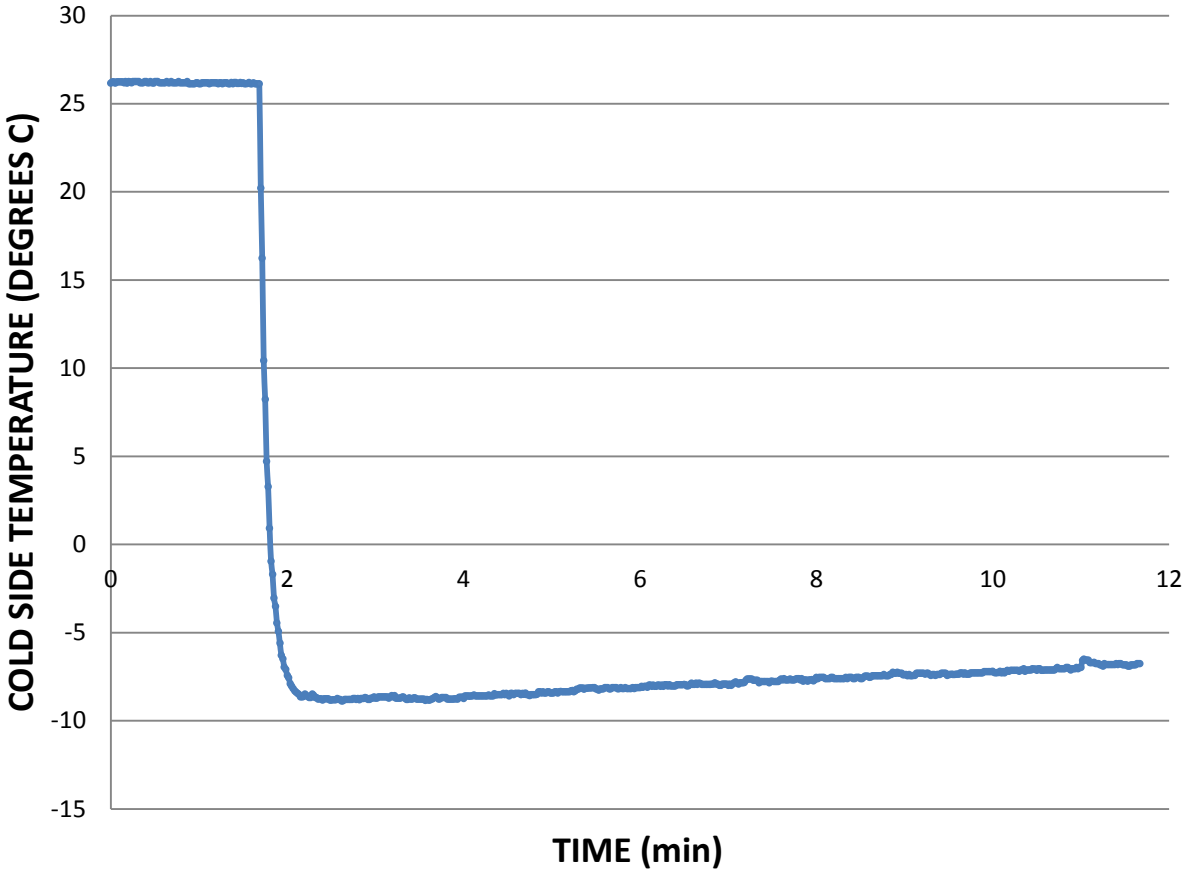

Figure 4.10: Cooling Performance of TEC 2 with HS – 5 on Rubber Surface

4.3.2 Experiment 3 Summary

Overall, the initial heat sink size of 254 cm^3 was reduced by 78% to 57 cm^3 by simply maintaining a sufficient exposed surface area to volume ratio (fins per unit volume) of the heat sinks, all the while maintaining a cold side temperature of at least -10°C. Statistically speaking, the effect of available surface area on observed cooling is greater than increased heat sink volume (stronger correlation). Thus, classifying heat sinks by their specific surface area (exposed surface area divided by the effective volume) is particularly useful when considering them for use in heat transfer applications. Continuing improvements such as introducing a phase change liquid and further size reductions to key components (fans, TEC, foam based heat sinks, etc.) can potentially help scale down the thermal management system even more.

4.4 Experiment 4 - Target Surface Analysis

The final set of experiments looked at the effect of the target surface on the achievable cold side temperature. In the first 3 experiments rubber was used as the target surface due to its deformability properties and relative ease-of-use. The setup for the experiments was therefore much simpler and quicker from run to run. However, rubber is not a practical option for a target surface as it is not widely used in electronics as a substrate. Ceramic and metallic surfaces are far more prevalent in electronics and thus need to be analyzed also. Initially, ceramic target surfaces were going to be primarily studied since they mimic closely the application of interest but due to difficulties in etching channels required for thermocouple insertion, this was abandoned. Instead, a comparative study of rubber and copper surfaces was conducted. Nevertheless, this experiment is still relevant since it is the thermal resistance of the surface that is of interest, with rubber and copper representing opposite ends of the heat transfer spectrum. The same experiments conducted in section 4.2 were used in this test with the only change being copper as the target surface.

4.4.1 Copper Surface Results

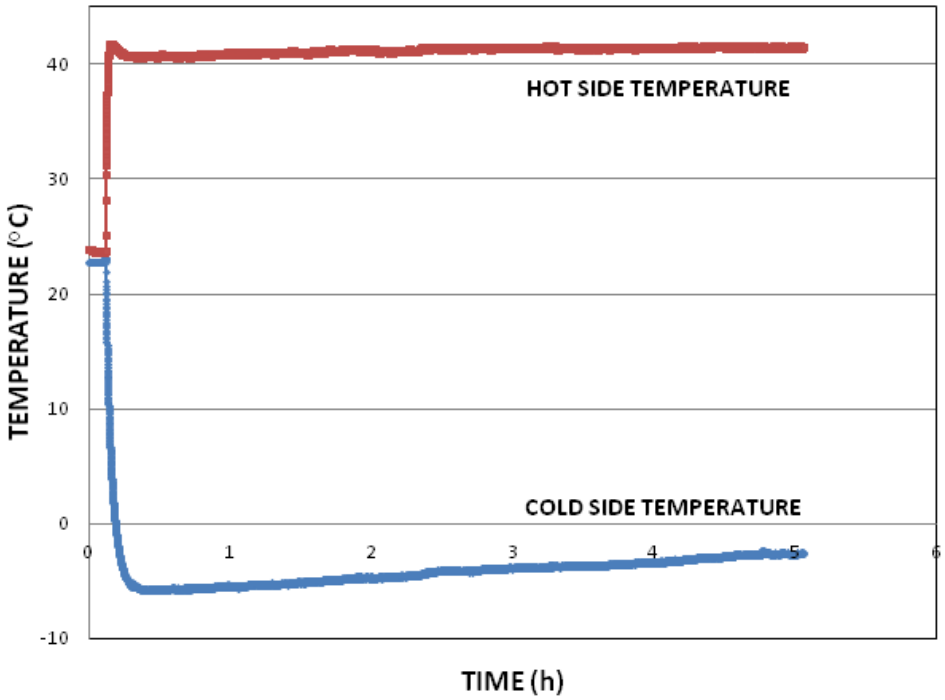

Figure 4.11: TEC 1 / HS - 3 Cooling Performance on Copper Target Surface

The TEC was again combined with HS – 3 in the exact same configuration as observed in section 4.2. The results of that experiment are shown in Fig. 4.11. Looking at Fig. 4.11 it is clear that the performance drops off considerably by switching the target surface from neoprene rubber to copper. The lowest temperature achieved in this scenario was -6°C with a warm up rate of 0.8°C/h which is 8 times higher than that observed with rubber as the target surface. The average cold side temperature was -3.75°C over the duration of the experiment. Upon examination of the thermal resistance network it is possible to explain this performance difference by analyzing the thermal conductivities of both surfaces.

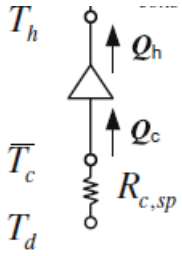

The focus in this case is $R_{c,sp}$, the spreading thermal resistance of the cold side target surface. Using copper as the target surface, T_d the surface edge temperature, was measured to be 0°C. $R_{c,sp}$ can be calculated using Eq. 4.19.

$$R_{c,sp} = \frac{\Delta T}{Q_c} = \frac{T_d - \bar{T}_c}{Q_c} = \frac{273.15\ K - 269.4\ K}{Q_c} = \frac{3.75}{Q_c} \tag{4.19}$$

Assuming a constant value for Q_c at steady-state the value of $R_{c,sp}$ in this case is much lower than the case where rubber was used as the target surface. Comparing the thermal conductivities of both surface materials it becomes obvious that copper has a much higher thermal conductivity (k = 401 W/m K) and therefore allows more heat to penetrate towards the desired cooling region on the cold side. Neoprene rubber on the other hand has a thermal conductivity of 0.19 W/m K which would help insulate against heat that could reach the cooled region. Also noticeable was the large amount of condensation produced in the scenario using copper as the target surface. Almost 10 mL of liquid condensate was collected from the area around the cooled region as well as a visible frozen exterior of the copper surface which was not visible in the case of rubber as

the target surface. This may explain the relatively high warm up rate when the copper surface was used since liquid condensate could have leaked into the cooled region.

4.4.2 Experiment 4 Summary

The impact of the target surface on desired cooling cannot be ignored. The higher the thermal conductivity of the target surface, the higher amount of thermal leakage should be expected. Since most integrated electronic systems use materials that are highly thermally conductive, this can present a challenge when it comes to localized cooling. In addition, condensation is greater if the thermal conductivity of the surface is higher. Nearly 10 mL of liquid condensate was collected from the copper surface at the end of the experiment which was not observed in the rubber surface experiment. From a thermal resistance standpoint, the rubber surface restricts heat flow into the cooling region and minimizes both leakage and condensation.

Chapter 5 – Conclusions and Recommendations

In summary, the project set out to assess the feasibility and practicality of implementing a TEC-based thermal management system for use in electronic packaging and in particular, for spectrometers in the nanophotonics industry. The key questions that needed to be answered centered on temperature stability, cooling capability, and scale down potential.

As far as maintaining a consistent temperature, there was no significant increase in temperatures once steady-state had been reached (on average 2 min into testing). An average warming rate of 0.10°C/h was observed for both the hot and cold side temperatures. In some cases, the temperatures decreased even further over time although at a much reduced rate. Temperature stability was observed in each case for a minimum of 5 hours.

Delivering at least -10°C temperature at the cold junction between the TEC and target surface proved to be feasible. The best cooling performance attained was -22.4°C, although the average maximum cooling, corrected to operation in 23°C ambient temperature, was approximately -21.5°C. Condensation was observed at these temperatures and it will need to be addressed in future experiments. Therefore, it is important to take into consideration the ambient conditions in order to put the results in perspective.

The overall size of the thermal management system was reduced 78% from the starting design to 57 cm^3. The results show a strong correlation between the exposed surface areas in the heat sink and the cooling capability. This factor will be the focus of future heat sink development, along with introducing phase change liquids and other micro-scale components.

The following are some recommendations and next steps regarding future research and development in this area:

1) Look further into methods to improve surface-to-surface contact

2) Quantify in a meaningful way the severity of condensation that occurs during operation
3) Investigate metallic sponges and microchannels to maximize the available surface area for heat transfer
4) Introduce phase change fluids to leverage heat transfer from the latent heat of vaporization (similar to heat pipes)
5) Source micro-components such as fans and TECs to address an even smaller region for cooling
6) Attempt to reduce the power consumption of the components if there are constraints
7) Test the system in various environments to determine robustness
8) Use a greater range of target surfaces to conduct the tests and compare results
9) Compare the costs of the different thermal management designs to determine the most economical option
10) Test thermal management system in a prototype spectrometer to determine effectiveness in the field
11) Investigate various materials that can be upgraded for better heat transfer (use of copper, thermal interface compound, etc.)
12) Improve heat sink design to minimize fluid pressure drop across fins

There is a strong case to be made regarding the practicality of an advanced TEC-based thermal management system for use in nanophotonics. The results presented above merely introduce the topic and the results demonstrate that there is great potential for further developments. A phase 2 research proposal is currently being discussed in hopes of continuing the progress achieved in this thesis.

References

[1] Asia Vital Components [2010] Relative Power Dissipation Plot. Asia Vital Components – Retrieved December, 2014 From – http://www.avc.com.tw/news_detail.asp?id=270

[2] Azar, K. [2000] The History of Power Dissipation. Electronics-Cooling.com – Retrieved October, 2014 From – http://www.electronics-cooling.com/2000/01/the-history-of-power-dissipation/

[3] Bale, G., Holland, A., Seller, P., Lowe, B. [1999] Cooled CdZnTe Detectors for X-Ray Astronomy. Nuclear Instruments and Methods in Physics Research – A 436, pp. 150 – 154

[4] Boppart, S. [2007] OCT Image of Sarcoma. Biophotonics Imaging Laboratory, University of Illinois at Urbana-Champaign. EB 005221 – NIBIB, Retrieved June, 2014 From – http://en.wikipedia.org/wiki/Sarcoma#mediaviewer/File:Nibib_030207_105309_sarcoma.jpg

[5] Buyincoins.com [2014] 12V 60W TEC1-12706 Thermoelectric Cooler Peltier Description. Retrieved June, 2014 From – http://www.buyincoins.com/images/review/1292049635-003.png

[6] Burris, M. [2015] Introduction to Thermal Management. – Retrieved March, 2014 From – http://components.about.com/od/Themal/a/Introduction-To-Thermal-Management.htm

[7] BWTEK.com [2015] Part 3a: The Detector. Retrieved January, 2014 From – http://bwtek.com/spectrometer-part-3a-the-detector/

[8] BWTEK.com [2015] Part 3b: The Detector. Retrieved January, 2014 From – http://bwtek.com/spectrometer-part-3b-the-detector/

[9] Chamberland, M., Farley, V., Vallieres, A., Villemaire, A., Belhumeur, L., Giroux, J., Legault, J.F. [2005] High-Performance Field-Portable Imaging Radiometric Spectrometer Technology for Hyperspectral Imaging Applications. Proceedings of SPIE – Vol. 5994

[10] Chang, Y.W., Chang, C.C., Ke, M.T., Chen, S.L. [2009] Thermoelectric Air-Cooling Module for Electronic Devices. Applied Thermal Engineering – Vol 29, pp. 2731 – 2737

[11] Chang, Y.W., Cheng, C.H., Wu, W.F., Chen, S.L. [2007] An Experimental Investigation of Thermoelectric Air-Cooling Module. International Journal of Mechanical, Aerospace, Industrial and Mechatronics Engineering – Vol. 1 No. 9, pp. 495 – 500

[12] Coulton, S. [2015] Condensation and Electronics. Kooltronic Inc. – Retrieved December, 2014 From – http://www.kooltronic.com/downloads/K1213.pdf

[13] Custom Thermoelectric [2007] TEC Specification Sheet. Rev. 4-15-2007 Retrieved June, 2014 From – http://www.customthermoelectric.com/tecs/pdf/12711-5L31-03CL_spec_sht.pdf

[14] Domingo, J. [2011] Ensuring Optimal High Power LED Performance with Thermal Management. Electronic Component News – Retrieved December, 2014 From – http://www.ecnmag.com/articles/2011/04/ensuring-optimal-high-power-led-performance-thermal-management

[15] Dunnivant, F. [2008] Components of a Flame Atomic Absorption/Emission Spectrometer System. Whitman College, Walla Walla, WA Retrieved January, 2015 From – http://people.whitman.edu/~dunnivfm/FAASICPMS_Ebook/CH2/2_2_9.html

[16] Ellsworth, M.J. [2005] High Powered Chip Cooling – Air and Beyond. Electronics-Cooling.com – Retrieved November, 2014 From – http://www.electronics-cooling.com/2005/08/high-powered-chip-cooling-air-and-beyond/

[17] Flir.com [2015] Cooled or Uncooled? Flir.com – Retrieved October, 2014 From – http://www.flir.com/science/display/?id=65982

[18] Frostytech.com [2010] Copper Heat Sink Image. Frostytech.com – Retrieved December, 2014 From – http://www.frostytech.com/articleview.cfm?articleid=2424&page=9

[19] Futuretimeline.net [2012] Microchip Transistor Sizes. Futuretimeline.net – Retrieved September, 2014 From – http://www.futuretimeline.net/subject/computers-internet.htm

[20] Hamamatsu.com [2013] What is the Micro PMT? Hamamatsu.com – Retrieved October, 2014 From – http://www.hamamatsu.com/us/en/community/optical_sensors/tutorials/what_is_micro_pmt/index.html

[21] Hickey, T. [2002] Temperature Dependence of Dark Current in Quantum Well Infrared Detectors. Master's Thesis – United States Navy Postgraduate School, Monterey, CA, USA

[22] Intechopen.com [2012] Photodetectors. – Retrieved October, 2014 From – http://www.intechopen.com/books/photodetectors

[23] Interfaceforce.com [2015] 1100 Ultra Precision LowProfile Load Cell – Retrieved May, 2014 From – http://www.interfaceforce.com/index.php?1100-Ultra-Precision-LowProfile-Load-Cell&mod=product&show=3

[24] Janesick, J.R. [2001] Scientific Charge-Coupled Devices. Washington – SPIE

[25] Keithley. [2002] Model 2700 Multimeter Data Acquisition System: User's Manual. Keithley Instruments Inc. Retrieved September, 2014 From – http://www.ee.bgu.ac.il/~acl/Equip/2700_900_01fnl.pdf

[26] Kleinfeld, D. [1979] Summary on Noise and Signal-to-Noise in Photodetector Systems. Retrieved June, 2014 From - https://physics.ucsd.edu/neurophysics/lab/DK_Photodetector_Noise.pdf

[27] Kumar, V. [2007] Heat Transfer Studies of a Heat Pipe. Heat Transfer Engineering – Vol. 28 No. 11, pp. 954 – 965

[28] Kurweil, R. [2005] The Singularity is Near: When Humans Transcend Biology. Viking Penguin – New York

[29] Lasance C. J. M. [2005] Advances in High Performance Cooling for Electronics. Retrieved June, 2014 From – http://www.electronics-cooling.com/2005/11/advances-in-high-performance-cooling-for-electronics/

[30] Luo, Z. [2008] A Simple Method to Estimate the Physical Characteristics of a Thermoelectric Cooler from Vendor Datasheets. Retrieved June, 2015 From – http://www.electronics-cooling.com/2008/08/a-simple-method-to-estimate-the-physical-characteristics-of-a-thermoelectric-cooler-from-vendor-datasheets/

[31] MacDonald, D.K.C. [1962] Thermoelectricity: An Introduction to the Principles. John Wiley & Sons – New York

[32] Mayer, P. M., Ram, R. J. [2006] Optimization of Heat Sink Limited Thermoelectric Generators. Nanoscale and Microscale Thermophysical Engineering – 10, pp. 143 – 156

[33] Moffat, R.J. [1999] Uncertainty Analysis. Retrieved June, 2015 From – http://www.electronics-cooling.com/1999/05/uncertainty-analysis/

[34] Mountain, C.M., Robertson, D.J., Lee, T.J., Wade, R. [1990] An Advanced Cooled Grating Spectrometer for UKIRT. SPIE Vol 1235 Instrumentation in Astronomy VII, pp. 25 – 33

[35] Overclockers.com [2005] Copper Foam Heat Sink. – Retrieved May, 2015 From – http://www.overclockers.com/copper-foam-heatsink/

[36] Ozmat, B. [2007] Reticulated Metal Foams Build Better Heatsinks. – Retrieved May, 2015 From – http://powerelectronics.com/thermal-management/reticulated-metal-foams-build-better-heatsinks

[37] Personal Correspondence 1. [2014] Phone conference 1 with Tornado Spectral Systems representatives Arsen Hajian and Andrew Cenko. January 2014, University of Waterloo, Ontario, CA

[38] Personal Correspondence 2. [2015] Phone conference 2 with Tornado Spectral Systems representatives Arsen Hajian and Andrew Cenko. March, 2014. University of Waterloo, Ontario, CA

[39] Prasad, P.N. [2004] Nanophotonics. John Wiley & Sons – New Jersey

[40] Redus, R.H., Huber, A.C., Pantazis, J.A. [2001] Thermoelectrically Cooled X/γ-ray Detectors and Electronics. Nuclear Instruments and Methods in Physics Research – A 458, pp. 214 – 219

[41] Rieder, R., Economou, T., Wanke, H., Turkevich, A. [1997] Determination of the Chemical Composition of Martian Soil and Rocks: The Alpha Proton X Ray Spectrometer. Journal of Geophysical Research – Vol 102 [2], pp. 4027 – 4044

[42] Riffat, S.B., Ma, X. [2004] Improving the Coefficient of Performance of Thermoelectric Cooling Systems: A Review. International Journal of Energy Research – Vol 28, pp. 753 – 768

[43] Shiokawa, K., Kadota, T., Otsuka, Y., Ogawa, T., Nakamura, T., Fukao, S. [2003] A Two-Channel Fabry-Perot Interferometer with Thermoelectric – Cooled CCD Detectors for Neutral Wind Measurement in the Upper Atmosphere. Earth Planets Space – Vol 55, pp. 271 – 275

[44] Silk, E. [2004] Spray Cooling of Electronics Image. NASA – Retrieved December, 2014 From – http://mscweb.gsfc.nasa.gov/msctech/spraycooling.htm

[45] Simons, R. [2010] Calculation Corner: Using Vendor Data to Estimate Thermoelectric Module Cooling Performance in an Application Environment. Retrieved June, 2015 From – http://www.electronics-cooling.com/2010/07/using-vendor-data-to-estimate-thermoelectric-module-cooling-performance-in-an-application-environment/

[46] Simons, R.E., Chu, R.C. [2000] Application of Thermoelectric Cooling to Electronic Equipment: A Review and Analysis. Sixteenth IEEE SEMI-THERM Symposium

[47] Sparrow, E. [2010] ME 3333 Lecture Essay. University of Minnesota, Minneapolis, MN Retrieved January, 2015 From – http://www.me.umn.edu/courses/old_me_course_pages/me3333/essays/essay%203.pdf

[48] Stucki, D., Ribordy, G., Stefanov, A., Zbinden, H., Rarity, J.G., Wall, T. [2001] Photon Counting for Quantum Key Distribution with Peltier Cooled InGaAs / InP APDs. Journal of Modern Optics – Vol 48 [13], pp. 1967 – 1981

[49] Tada, H. [2002] EN43ME Lecture Notes. Tufts University, Medford, MA – Retrieved December, 2014 From – http://www.tufts.edu/as/tampl/en43/lecture_notes/ch5.html

[50] Teertstra, P. [1997] Calculating Interface Resistance. Retrieved June, 2015 From – http://www.electronics-cooling.com/1997/05/calculating-interface-resistance/

[51] Thermopedia.com [2011] Thermal Contact Resistance – Retrieved May, 2015 From – http://www.thermopedia.com/content/1188/

[52] Thome J. R. [2006] State–of–the–Art Overview of Boiling and Two–Phase Flows in Micro–Channels. Heat Transfer Engineering – Vol 27 [9], pp. 4 – 19

[53] Thorlabs Inc. [2014] 3D OCT Data of in Vitro Porcine Artery Wall. Retrieved June, 2014 From – http://www.thorlabs.com/laserimaging/index.cfm?pageref=30&page=OCT-Blood-Vessel

[54] Timmerhaus, K.D., Reed, R.P. [2007] Cryogenic Engineering – Fifty Years of Progress. International Cryogenics Monograph Series, Springer – New York

[55] Toon, J. [2005] Beating the Heat: Liquid Cooling Technique Uses Microfluidic Channels Integrated onto the Backs of Chips. Georgia Institute of Technology, Atlanta, GA – Retrieved May, 2015 From – http://www.gtresearchnews.gatech.edu/newsrelease/cooling.htm

[56] Tornado Spectral Systems [2013] OCT for Non-Destructive Testing (NDT) - Nanophotonic Spectroscopy. Retrieved June, 2014 From – http://tornado-spectral.com/wp-content/uploads/2013/06/TSS_app-note_OCT-NDT.pdf

[57] Tuckerman, D.B., Pease, R.F.W. [1981] High-Performance Heat Sinking for VLSI. IEEE Electron Device Letters – Vol. 2 No. 5, pp. 126 – 129

[58] Upadhya, G., Zhou, P., Hom, J., Goodson, K., Munch, M. [2004] Electro-Kinetic Microchannel Cooling System for Servers. Inter Society Conference on Thermal Phenomena – pp. 367 – 371

[59] van Es, J., van Gerner, H.J. [2013] Benefits and Drawbacks of using Two-Phase Cooling Technologies in Military Platforms. Electronics-Cooling.com – Retrieved December, 2014 From – http://www.electronics-cooling.com/2013/03/benefits-and-drawbacks-of-using-two-phase-cooling-technologies-in-military-platforms/

[60] Virtual Outcrop Geology Group [2014] Ground-Based Hyperspectral Imaging for Geological Outcrop Analysis. CIPR – University of Bergen, Bergen Norway

[61] Wgsimon. [2011] Microprocessor Transistor Counts and Moore's Law. Wikipedia.org – Retrieved November, 2014 From – http://en.wikipedia.org/wiki/Moore's_law#mediaviewer/File:Transistor_Count_and_Moore%27s_Law_-_2011.svg

[62] Wilcox, J.R., Grosskopf, C.T., Kelly, M.S., Cole, M.S. [2011] Managing Temperature Sensitive Components in Pb-free Power Assemblies. IBM Power Symposium, Research Triangle Park, NC, USA. Retrieved September, 2014 From – http://www-03.ibm.com/procurement/proweb.nsf/7a84535a0acd580885256b3f000e250a/526ec552cd0da6c7852578a1006c7e45/$FILE/6-IBM-Wilcox-Power%20Symp%202011%20-%20TSC%20Mgmt.pdf

[63] Wolpert, D., Ampadu, P. [2012] Managing Temperature Effects in Nanoscale Adaptive Systems. Springer Publishing – New York

[64] Yadav, L.D.S. [2005] Organic Spectroscopy. Springer Publishing – Netherlands

[65] Yeh, L.T. [1995] Review of Heat Transfer Technologies in Electronic Equipment. Journal of Electronic Packaging – Vol. 117, pp. 333 – 339

Appendix A – Surface Pressure Calibration

Voltage (V)	Mass (kg)	Mass (lbs)	Force (N)	Surface Pressure (Pa)	Surface Pressure (kPa)	Surface Pressure (psi)
0.5	2.235	4.917	21.92535	24361.5	24.3615	3.533336854
1	4.476	9.8472	43.90956	48788.4	48.7884	7.076159177
1.495	6.714	14.7708	65.86434	73182.6	73.1826	10.61423876
2.026	9.084	19.9848	89.11404	99015.6	99.0156	14.36099865
2.526	11.325	24.915	111.0983	123442.5	123.4425	17.90382097

TEC 1 Surface Area

Length (m)	0.03
Width (m)	0.03
Area (m^2)	0.0009

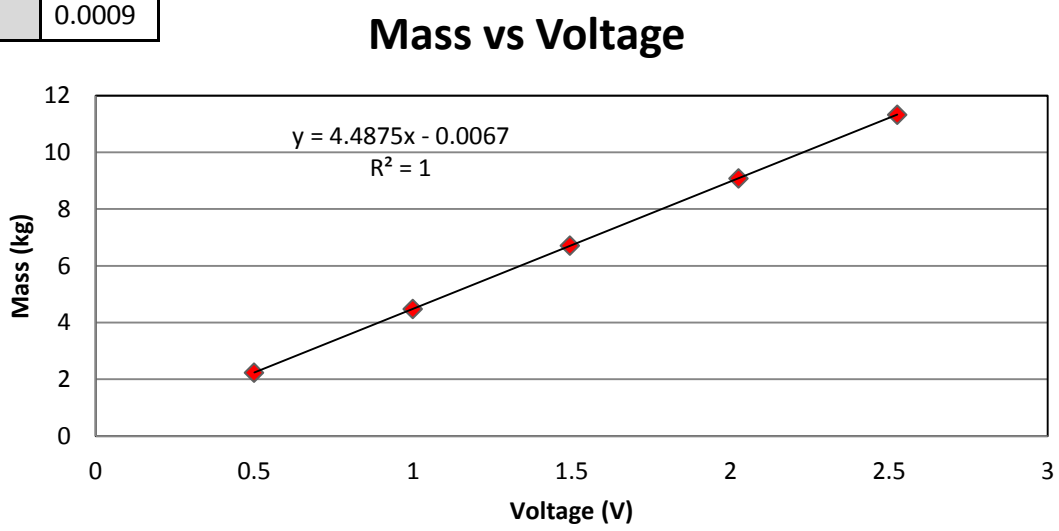

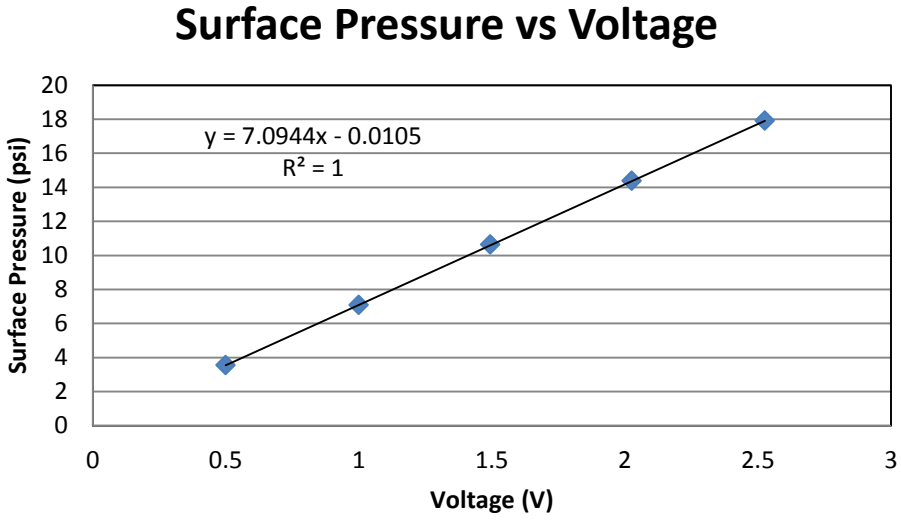

Appendix B – TEC Vendor Data

TEC Specification Sheet

CUSTOM THERMOELECTRIC
Your Thermoelectric Partner

Part #	I_{max} (Amps)	Q_{max} (Watts)	V_{max} (Volts)	DT_{max} (°C)	T_{max} (°C)
12711-5L31-04CL	4.0	33.4	15.4	67°C	125°C

(TEC 1)

Lapped

X_n Codes:

X_2=Wire type. See Wire type codes or call for custom wires.

X_3=Height Tolerance specification. See Tolerance codes or call for custom tolerances.

X_4=Options. See Options codes or call for custom options.

Bottom Plate				Top Plate				Metallized Height		Lapped Height	
A		B		C		D		H		H	
mm	in	mm	in	mm	in	mm	in	mm	in	mm	in
30.0	1.18	30.0	1.18	30.0	1.18	30.0	1.18	NA	NA	3.3	.130

Weight (w/o leads)
10 grams

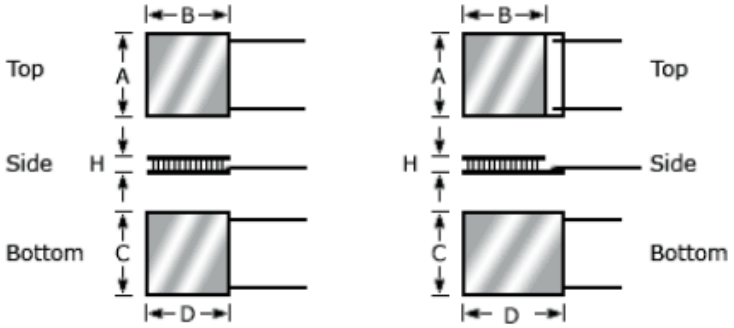

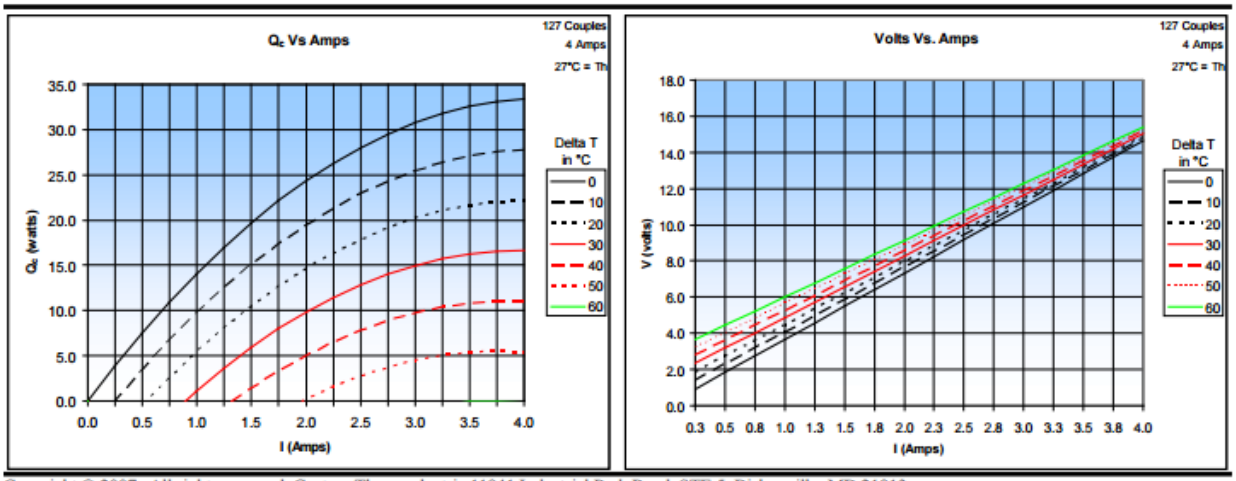

Laird
Smart Technology. Delivered.

(TEC 2)

Tlam OptoTEC™ Series OT08,66,F0T,1009 Thermoelectric Module

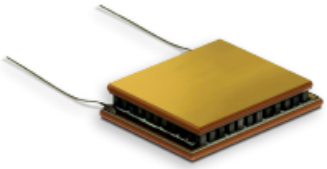

The Tlam OptoTEC™ Series is a miniature thermoelectric module (TEM) that uses a thermally conductive dielectric with copper exteriors as substrates. This product line has improved heat spreading, higher mechanical integrity and can provide cost savings over standard ceramic based TEMs with similar form factors in high volume. This product series has been created for applications to stabilize the temperature of sensitive optical components in telecom, photonics, medical and consumer markets.

This product line is available in multiple configurations and surface finishing options. The Tlam OptoTEC™ Series is designed for lower current and lower heat-pumping applications and are easily customizatable to accomodate alternate sizes, heat pumping capacities, pretinning, unique circuit patterns, or solder posts, however MOQ applies.

FEATURES RoHS

- Miniature geometric sizes
- Precise temperature control
- Reliable solid state operation
- No sound or vibration
- DC operation
- RoHS compliant

APPLICATIONS

- Laser diodes
- CCD cameras
- Infrared (IR) sensors
- Pump lasers
- Crystal oscillators
- Optical transceivers

PERFORMANCE SPECIFICATIONS		
Hot Side Temperature (°C)	25	50
Qmax (Watts)	3.6	4.0
Delta Tmax (°C)	67	77
Imax (Amps)	0.8	0.8
Vmax (Volts)	7.6	8.5
Module Resistance (ohms)	8.61	9.71

SUFFIX	THICKNESS (PRIOR TO TINNING)	FLATNESS & PARALLELISM	HOT FACE	COLD FACE	LEAD LENGTH
22	0.114"± 0.005"	NA / NA	Pre-tinned	Pre-tinned	2.0"
GG	0.114"± 0.005"	NA / NA	Au plated	Au plated	2.0"

SEALING OPTION

SUFFIX	SEALANT	COLOR	TEMP RANGE	DESCRIPTION
RT	RTV	White	-60 to 204 °C	Non-corrosive, silicone adhesive sealant
EP	Epoxy	Black	-55 to 150 °C	Low density syntactic foam epoxy encapsulant

Americas: +1 888.246.9050
Europe: +46.31.704.67.57
Asia: +86.755.2714.1166

clv.customerpos@lairdtech.com
www.lairdtech.com

Laird
Smart Technology. Delivered.

(TEC 2)

Tlam OptoTEC™ Series
OT08,66,F0T,1009
Thermoelectric Module

PERFORMANCE CURVES

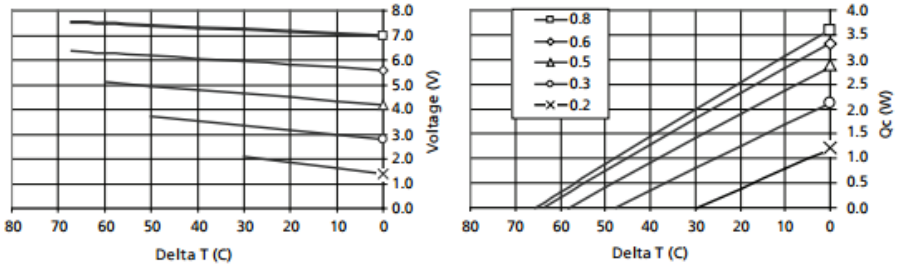

MECHANICAL DRAWING

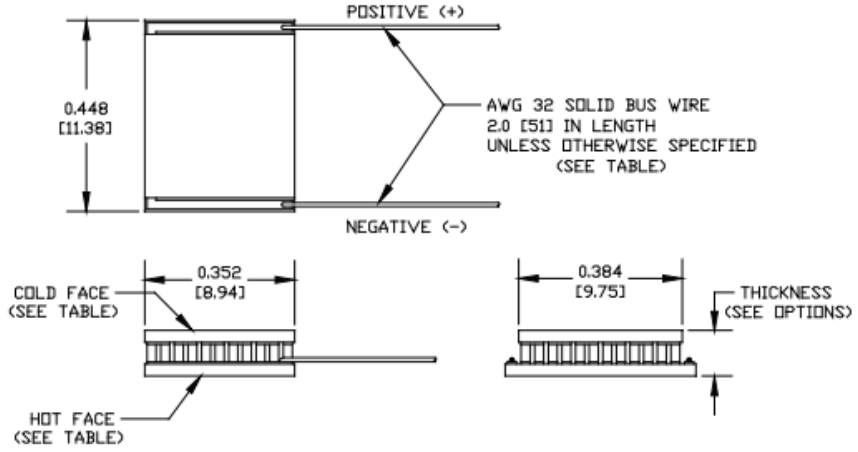

Ceramic Material 96% Alumina Ceramics
Solder Construction: 138°C, Bismuth Tin

OPERATING TIPS

- Max Operating Temperature: 80°C
- Do not exceed Imax or Vmax when operating module
- Reference assembly guidelines for recommended installation
- Solder tinning also available on metallized ceramics

Appendix C – Fan Specs

600N Series Tubeaxial

60x60x25mm

- DC fans with electronically commutated external rotor motor. Fully integrated commutation electronics.
- With electronic protection against reverse polarity, blocking and overloading.
- Mounting from either face using four 3.7 mm holes.
- Fan of fiberglass reinforced plastic. PBTP housing, PA impeller.
- Air exhaust over struts, Rotational direction CCW looking at rotor.
- Electrical connection via 2 leads AWG 22, TR 64. Stripped and tinned ends.
- UL, CSA, VDE approvals on most models, please contact application engineering.

Part Number	Curve	CFM @ 0	VDC	Volt. Range	Power (W)	dBA	Max Amb. Temp C	Bearing Type	Features	Wgt. (lbs)
612NLE	1	12.4	12	8 to 15	0.4	16	85	Ball	Leads	0.19
612NMLE	2	14.7	12	8 to 15	0.4	19	85	Ball	Leads	0.19
612NME	3	20.6	12	8 to 15	0.8	28	75	Ball	Leads	0.19
612NN	4	24.7	12	8 to 15	1.6	35	70	Ball	Leads	0.19
612NH	5	27.1	12	8 to 15	2.0	38	70	Ball	Leads	0.19
612NHH	6	33.0	12	8 to 13.2	3.0	43	70	Ball	Leads	0.19
614NL	1	12.4	24	18 to 28	0.9	16	70	Ball	Leads	0.19
614NML	2	14.7	24	18 to 28	1.0	19	70	Ball	Leads	0.19
614NM	3	20.6	24	18 to 28	1.4	28	70	Ball	Leads	0.19
614NN	4	24.7	24	18 to 28	1.8	35	70	Ball	Leads	0.19
614NH	5	27.1	24	18 to 26	2.1	38	70	Ball	Leads	0.19
614NHH	6	33.0	24	18 to 26	3.0	43	70	Ball	Leads	0.19
618NN	4	24.7	48	36 to 56	2.1	35	65	Ball	Leads	0.19

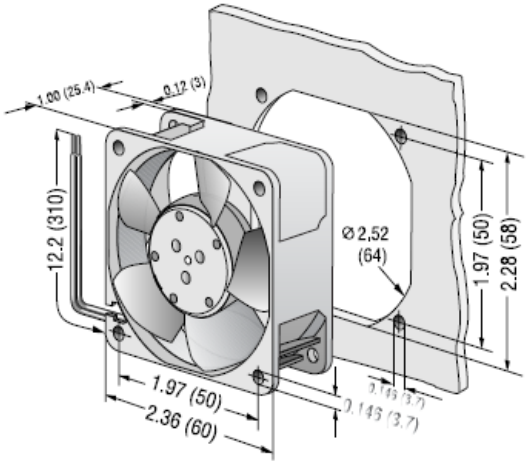

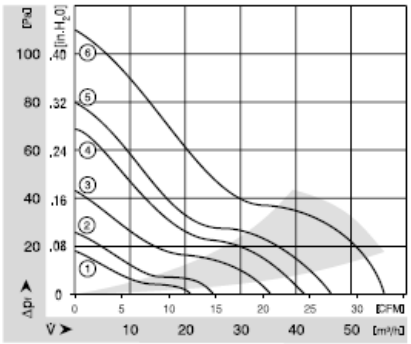

ebmpapst

e-mail: sales@us.ebmpapst.com · TEL: 860-674-1515 · FAX: 860-674-8536
ebm-papst Inc., 100 Hyde Road, Farmington, CT 06034 USA

Appendix D – Load Cell Specs

SPECIFICATIONS

PARAMETERS	MODEL				
	1110	1110	1120	1132	1140
	CAPACITY				
U.S. Models (lbf)	300, 500, 1K, 2K, 3K	5K, 10K	25K, 50K	100K	200K
Metric Models (kN)	1.5, 2.5, 5, 10	25, 50	100, 250	450	900
ACCURACY – (MAX ERROR)					
Static Error Band–% FS	±0.02	±0.025	±0.035	±0.05	±0.06
Nonlinearity–% FS	±0.03	±0.035	±0.035	±0.05	±0.06
Hysteresis–% FS	±0.02	±0.035	±0.045	±0.05	±0.06
Nonrepeatability–% RO	±0.01	±0.01	±0.01	±0.01	±0.01
Creep, in 20 min–%	±0.025	±0.025	±0.025	±0.025	±0.025
Side Load Sensitivity–%	±0.1	±0.1	±0.1	±0.1	±0.1
Eccentric Load Sensitivity–%/in	±0.1	±0.1	±0.1	±0.1	±0.1
TEMPERATURE					
Compensated Range–°F	15 to 115	15 to 115	15 to 115	15 to 115	15 to 115
Compensated Range–°C	-10 to 45	-10 to 45	-10 to 45	-10 to 45	-10 to 45
Operating Range–°F	-65 to 200	-65 to 200	-65 to 200	-65 to 200	-65 to 200
Operating Range–°C	-55 to 90	-55 to 90	-55 to 90	-55 to 90	-55 to 90
Effect on Zero–%RO/°F – MAX	±0.0004	±0.0004	±0.0004	±0.0004	±0.0004
Effect on Zero–%RO/°C – MAX	±0.0007	±0.0007	±0.0007	±0.0007	±0.0007
Effect on Output–%RO/°F – MAX	±0.0008	±0.0008	±0.0008	±0.0008	±0.0008
Effect on Output–%RO/°C – MAX	±0.0015	±0.0015	±0.0015	±0.0015	±0.0015
ELECTRICAL					
Rated Output–mV/V (Nominal)	2.0	4.0	4.0	4.0	4.0
Excitation Voltage–VDC MAX	20	20	20	20	20
Bridge Resistance–Ohm (Nominal)	350	350	350	350	350
Zero Balance–% RO	±1.0	±1.0	±1.0	±1.0	±1.0
Insulation Resistance–Megohm	5000	5000	5000	5000	5000
MECHANICAL					
Safe Overload–% CAP	±150	±150	±150	±150	±150
Deflection @ RO–inch	0.002	0.004	0.004	0.006	0.012
Deflection @ RO–mm	0.05	0.10	0.10	0.15	0.20
Base–P/N (Ref) (Metric)	B101 (m)	B102 (m)	B103 (m)	B112 (m)	B105 (m)
Natural Frequency–kHz	2.7, 3.5, 4.9 7.0, 8.5	4.7, 6.6	4.6, 5.0	4.0	3.5
Weight–lb	3.3	7.3	21.5	52	146
Weight–kg	1.5	3.3	9.8	24	66
Connector	PC04E-10-6P	PC04E-10-6P	PC04E-10-6P	PC04E-10-6P	PC04E-10-6P
Calibration	T & C	T & C	T & C	T & C	T & C

OPTIONS

Compression Overload Protection
Integral 10 ft Cable
Bayonet Connector
Multiple Bridge
Standardized Output
Connector Protection
Transducer Electronic Data Sheet (TEDS)

ACCESSORIES

Mating Connector
Instrumentation
Loading Hardware

STANDARD CONFIGURATIONS

10 ft Integral Cable (11xxAJ-nn)
<or> PC04E-10-6P Connector (11xxAF-nn)
<or> PT02E-10-6P Bayonet Connector (11xxACK-nn)

Appendix E – Uncertainty Analysis

E.1 Uncertainty in Measured Values

E.1.1 Temperature

All temperature measurements were recorded using T-Type Thermocouples and a Keithley 2700 data acquisition system. Using the specifications determined by Keithley [Keithley – 2002], the accuracy of T-Type thermocouple measurements can be determined using the following expression.

$$\frac{\delta T}{T} = \pm \frac{0.02℃}{T[℃]} \tag{E.1}$$

E.1.2 Surface Pressure

The surface pressure was recorded using an Interface Model 1100 (1K lbf) load cell connected to the Keithley data logger system. The pressure is calculated as follows:

$$P = C * V_{pressure} \tag{E.2}$$

where C is the correlation constant and Vpressure is the voltage signal as a result of the applied pressure. Therefore using the method described previously, the uncertainty in the pressure measurement is determined by Eq. (E.3).

$$\frac{\delta P}{P} = \pm \left[\left(\frac{\delta C}{C} \right)^2 + \left(\frac{\delta V_{pressure}}{V_{pressure}} \right)^2 \right]^{1/2} \tag{E.3}$$

The accuracy of the load cell is given in the manufacturer's specification sheet as follows:

$$\frac{\delta C}{C} = \pm 0.02\ \%\ of\ full\ scale\ (FS) \tag{E.4}$$

Full scale for the load cell is 1000 lbf / 12.57 in^2 = 79.58 psi. Therefore the uncertainty in C becomes the following.

$$\frac{\delta C}{C} = \pm \frac{0.0159\ psi}{P\ [psi]} \tag{E.5}$$

For the 10 V range used by the data logger to record the output signal, the corresponding uncertainty is as follows.

$$\frac{\delta V_{pressure}}{V_{pressure}} = \pm \left(3.0 \times 10^{-5} + \frac{5 \times 10^{-5}\ V}{V_{pressure}\ [V]} \right) \tag{E.6}$$

Based on the expressions above, the uncertainty in the surface pressure readings can be determined by substituting Eq. (E.5) and Eq. (E.6) into Eq. (E.3).

$$\frac{\delta P}{P} = \pm \left[\left(\frac{0.0159\ psi}{P\ [psi]} \right)^2 + \left(3.0 \times 10^{-5} + \frac{5 \times 10^{-5}\ V}{V_{pressure}\ [V]} \right)^2 \right]^{1/2} \tag{E.7}$$

E.1.3 Heat Sink Surface Area

The surface area of the heat sinks was calculated manually by measuring the individual length (L_i) and width (w_i) of the internal surfaces. Due to symmetry within the heat sink design the internal surface areas (A_i) could be multiplied to attain the overall heat sink surface area (A_{HS}) as seen in Eq. (E.8) and Eq. (E.9).

$$A_{HS} = \sum N_i * A_i \tag{E.8}$$

$$A_i = L_i * w_i \tag{E.9}$$

Therefore the uncertainty in the individual heat sink surface areas can be determined as follows:

$$\frac{\delta A_i}{A_i} = \pm \left[\left(\frac{\delta L_i}{L_i} \right)^2 + \left(\frac{\delta w_i}{w_i} \right)^2 \right]^{1/2} \tag{E.10}$$

The length (l_i) and width (w_i) of each surface was measured using an electronic digital caliper with a resolution of ±0.0005 cm.

$$\frac{\delta L_i}{L_i} = \pm \frac{0.0005\ cm}{L_i\ [cm]} \tag{E.11}$$

$$\frac{\delta w_i}{w_i} = \pm \frac{0.0005\ cm}{w_i\ [cm]} \tag{E.12}$$

Substituting Eq. (E.11) and Eq. (E.12) into Eq. (E.10), the uncertainty in the individual surface areas can be determined.

$$\frac{\delta A_i}{A_i} = \pm \left[\left(\frac{0.0005\ cm}{L_i\ [cm]} \right)^2 + \left(\frac{0.0005\ cm}{w_i\ [cm]} \right)^2 \right]^{1/2} \tag{E.13}$$

E.1.4 Effective Heat Sink Volume

The effective heat sink volume is calculated simply by multiplying the length, width, and height. This gives the practical occupying volume of the heat sink including the void spaces.

$$Vol_{HS} = L_{HS} * w_{HS} * h_{HS} \tag{E.14}$$

Using the same methodology as earlier and the same digital caliper to make measurements, the following expression can be used to determine the uncertainty in the effective heat sink volume.

$$\frac{\delta Vol_{HS}}{Vol_{HS}} = \pm\left[\left(\frac{0.0005\ cm}{L_{HS}\ [cm]}\right)^2 + \left(\frac{0.0005\ cm}{w_{HS}\ [cm]}\right)^2 + \left(\frac{0.0005\ cm}{h_{HS}\ [cm]}\right)^2\right]^{1/2} \quad \text{(E.15)}$$

E.1.5 Time

The timer function in the data acquisition program is used to access the computer's system clock and record the time values. The timer function has a 1 ms accuracy level and thus the uncertainty can be determined via Eq. (E.16).

$$\frac{\delta t}{t} = \pm\frac{0.001\ s}{t\ [s]} \quad \text{(E.16)}$$

E.1.6 Applied Voltage and Current (TEC and Fan)

The uncertainty in the applied voltage and current measurements is given in the power supply manufacturer's specification sheet and shown in Eq. (E.17) and Eq. (E.18).

$$\frac{\delta V_{applied}}{V_{applied}} = \pm(0.5\ \%\ of\ reading + 2\ digits) \quad \text{(E.17)}$$

$$\frac{\delta I_{applied}}{I_{applied}} = \pm(0.5\ \%\ of\ reading + 2\ digits) \quad \text{(E.18)}$$

E.2 Uncertainty in Calculated Values

E.2.1 Conduction Thermal Resistance

The conduction thermal resistance is calculated using Eq. (4.6). Therefore the uncertainty of thermal conduction resistances can be determined as follows:

$$\frac{\delta R_{cond}}{R_{cond}} = \pm\left[\left(\frac{\delta k}{k}\right)^2 + \left(\frac{\delta L_2}{L_2}\right)^2 + \left(\frac{\delta A}{A}\right)^2\right]^{1/2} \tag{E.19}$$

Assuming the thermal conductivity given by [EngineeringToolBox.com] has 6 % uncertainty (standard value for thermal conductivity determination), the uncertainty in conduction resistance can be calculated by substituting Eq. (E.11) and Eq. (E.13) into Eq. (E.19).

$$\frac{\delta R_{cond}}{R_{cond}} = \pm\left[(0.06)^2 + \left(\frac{0.0005\ cm}{L_2\ [cm]}\right)^2 + \left(\frac{0.0005\ cm}{L_1\ [cm]}\right)^2 + \left(\frac{0.0005\ cm}{w_1\ [cm]}\right)^2\right]^{1/2} \tag{E.20}$$

L_1 and w_1 are the length and width of the cross-sectional area and L_2 is the thickness of the conducting material (ie. Aluminum).

E.2.2 Heat Flow

The heat flow is calculated by dividing the temperature difference across a conductive path by the thermal resistance. This is expression was given again in Eq. (E.21).

$$Q = \frac{T_{max} - T_{min}}{R_{cond}} \tag{E.21}$$

Therefore the uncertainty in the heat flow can be expressed as shown in Eq. (E.22).

$$\frac{\delta Q}{Q} = \pm\left\{\left[\left(\frac{T_{max}}{T_{max}-T_{min}}\right)\frac{\delta T_{max}}{T_{max}}\right]^2 + \left[\left(\frac{T_{min}}{T_{max}-T_{min}}\right)\frac{\delta T_{min}}{T_{min}}\right]^2 + \left(\frac{\delta R}{R}\right)^2\right\}^{1/2} \quad \text{(E.22)}$$

Substituting Eq. (E.1) and Eq. (E.19) for the uncertainties in temperature and thermal conduction resistance respectively, the following expression can be obtained for the uncertainty in heat flow.

$$\frac{\delta Q}{Q} = \pm\left\{\left[\left(\frac{T_{max}}{T_{max}-T_{min}}\right)\frac{0.02℃}{T_{max}[℃]}\right]^2 + \left[\left(\frac{T_{min}}{T_{max}-T_{min}}\right)\frac{0.02℃}{T_{min}[℃]}\right]^2 + \left(\frac{0.0005\ cm}{L_2\ [cm]}\right)^2 + \left(\frac{0.0005\ cm}{L_1\ [cm]}\right)^2 + \left(\frac{0.0005\ cm}{w_1\ [cm]}\right)^2\right\}^{1/2} \quad \text{(E.23)}$$

E.2.3 Convection, Spreading, and Contact Thermal Resistance

The convection, spreading, and contact resistance was calculated using a variation of Eq. (E.24).

$$R_{conv}\ or\ R_{sp}\ or\ R_{cont} = \frac{T_{max}-T_{min}}{Q} \quad \text{(E.24)}$$

In this case $T_{max} - T_{min}$ represents the temperature difference across the specific region of interest. For convective thermal resistance for example, the temperature difference is between the heat sink fins and the ambient. For spreading thermal resistance, the temperature gradient is between the center of the heat sink base and the heat sink base edge. Finally, for the contact thermal resistance, the temperature gradient exists between the TEC hot side and the heat sink base. Using a general term to denote any of these resistances, R_i, the following uncertainty can be calculated.

$$\frac{\delta R_i}{R_i} = \pm\left\{\left[\left(\frac{T_{max}}{T_{max}-T_{min}}\right)\frac{\delta T_{max}}{T_{max}}\right]^2 + \left[\left(\frac{T_{min}}{T_{max}-T_{min}}\right)\frac{\delta T_{min}}{T_{min}}\right]^2 + \left(\frac{\delta Q}{Q}\right)^2\right\}^{1/2} \quad \text{(E.25)}$$

E.2.4 Power

The uncertainty in applied power to the TEC and fan can be calculated using the following equations.

$$P_{applied} = V * I \tag{E.26}$$

$$\frac{\delta P_{applied}}{P_{applied}} = \pm\left[\left(\frac{\delta V_{applied}}{V_{applied}}\right)^2 + \left(\frac{\delta I_{applied}}{I_{applied}}\right)^2\right]^{1/2} \tag{E.27}$$

Substituting Eq. (E.17) and Eq. (E.18) into Eq. (E.27) the uncertainty in the applied power can be determined.

$$\frac{\delta P_{applied}}{P_{applied}} = \pm[(0.5\ \%\ of\ voltage\ reading)^2 + (0.5\ \%\ of\ current\ reading)^2]^{1/2} \tag{E.26}$$

Appendix F – Raw Data

F.1 TEC Performance Data w/o Heat Sink (Compressed – 10 s intervals)

Time (s)	T_h (°C)	T_c (°C)
150	26.357	26.419
155	26.294	26.481
160	26.357	26.481
165	26.419	24.675
170	28.038	11.22
175	28.536	16.953
180	28.926	25.002
185	29.175	32.911
190	29.47	39.621
195	28.49	60.489
200	28.178	67.634
205	27.992	69.017
210	27.929	68.383
215	27.867	67.461
220	27.805	66.309
225	27.805	64.811
230	27.743	63.543

F.2 Experiment 1 – Temperature Stability Data

F.2.1 Temperature Stability Data (Compressed to 20 min Intervals)

	Replicate 1	Replicate 2	Replicate 3	Replicate 4	Replicate 5
Time (min)	**T_c (°C)**	**T_c (°C)**	**T_c (°C)**	**T_c (°C)**	**T_c (°C)**
0	23	23	23	23	23
20	-6.8	-8.25	-7.5	-7.95	-9
40	-6.7	-8.2	-7.25	-7.95	-8.6
60	-6.75	-8.05	-7.1	-7.95	-8.55
80	-6.6	-7.9	-7	-7.9	-8.5
100	-6.8	-8	-7	-7.9	-8.45
120	-6.55	-7.8	-6.95	-7.75	-8.5
140	-6.45	-7.95	-7.25	-7.6	-8.4
160	-6.25	-7.95	-7.25	-7.25	-8.45
180	-6.25	-7.75	-7.35	-7.25	-8.5
200	-6.3	-7.7	-7.4	-7.25	-8.5
220	-6.3	-7.7	-7.45	-7.45	-8.4
240	-6.25	-8	-7.5	-7.5	-8.4
260	-6.25	-7.85	-7.5	-7.5	-8.5
280	-6.2	-7.85	-7.3	-7.25	-8.5
300	-6.2	-7.85	-7.25	-7.15	-8.55
320	-6.15	-7.8	-7	-7.1	-8.6

F.2.2 Surface Pressure Adjustment Data (Compressed to 2.5 min Intervals)

Time (min)	**T_c (°C)**
0	20
2.5	20
5	20
7.5	-8.5
10	-9.5
12.5	-9.75
*13.25	-9.25
15	-10.5
17.5	-10.75
*18.3	-10.8
20	-11.25
22.5	-11.5
25	-11.5

* Pressure Adjustment Times

F.2.3 Effect of Surface Pressure on Cooling Data (Compressed to 2.5 min Intervals)

	7.07 psi	28.3 psi
Time (min)	**T_c (°C)**	**T_c (°C)**
0	23.0	23.0
20	-13.25	-14.75
40	-12.85	-14.25
60	-12.75	-14
80	-12.65	-13.85
100	-12.5	-13.85
120	-12.4	-13.8
140	-12.3	-13.75
160	-12.2	-13.7
180	-12.15	-13.65
200	-12.25	-13.7
220	-12.25	-13.75
240	-12.25	-13.6
260	-12.2	-13.55
280	-12.3	-13.5
300	-12.25	-13.3
320	-12.15	-13.4

F.3 Experiment 2 – Enhanced Cooling Data (Compressed to 0.5 h Intervals)

	Replicate 1 (Green Line)		Replicate 2 (Cyan Line)		Replicate 3 (Red Line)		Replicate 4 (Blue Line)	
Time (h)	**T_h (°C)**	**T_c (°C)**	**T_h (°C)**	**T_c (°C)**	**T_h (°C)**	**T_c (°C)**	**T_h (°C)**	**T_c (°C)**
0	21	21	22.5	22.5	24	24	25	25
0.5	34	-22.4	35	-21	37	-20	38	-18
1	34.5	-22	35.5	-21	37	-20	38.5	-17.5
1.5	34.75	-21.75	35.5	-20.75	37	-20	38.5	-17.5
2	34.9	-21.5	35	-20.75	36.5	-20.25	38.5	-17.5
2.5	35	-21.25	34.5	-21.25	37.5	-19.5	38.75	-17.5
3	35	-21.5	34.5	-21.5	37.5	-19.5	38.25	-17.75
3.5	35	-21.5	35	-21	37.5	-19.5	38.25	-17.75
4	35.1	-21.5	35	-21	37.5	-19.5	38	-17.75
4.5	35	-21.5	34	-21.5	37	-20	38	-17.75
5	35	-21.25	33.75	-22	37.5	-19.75	38	-17.5
5.5	35	-21.5	33.75	-22	37.5	-20	38.5	-17.25
6	34.95	-21.75	33.75	-21.75	37	-20	38.75	-17.5

F.4 Experiment 3 – Thermal Management Scale Down Data

F.4.1 Effect of Surface Pressure on Cooling Data (Compressed to 2.5 min Intervals)

	HS – 1 (Red Line)		HS – 2 (Cyan Line)		HS – 3 (Blue Line)		HS – 4 (Yellow Line)		HS – 5 (Green Line)	
Time (h)	T_h (°C)	T_c (°C)	T_h (°C)	T_c (°C)	T_h (°C)	T_c (°C)	T_h (°C)	T_c (°C)	T_h (°C)	T_c (°C)
0	23	23	23	23	23	23	23	23	23	23
0.5	32	-22.4	35.5	-19.75	36.5	-21	37.5	-9.75	36	-11.25
1	32	-22	35.5	-19.75	37	-20.5	37.5	-9.5	36	-10.75
1.5	32	-22	36	-19.5	36.5	-21	37.5	-10	36	-10.5
2	32	-22	36	-19	36.75	-20.5	38	-10.25	36	-10.25
2.5	32	-22	36.25	-19.5	37.25	-20	38.25	-10	36.25	-10.25
3	31.75	-21.75	36	-19.5	37	-20	38.5	-10	36	-10.25
3.5	31.5	-21.5	35.75	-19.5	37.5	-20	38.75	-10.25	36	-10.25
4	31	-20.75	35.5	-19.5	37.5	-20	38.5	-10.25	36.25	-10.25
4.5	31	-20.5	35.5	-19.5	36.5	-20.5	38.75	-10.25	36.25	-10.25
5	31	-20.5	35.25	-19.5	36.5	-20.75	38.5	-10	36.5	-10.75
5.5	31.5	-20.25	35.25	-19.5	36	-20.5	38.5	-9.75	36.25	-11

F.4.2 Cooling Performance of TEC 2 + HS – 5 Data (Compressed to 1 min Intervals)

TEC 2, HS – 5	
Time (min)	T_c (°C)
0	26.5
1	26.5
2	-6.5
3	-9
4	-8.5
5	-8
6	-7.75
7	-7.65
8	-7.5
9	-7.35
10	-7
11	-6.85
12	-6.5

F.5 Experiment 4 – Copper Cooling Data (Compressed to 0.5 h Intervals)

	Copper Surface	
Time (h)	**T_h (°C)**	**T_c (°C)**
0	23	23
0.5	41	-6
1	41	-5.5
1.5	42	-4
2	42.5	-3.5
2.5	42.5	-3
3	42.5	-3
3.5	42.5	-2.75
4	42.5	-2.5
4.5	42.75	-2.25
5	42.75	-2
5.5	42.75	-2